The Islamic University of Gaza
Deanship and Postgraduate Affairs
Faculty of Engineering
Electrical Engineering Department
Master of Communications Systems

الجامعـــة الإســلاميـة بغزة
عمادة البحث العلمي والدراسات العليا
كليــة الهندسة
قسم الهندسة الكهربائية
ماجستير أنظمة الاتصالات

Design of Multi-Band RF Energy Harvesting System

تصميم نظام متعدد النطاقات لحصاد طاقة موجات الراديو

By:

Salman Y. Mansour

Supervised by

Dr. Talal F. Skaik

PhD Communications Engineering

A thesis submitted in partial fulfillment
of the requirements for the degree of
Master of Communications Systems

March/2018

إقـــــرار

أنا الموقع أدناه مقدم الرسالة التي تحمل العنوان:

Design of Multi-Band RF Energy Harvesting System

تصميم نظام متعدد النطاقات لحصاد طاقة موجات الراديو

أقر بأن ما اشتملت عليه هذه الرسالة إنما هو نتاج جهدي الخاص، باستثناء ما تمت الإشارة إليه حيثما ورد، وأن هذه الرسالة ككل أو أي جزء منها لم يقدم من قبل الاخرين لنيل درجة أو لقب علمي أو بحثي لدى أي مؤسسة تعليمية أو بحثية أخرى.

Declaration

I understand the nature of plagiarism, and I am aware of the University's policy on this. The work provided in this thesis, unless otherwise referenced, is the researcher's own work, and has not been submitted by others elsewhere for any other degree or qualification.

Student's name:	سلمان يوسف منصور	**اسم الطالب:**
Signature:	*Salman Y. Mansour*	**التوقيع:**
Date:	**06/03/2018**	**التاريخ:**

بسم الله الرحمن الرحيم

الجامعة الإسلامية غزة
The Islamic University of Gaza
عمادة البحث العلمي والدراسات العليا
هاتف داخلي: 1150

الرقم: ج س غ/35/
Ref: 2018/03/06م
التاريخ:
Date:

نتيجة الحكم على أطروحة ماجستير

بناءً على موافقة عمادة البحث العلمي والدراسات العليا بالجامعة الإسلامية بغزة على تشكيل لجنة الحكم على أطروحة الباحث/ **سلمان يوسف سلمان منصور** لنيل درجة الماجستير في كلية **الهندسة**/ قسم **الهندسة الكهربية/أنظمة الاتصالات** وموضوعها:

تصميم نظام متعدد نطاقات التردد لحصاد طاقة موجات الراديو

Design of Multi-Band RF Energy Harvesting System

وبعد المناقشة العلنية التي تمت اليوم **الثلاثاء 18 جمادي الثانية** 1439هـ الموافق **2018/03/06م** الساعة **الواحدة مساءً**، في قاعة مبنى **القدس** اجتمعت لجنة الحكم على الأطروحة والمكونة من:

د. طلال فايز سكيك	**مشرفاً ورئيساً**	.....
د. عمار محمد رمضان/ أبو هدروس	**مناقشاً داخلياً**	.....
د. تامر كمال أبو فول	**مناقشاً خارجياً**	.....

وبعد المداولة أوصت اللجنة بمنح الباحث درجة الماجستير في **كلية الهندسة/قسم الهندسة الكهربية/أنظمة الاتصالات.**

واللجنة إذ تمنحه هذه الدرجة فإنها توصيه بتقوى الله تعالى ولزوم طاعته وأن يسخر علمه في خدمة دينه ووطنه.

والله ولي التوفيق،،،

عميد البحث العلمي والدراسات العليا

أ. د. مازن إسماعيل هنية

Abstract

Energy harvesting technology has received a lot of attention at a time of great proliferation in the use of wireless devices. It has also become one of the most research topics in the world because of its importance in providing easy and free energy for important applications that are not easily accessible.

This thesis presents design of multi-Band RF energy harvesting system which consists of three main blocks connected together, rectenna (antenna, rectifier circuit) and matching circuit.

Microstrip Ultra-wideband star patch antenna was designed to harvest multi-band signals including 900MHz (GSM band) Global System for Mobile communication ,1800MHz (GSM band), UMTS (3G Band) Universal Mobile Telecommunications System and WiFi (Wireless Fidelity) frequencies bands. The designed antenna has good return loss performance. The design and optimizing of the performance of proposed antenna are performed by using Computer Simulation Technology software CST studio design and ANSYS HFSS 15 software. The antenna has been fabricated and tested and the measurements were in acceptable agreement with simulations but with some shift in frequency.

Next, rectifier circuits are proposed for RF to DC conversion and obtaining high voltage output. Rectifier circuits with four-stage voltage doubler using Schottky diodes were designed to convert the RF energy into a DC output. Many matching techniques were used in the design, the first design included T-Lumped element matching network used for single band and multi-band rectifiers by using Advanced Design System (ADS 2016) and Smith Ver3 software. On the second design Taper matching technique was used to match the complex input impedance of the rectifier circuit to the standard 50 Ω. The design of the rectifier circuits is performed by Advanced Design System (ADS 2016) software and the RF-DC conversion efficiency and output voltage were simulated and the max output voltage of rectifier at 0dBm was 5.8V. The circuit with tapered matching has been fabricated and tested.

الملخص

لقد حظيت تكنولوجيا حصاد الطاقة على الكثير من الاهتمام في ظل الانتشار الواسع لاستعمال الأجهزة الالكترونية وخصوصا اللاسلكية منها، حيث كانت ومازالت محور الباحثين حيث أصبحت واحدة من أكثر المواضيع البحثية في العالم نظرا لأهميتها في توفير مصادر طاقة سهلة ومجانية، إضافة الى إمكانية استعمالها في التطبيقات الالكترونية صعبة الوصول.

ولحصاد الطاقة اشكال متعددة من أهمها حصاد الطاقة من خلال حركة الرياح أو أشعة الشمس أو حركة الامواج إضافة الى حصاد طاقة الموجات الكهرومغناطيسية المنتشرة في الجو من خلال أنظمة الاتصالات اللاسلكية المتعددة، في هذه الأطروحة تم تصميم نظام متعدد النطاقات لحصاد طاقة الترددات الراديوية والذي يتألف من ثلاث كتل رئيسية متصلة معا وهم: الهوائي ودائرة المعدل والدائرة المطابقة (دائرة التوافق).

في الدائرة الأولى تم تصميم هوائي ذي نطاق عريض ليكون مناسبا للعمل في حصاد النطاقات المتعددة، حيث يعمل على تغطية أكثر النطاقات العالمية أهمية وهي (تردد الخلوي (GSM900)، تردد الخلوي(GSM1800)، وتردد الشبكات اللاسلكية (WiFi)، وتردد الجيل الثالث (UMTS)، وتردد(LTE).

كما تم تصميم دائرة المعدل ومضاعف الجهد المستقبل من خلال دائرة الهوائي باستخدام ثنائيات خاصة (Schottky diodes) تتميز بصغر جهد التشغيل، حيث تعمل على تحويل طاقة ترددات الراديو المستقبلة الى تيار كهربائي مستمر ومضاعفته أربعة اضعاف.

ولكي تتوافق الدائرة الأولى مع الثانية ونحصل على اعلى كفاءة لها تم استخدام عدة تقنيات لدوائر التوافق، ففي التصميم الأول استعمل نموذج العناصر المجمع في دائرة التوافق لدائرة النطاق وكذلك متعددة النطاقات، وكإضافة لإثراء البحث تم عمل دائرة التوافق المغزلية (مستدقة الرأس Taper) مما جعل دائرة التوافق أكبر كفاءة وأقل تكلفة.

في هذه الأطروحة تم استعمال برامج المحاكاة:(CST 2014, ADS 2016, Smith Ver3, HFSS 15).

Nothing's impossible if you put your mind to it.

Dedication

To

My Parents Yousuf & Naema

My Wife Rodaina

My children

Yazan, Dana

and

My Family

Acknowledgment

First and foremost, I thank almighty **ALLAH** for giving me the courage and determination, as well as guidance in conducting this research study, deposits all difficulties.

I would like to start out by expressing my deepest gratitude to my advisor, **Dr. Talal Skaik**, for providing me the opportunity to work on this project and for his guidance throughout my research. He is an amazing professor and advisor and it was an honor to work with him.

I am also very grateful to my thesis committee members, **Dr. Ammar Abo Hadrouss** and **Dr. Tamer Aboufoul** who reviewed the proposal and development of important notes, cooperation and constructive advices.

My heartiest thanks and deepest appreciation is due to my parents, my wife, my children, my brothers and sisters for standing beside me, encouraging and supporting me all the time I have been working on this thesis.

Special thanks For **INTERPAL** Palestine for choosing my thesis and support, and most especially thanks for my dear friend **Eng. Khaled Daoud** for his outstanding support and encourage,

Thanks to all those who assisted me in all terms and helped me to bring out this work.

Table of Contents

List of Tables

List of Figures

List of Abbreviations

2D	Two dimensions
3D	Third dimension
AC	Alternating Current
ADS	Advanced Design System
BTS	Base Transceiver Station
CST	Computer Simulation Technology
dB	Decibel
dBi	decibels relative to isotropic radiator
DC	Direct Current
DCS	Digital Cellular Service.
E	Electric fields
EH	Energy Harvesting
EM	Electro Magnetic
FNBW	First-Null Beam Width
GHz	Gigahertz
GSM	Global System for Mobile
GSM	Global System for Mobile Communications
H	Magnetic fields
HFSS	ANSYS High-Frequency Electromagnetic Fields
HPBW	Half Power Beam Width
IEEE	Institute of Electrical and Electronics Engineers
ISM	The industrial, scientific and medical (ISM) radio bands.
LAN	Local Area Network
MHz	Megahertz
PFD	Power Flux Density
RF	Radio Frequency
RFID	radio frequency identification
RL	Return Loss
SHF	Super high frequency.
TV	Television
UHF	Ultra-high frequency.
UMTS	Universal Mobile Telecommunications System
VSWR	Voltage Standing Wave Ratio
WiFi	Wireless Fidelity, wireless internet
WiMAX	Worldwide Interoperability for Microwave Access.
WLAN	Wireless Local Area Network
WSNs	Wireless Sensor Networks.
µW	Microwatt
Ω	Omega in ohm
Mbps	megabits per second

Chapter 1

Introduction

Chapter 1
Introduction

Recently, RF energy harvesting is increasingly attracting researchers as an alternative solution to short-life batteries. Harvesting of ambient energy available in RF signals enables empowering low power devices like network wireless sensors and medical implants.

Since the 1980s mobile phone technology has grown rapidly and the needs for longer battery life have risen (Mitcheson, Yeatman, Rao, Holmes, & Green, 2008). Beside of improving the energy of batteries has been a major research field, energy harvesting as new developments has helped manufacturers in their search for better power supplies (Mitcheson et al., 2008). Energy harvesting has many forms, such as wind, sun and waves harvesting, as well as the harvesting of RF energy from wireless telecommunication systems. These RF signals can be utilized and converted as usable DC power by using Energy harvesting system. The surrounded RF energy has an advantage that is available during all the day and night unlike a solar energy, which is available only when sunlight is present but sun has higher energy.

Manufacturers looking to harvest energy through other means have to consider the following four factors: the device's power consumption; its usage pattern; its size; and the motion and vibration to which the device is generally subjected (Mitcheson et al., 2008)

RF energy harvesting is one of the most important energy harvester types, there are several energy harvesting technologies have been used, which have innovative techniques at use. such as vibration, solar and wind that can be harvested look at Table 1.1 to see the power of energy harvesting sources that is available.

Table 1.1: Available power from sources of energy harvesting

Source	Source Power	Harvested Power	Advantages	Disadvantages
Light				
Indoor	0.1 mW/cm²	10 µW/cm²	• High power density • Mature	• Not available always • Required exposure to light costly
Outdoor	100 mW/cm²	10 mW/cm²		
Vibration/Motion				
Human	0.5m at 1 Hz		• Implantable • High efficiency	• Not available always • Material physical limitation
	1m/s² at 50 Hz	4 µW/cm²		
Machine	1m at 5 Hz			
	10m/s² at 1 kHz	100 µW/cm²		
Thermal				
Human	20 mW/cm²	30 µW/cm²	• High power density • Implantable	• Not available always • Overflow heat
Machine	100 mW/cm²	1-10 mW/cm²		
RF				
GSM	0.3 µW/cm²	0.1 µW/cm²	• Always available • Implantable	• Low density • Efficiency inversely proportional to distance

The idea of RF energy harvesting is to capture transmitted RF energy at ambient and using it directly for low power circuit or store it to use it later. The concept to convert RF signals to DC voltage needs an efficient antenna with side by side a rectifier circuit. The efficiency of RF energy harvesting depends on the efficiency of antenna which depends on its impedance and the rectifier circuit impedance. all the ambient available RF power will not be received from the free space at the desired frequency band If the two impedances aren't matched.

The impedances matching means that the impedance of the rectifier circuit (voltage doubler circuit) is the complex conjugate of the impedance of antenna.

The basic energy harvesting system block diagram is shown in Figure 1.1, which consists of RF source from antenna, matching network, RF to DC conversion and load circuits.

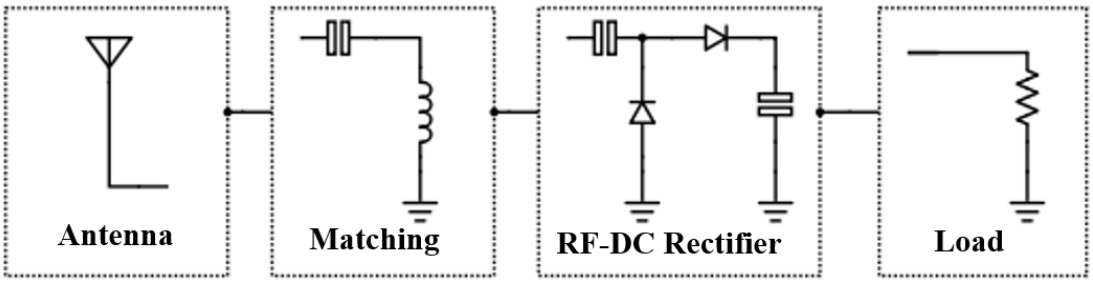

Figure 1.1: Energy harvesting system block diagram

The ambient electromagnetic energy harvested by using antenna and the harvested energy is filtered and rectified. Then the recovered direct current (DC) can be used directly at low powered device, or stored in a super capacitor and batteries for higher power low duty-cycle operation. (Bouchouicha, Dupont, Latrach, & Ventura, 2010). Voltage doubler can be used to multiply voltage for devices required.

1.1 Background and Context

Nowadays, world looks forward to rationalize and reduce energy consumption, and trying to conserve energy and raising the efficiency of energy utilization by preventing any loss of energy or use energy in other ways, RF energy harvesting is common in metropolitan centers, which are saturated by Television (TV), AM (Amplitude Modulation), FM (Frequency Modulation), cellular GSM (Global System for Mobile communication) 2G, 3G, UMTS (The Universal Mobile Telecommunications System), WiFi, WiMAX(Worldwide Interoperability for Microwave Access), and other instruments that transmit RF signals. (Paradiso & Starner, 2005) high electromagnetic fields generated from Radio frequency emitted by such sources contain electromagnetic energy that can be converted into DC voltage using a rectifier voltage doubler circuit linked to the receiving antenna. (Le, Mayaram, & Fiez, 2008) This circuit system can convert the RF (Radio frequency) signal to DC (Direct Current) power at distances over 100 meters. To maintain a sufficient supply of energy in midst of varying RF concentrations, a capacitor can be attached to the circuit system to output the required constant voltage. (Le et al., 2008)

The following sub-sections provide a brief background on the wireless systems of interest for harvesting.

1.1.1 GSM 900-1800

GSM900 and GSM1800 (Global System for Mobile Communications) are open digital cellular technology used to transmit mobile data and voice services. Which is used in most parts of the world as we see at the following in Figure 1.2.

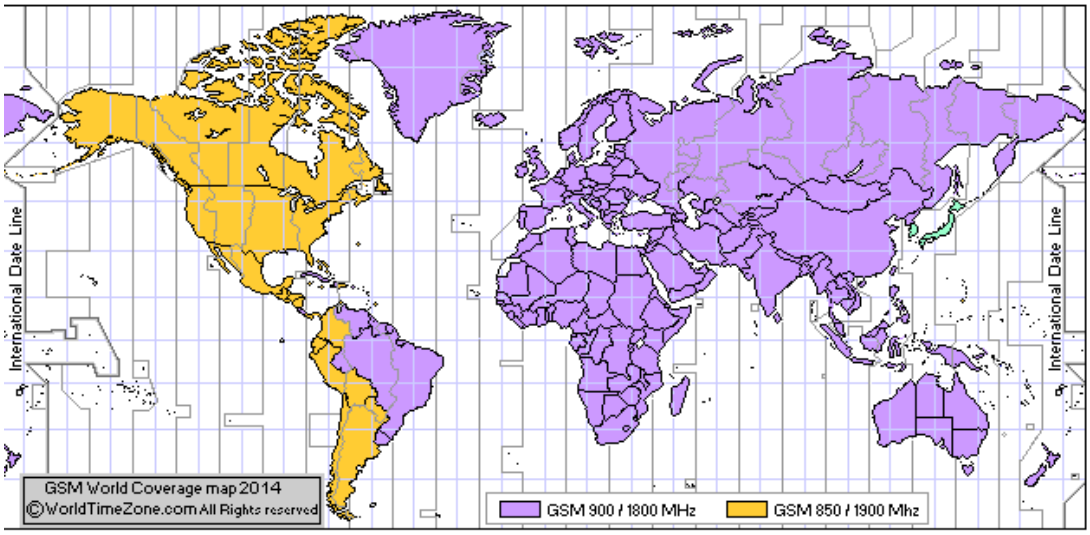

Figure 1.2: GSM Global System for Mobile communications - most popular standard for phones in the world.(Poranki, Perwej, & Perwej, 2015)

GSM900 in Figure 1.3 is using for uplink (sending information to the Base Transceiver Station (BTS) from the Mobile Station) frequency of 890 - 915 MHz and 935 - 960 MHz for the downlink (receiving information from the Base Transceiver Station (BTS) to the Mobile Station). Every GSM band (uplink /downlink) consist of 124 RF channels (channel numbers 1 to 124) have bandwidth of 200 kHz for channels and Duplex spacing of 45 MHz at either end of the range of frequencies the guard bands of 100 kHz wide are placed.(Huurdeman, 2003)

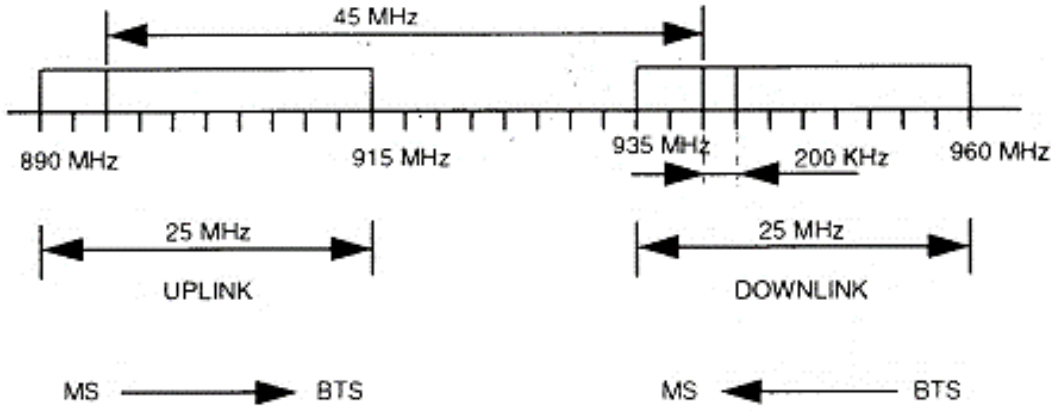

Figure 1.3: GSM 900 band (uplink /downlink).

GSM1800 using for uplink (sending information to the Base Transceiver Station (BTS) from the Mobile Station) frequency of 1710 - 1785 MHz and 1805–1880 MHz for the downlink (receiving information from the Base Transceiver Station (BTS) to the Mobile Station), every GSM band (uplink /downlink) consist of 374 RF channels (channel numbers 512 to 885) as shown in Figure 1.4. Duplex spacing is 95 MHz.

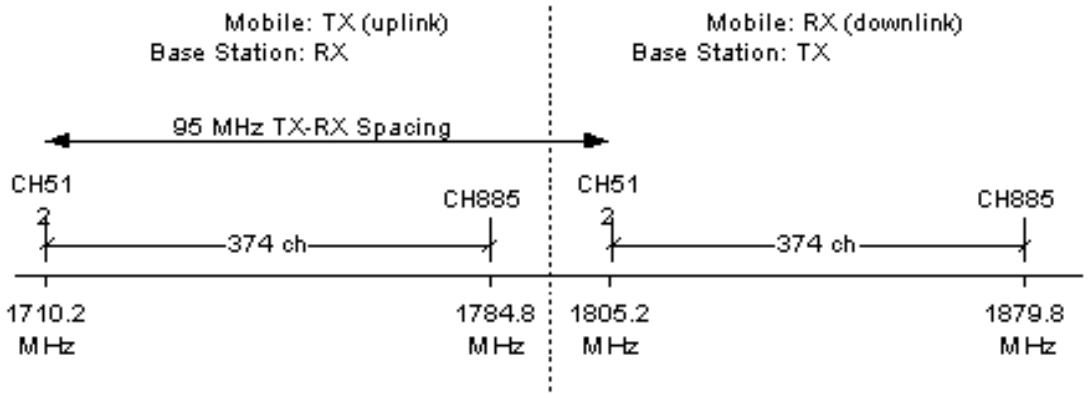

Figure 1.4: GSM 1800 band (uplink /downlink).

1.1.2 Universal Mobile Telecommunications Service (UMTS)

UMTS (Universal Mobile Telecommunications Service) is a third generation (3G) mobile cellular system for networks based on the GSM standard. Which send packet based of text, voice, video, and multimedia with data rate up to 2 Mbps (megabits per second).

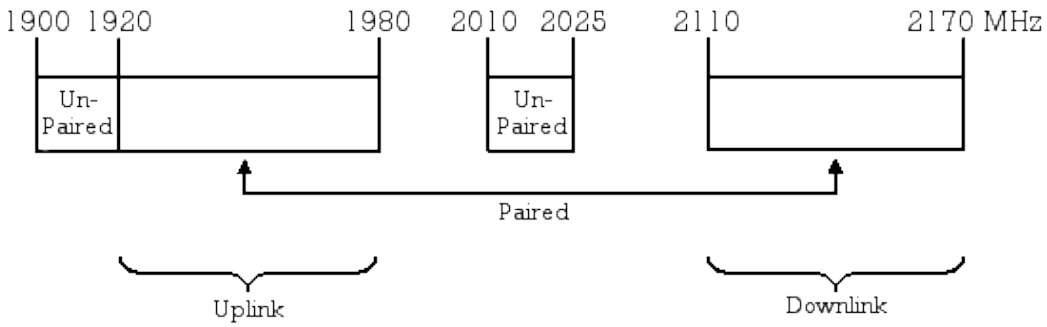

Figure 1.5: UMTS band uplink and downlink

UMTS using for uplink (sending information to the Base Transceiver Station (BTS) from the Mobile Station) frequency of 1900 - 2025 MHz and 2110 - 2170 MHz for the downlink (receiving information from the Base Transceiver Station (BTS) to the Mobile Station) as shown in Figure 1.5. A convenient set of services to mobile and smart phone users offered by UMTS, in anywhere in the world they are located. UMTS is based on GSM (the Global System for Mobile) communication standard and endorsed by manufacturers and major standards organizations as the standard for mobile users around the world. On UMTS computer and phone users can be contacted to the Internet constantly every time and everywhere, they will have the same set of capabilities. Through a combination of wireless and satellite transmissions users can be reach.(Samukic, 1998)

1.1.3 WiFi

WiFi is a short name for Wireless Fidelity, that is the name of a wireless networking technology, WiFi uses radio frequencies to provide Internet connections and high-speed networks. this allows modern devices to connect to the network.

WiFi was used in place of only the 2.4GHz 802.11b standard (IEEE 802.11 WiFi / WLAN standards) initially, but the generic use of the WiFi term expanded by the WiFi Alliance to include any type of network or WLAN (wireless local area network) product based on any of the 802.11 standards, including 802.11b, 802.11a, dual-band, and others, in an effort to stop interference about wireless LAN interoperability, the main bands used for carrying WiFi are 2400-2500 MHz for lower and upper frequencies, and 5725-5875 MHz for lower and upper frequencies, the ISM (The industrial, scientific and medical) band 2400 submitted into fourteen channels defined

for use by WiFi 802.11 for the 2400 MHz which is used for up and down link, the 802.11 WLAN standards specify a bandwidth of 22 MHz and channels are on a 5 MHz incremental step as shown in Figure 1.6.

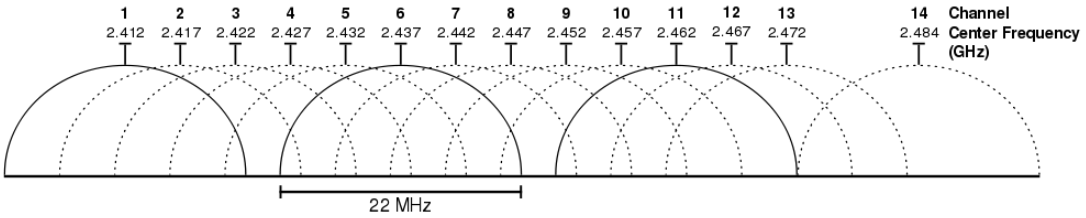

Figure 1.6: WiFi standards channels.

Many devices depends on using of WiFi, as e.g. smart homes, surveillance systems, smart devices, personal computers, video-game consoles, printers, smartphones, and tablet computers. These can connect to a network resource by using access points.(Varma, 2012)

1.2 Rectifier circuit

For needed to convert an input RF signal into DC voltage rectifier circuit is required. Designing rectifier is one of the challenging parts due to low power threshold, the efficiency of rectifier is not high enough to have reasonable efficiency. (Keyrouz, Visser, & Tijhuis, 2013)

Rectifier circuit is the third important part of the energy harvesting system, which used to convert AC voltage into DC voltage that received from impedance matching circuit. In chapter 5 more details will be discussed about rectifier circuit.

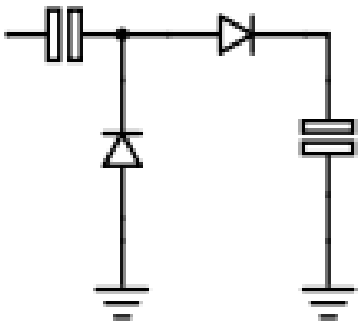

Figure 1.7: Simple rectifier circuit

1.3 Impedance matching circuit

Impedance matching circuit is used to transfer the maximum RF power from source to load. Since the RF source impedance (50Ω) is different from the input impedance of the rectifier, so in this case the impedance matching is needed for transferring maximum power into the circuit (Khonsari, Björninen, Tentzeris, Sydänheimo, & Ukkonen, 2015).

Impedance matching is an important part for RF circuits and a microwave component design. The term "impedance matching" is rather clear. It is simply defined as the process of making one impedance equal to another. look at the circuit below shown in Figure 1.8. It is necessary to match the load impedance to the source impedance or input impedance of a driving source. At chapter 3, more details will be discussed about impedance matching techniques.

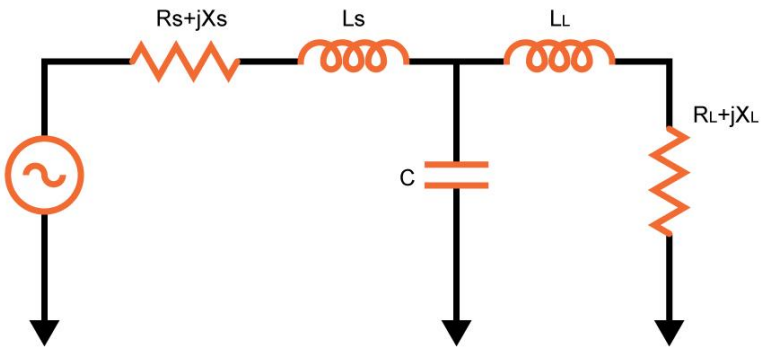

Figure 1.8: T-Match Impedance Matching Circuits

1.4 Scope and Objectives

The main purpose of the research is to design an efficient multiband energy harvesting system to collect RF signals from the GSM, WiFi, UMTS, and implement the design practically. The system consists of a UWB (Ultra-Wide Band) antenna, a rectifier circuit and a matching network. The design is based on microstrip technology. The simulated results will be compared with practical results after implementing the design.

1.5 Signification

In light of the spread of wireless devices, as well as scientific development in the medical fields, and wireless remote sensors have led to an increased demand and dependence on the use of batteries.

From this point, since 1950s researchers work on RF energy harvesting system and due to available technologies at that time they use high RF energy sources, as more of a proof of concept rather than a practical energy source. In the modern environment and current life there are many wireless sources of different frequencies bands radiating RF power in all directions.

This makes RF energy harvesting cornerstone in precision industries, that enters into commercial manufacturing in various important fields like medical fields, Radio-frequency Identification (RFID) and Wireless sensor network (WSN).

In this thesis, multi-band RF energy harvesting system will be designed and a study will be done on that which gives sufficient output voltage for input RF power of 0dBm or less, that is efficient for medical fields, and Wireless sensor network (WSN) use.

1.6 Limitations

The incident RF energy needs to be converted into usable dc power and this requires an antenna with high directivity to receive more incident RF energy because the amount of the received power by the antenna is directly proportional to its directivity (Barnett, Lazar, & Liu, 2006). The received power according to Friis transmission equation 1.1: (Gaur et al., 2013)

$$Pr = \frac{P_t G_t G_r \lambda^2}{(4\pi R)^2} \tag{1.1}$$

Pr = Received power by the antenna (w).
Pt = Transmitted power from the source (w).
Gt = The gain of the transmitter antenna (dB).
Gr = The gain of the receiver antenna (dB).
R = Distance between the transmitter and receiver antennas (m).
λ = wavelength of the transmitted signal (m).

Received power is low which can be used only on devices of low power needed. Also, the most important limitation at our country is design fabrication due to lack of required measuring devices and electronic components required for design.

1.7 Applications

Energy harvesting appears as a reasonable solution for safe and unlimited energy supply to communication networks (Shahzad, 2013). Environmental energy harvesting system has been recently taken into consideration for improving the prospective lifetimes of systems e.g., medical and healthcare, wearable computers and sensor networks, RFID (Radio-frequency Identification) etc.

1.7.1 RF power harvesting in medical and healthcare

For the protection and managing of chronic diseases the continual monitoring of physiological signals is needed by using the wearable biomedical sensors for the continuous monitoring of physiological signals.

However, the widespread of wearable biomedical devices based on their ability to work for long time without the need to change batteries frequently or recharge or even use batteries.

In this case, energy harvesting is the attractive modern technology that can facilitate the way towards large utilization of wireless wearable sensors devices for patient self-oversight and daily healthcare. Radio waves that transmitted from wireless communication networks, like GSM, WiFi, UMTS, TV, GPS. etc. represent ambient radio frequency energy that can be harvested as they are available in suburban and urban areas.

Radio frequency energy is used to recharge the batteries in pacemakers and planted transcutaneous electrical nerve stimulation (TENS) devices. The patient sits in room that contains radio frequency source works on a low frequency, who's the wearable biomedical devices receive, rectifies, and store the output energy for long life use.

1.7.2 Radio frequency identification (RFID)

Radio frequency identification (RFID) systems have been used in many fields successfully as example of this services are manufacturing, agriculture, transportation, supply chain, and medical care etc.

Objects in RFID system can be identified by using tags, or labels attached to it. Two-way radio transceivers called readers which send RF signal to the tags or labels and read its response.

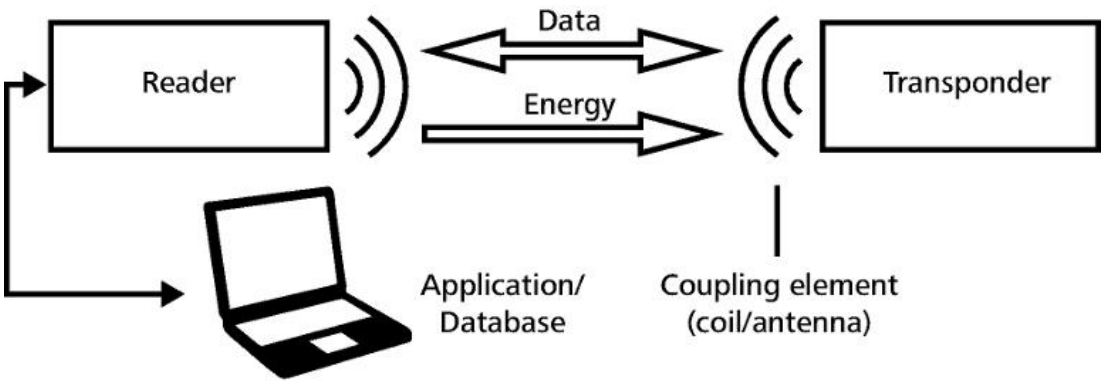

Figure 1.9: RFID System structure.

There are many types of RFID tags, it can be passive, active tags or A battery-assisted passive (BAP). The active tags have a battery and periodically transmits RF signal contain its ID. A battery-assisted passive (BAP) has a small battery on board, and it can be activated when in the existence of an RFID reader in the place. Passive tags are smaller and cheaper because it does not contain any battery on-board; Instead of, the tags use the RF energy transmitted by the reader to operate as shown in Figure 1.9. However, to operate a passive tag, it must be work with stronger than power level nearly a thousand times for transmit the signal. That makes a difference in exposure and in interference to radiation.(Raina, 2017)

The RFID technology can transmit information to goods without direct contact and line of sight contact. Passive RFID tag can be used for applications such as: Hotels, transportation, Resource and asset management, stealing preventing and traceability, security, essential maintenance, vehicle identification attendance and time recording,

leak detection, baggage tagging and automation processes. Different types of Tags shown in Figure 1.10.

Figure 1.10: Used RFID tags.

1.7.3 A wireless sensor network (WSN)

A wireless sensor network (WSN) is a device that has a microprocessor which is capable of monitoring and wireless communication. It contains fixed and temporary memory, it needs to energy source to operate it.

In last years, many projects and researches have been presented in the area of wireless sensor network (WSN) because of its importance. A wireless sensor network (WSN) is consist of autonomous sensors of spatially distributed that can be used to monitor environmental or physical conditions, such as movements, Vibrations, temperature, sound, pressure, etc., and to mutual transmit their data through the wireless network to a main location. There are various types of network sensors, the modern network sensors are bidirectional, for sensors control. The main motivated development, of wireless sensor networks is for military applications such as battlefield surveillance; this networks are used in many consumer and industrial fields,

such as control of industrial process and monitoring, machine validity monitoring, and many other applications. (Prittopaul & Shankarram)

1.8 Literature Review

Several studies about energy harvesting systems and their applications have been studied and presented in literature:

In (Keyrouz et al., 2013), a multi-band simultaneous RF energy harvesting system was designed and simulated, at 800MHz, 900MHz and 2.45 GHz as shown in Figure 1.11. A voltage multiplier is uses to rectify the captured radio frequencies and to decrease the rectifier impedance in order to match it to a 50 antenna. The combined system can achieve 15% more efficiency when compared to single-frequency RF harvester. It Good simulated results were presented but no practical results were introduced for rectifier.

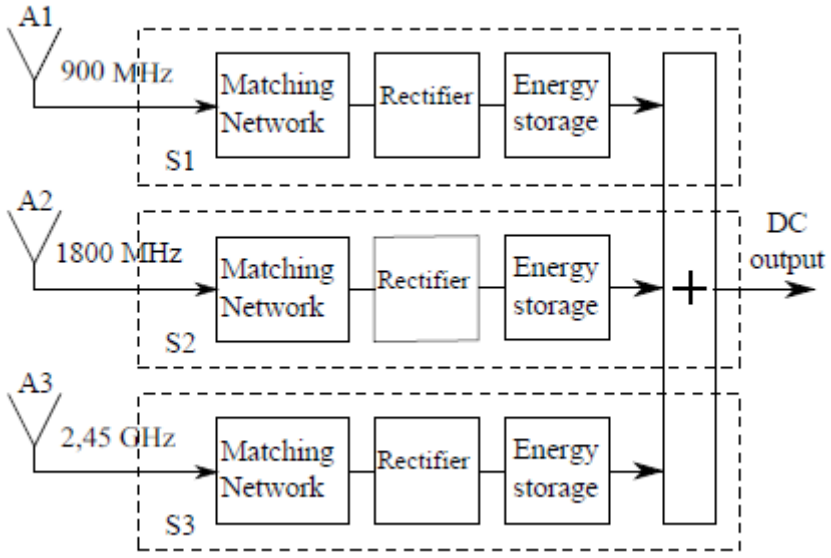

Figure 1.11: Multi-band simultaneous RF energy harvesting system.

In (Kitazawa, Ban, & Kobayashi, 2012), Energy Harvesting from Ambient RF Sources was presented. This paper shows a feasibility study of energy harvesting from surrounding radio frequency (RF) sources. The results showed that the median value of received power obtained was -25dBm from 800 MHz band mobile telephone base station (BS) was averagely 13dB stronger than that from Digital TV broadcasting. A

multi-stage rectifier was employed for the RF-DC conversion circuit to get a higher DC output. Here in this thesis we propose Dual band rectifier at GSM, TV frequencies which is more efficient.

In (Sun, Guo, He, & Zhong, 2013), A dual-band rectenna using broadband Yagi antenna array for ambient RF power harvesting was presented. A new rectenna with broadband quasi-Yagi array antenna and a dual-band rectifier as shown in Figure 1.12 has been designed to harvest the ambient RF power of GSM-1800 and UMTS-2100 bands. The measured output DC voltage was between 300 to 400 mV when measured in the ambience. But using of Yagi Antenna Array makes device very large and needs to be used in radiation direction only. Multi sage rectifier can be used to satisfy required voltage for other applications.

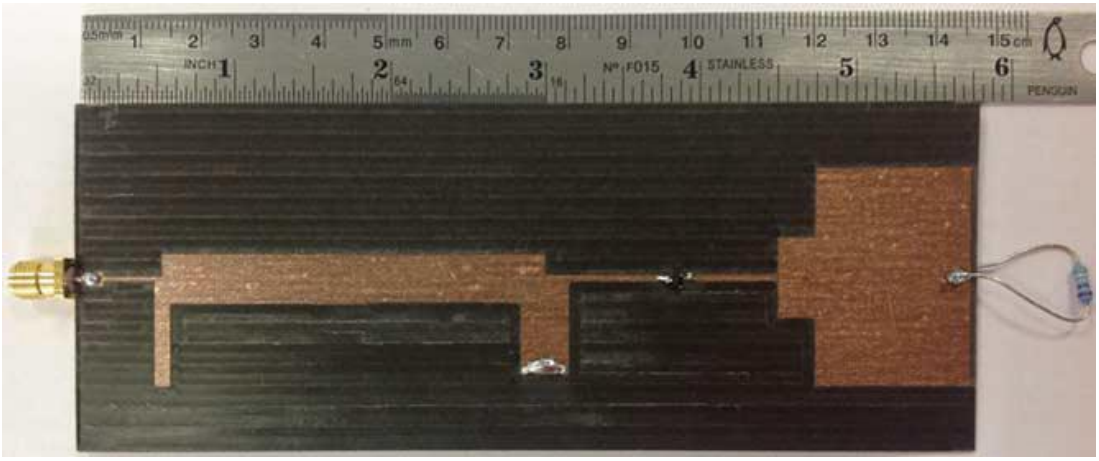

Figure 1.12: Dual-band rectifier.

In (Zakaria, Zainuddin, Aziz, Husain, & Mutalib, 2013), a planar dual-band monopole antenna has been presented. It operates at 915MHz and 1800MHz for GSM band application. Simulation of the design and implementation is done and the measured results is better than the simulation value. The monopole antenna achieves good return loss at frequencies of 915 MHz and 1800 MHz with bandwidth value of 124.2 MHz and 196.9 MHz with gain 1.97 dB and 3 dB, respectively.

In (D. Wang & Negra, 2014), novel tri-band RF rectifier design as shown in Figure 1.13 for wireless energy harvesting on frequencies of 1050, 2050 and 2600 MHz to achieve a 10 mW and it has the ability to harvest RF energy from the corresponding

operating frequencies sources. Rectifier is designed and fabricated on a Rogers RO4003CTM substrate. Here in this thesis we propose to use several stages of rectifier which leads to higher output voltage.

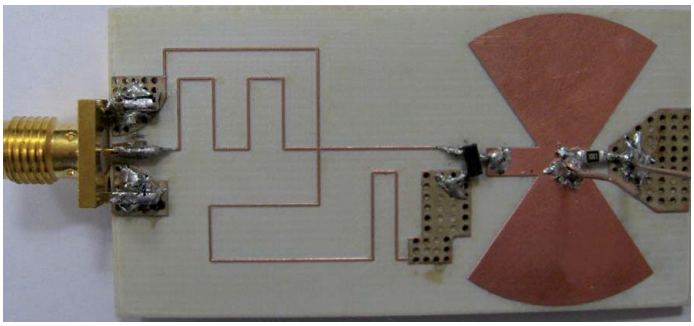

Figure 1.13: Prototype of the triband rectifier.

In (Khansalee, Zhao, Leelarasmee, & Nuanyai, 2014), a dual-band rectifier was proposed to support the RF energy harvesting at 2.1 GHz and 2.45 GHz that are UMTS-2100 and WiFi operating frequencies, respectively. In order to harvest at both frequencies, the input matching of the rectifier was designed to provide the high conversion efficiency at both frequencies; also, a high sensitivity Schottky diode was selected to be a small signal detector for the rectifier circuit. The simulation and experimental results are compared and discussed.

In (Borges et al., 2014), RF energy harvesting circuits specifically developed for GSM bands (900/1800) and a wearable dual-band antenna suitable for possible implementation. Besides, a wearable dual-band printed antenna with gains of the order of 1.8-2.06 dBi and 77.6-82% efficiency capable of harvesting electromagnetic energy from the GSM (900/1800) frequency bands. The authors also simulated the behavior of a 5-stage Dickson voltage multiplier for power supplying an IRIS node. Three prototypes for the 5-stage Dickson voltage multiplier with match impedance were proposed and experimentally characterized. Results show that all three prototypes can power supply the IRIS sensor node for RF received powers of -4 dBm, -6 dBm and -5 dBm, and conversion efficiencies of 20, 32 and 26%, respectively. Very good results but using lossy material as stub matching and FR4 lead to low efficiency look at Figure 1.14.

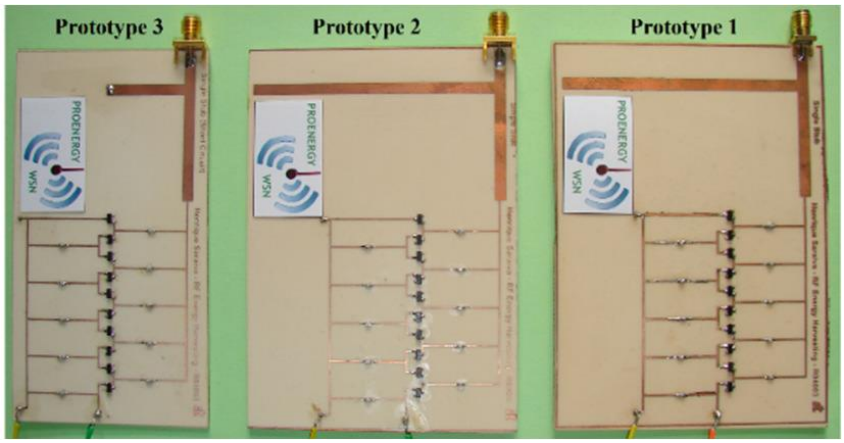

Figure 1.14: Prototypes of the five stages Dickson voltage multiplier with impedance matching.

In (Hoang, Phan, Van Hoang, & Vuong, 2014), two efficient compact dual-band antennas for RF energy harvesters were proposed. the first is a Printed-IFA for GSM bands with 1.3 dBi gain at 900 MHz band and 3.2 dBi gain at 1800 MHz band; and the second antenna is a quasi-Yagi for WiFi bands with 5.7 dBi gain at 2.45 GHz band and 5.9 dBi gain at 5.3 GHz band as shown in Figure 1.15. The proposed antenna's size is λ./6 × λ./5.5 and it achieves 1.3 dBi and 3.2 dBi at 900 MHz and 1800 MHz bands, respectively.

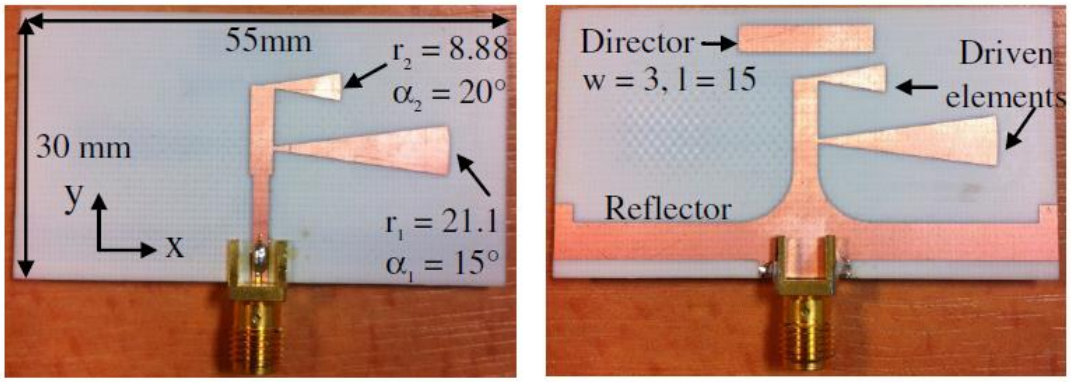

Figure 1.15: Geometry of the quasi-Yagi Wi-Fi antenna (dimensions in millimeters).

In (Belo & Carvalho, 2014), behavior of multi-band RF-DC converters in presence of modulated signals for space based wireless sensors is presented at frequencies 810MHz and 1580MHz. The RF-DC converter is optimized to operate in two bands. It is shown that the behavior of the two-bands combined can be of interest for the

harvesting of extra power. Multi band converters are proposed in this thesis with several stages.

In (Kuhn, Lahuec, Seguin, & Person, 2015), A rectenna with four-RF band has been designed for RF energy harvesting using in the status of the wireless sensor network. the architecture has been designed to cover GSM (900-1800), UMTS, and WiFi bands as shown in Figure 1.16. The fabricated prototype shows an 84% of RF-to-dc conversion efficiency at 0-dBm input power set on each of the four RF branches. The efficiency is more than doubled in the entity of all of the RF sources compared to a single band rectenna. Here in this thesis we propose to use several stages of rectifier which lead to higher output voltage which will be suitable for applications required.

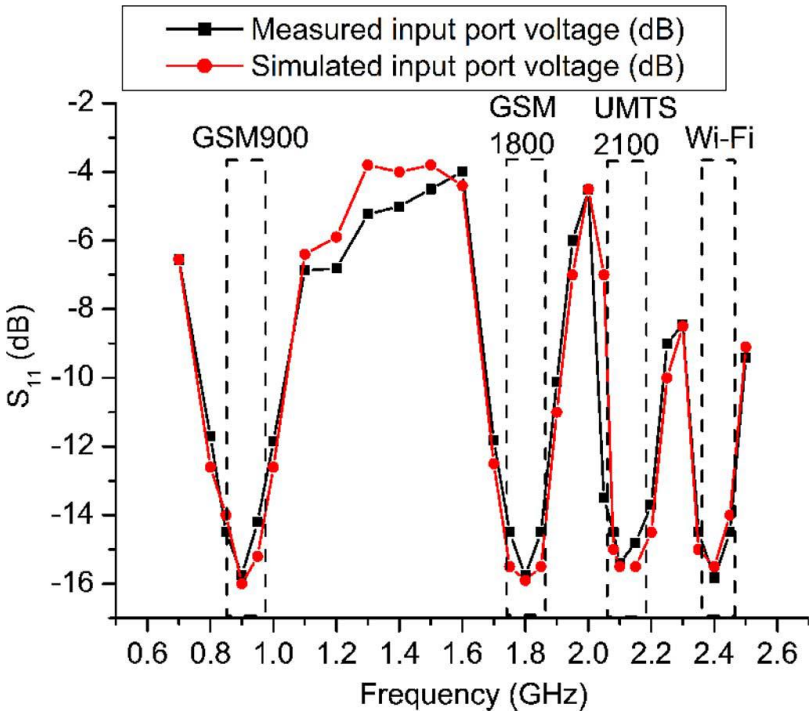

Figure 1.16: Simulated and measured S11 of the RF harvester at -15 dBm.

1.9 Overview of Thesis

This thesis is composed of six chapters, each dealing with different aspect of energy harvesting structure parts:

Chapter 1 is introductory and defines and describes energy harvesting systems, frequency bands, literature review, and application of the system.

Chapter 2 provides and introduces a background on the antenna basics, Maxwell's equations and radiation pattern of the antenna. Antenna parameters such as directivity, gain and polarization and microstrip antenna design equations are also discussed.

Chapter 3 is subdivided into three parts and provides an outline of relevant impedance matching techniques. Part 1 illustrates lumped element matching, Part 2 illustrates stub matching, and Part 3 illustrates matching with taper.

Chapter 4 concentrates on design of efficient Ultra-wideband star antenna, and describes antenna parameters, the measured results of design are compared with the simulation.

Chapter 5 presents single and multi-band voltage doubler rectifier design and exhibits the simulation results of the efficiency and output voltage of the proposed circuits.

Finally, the conclusion of the research and the suggestions for future work are presented in **chapter 6**.

Chapter 2

Antenna Theory

Chapter 2

Antenna Theory

2.1 Introduction:

An antenna can be defined as a specialized transducer that converts electromagnetic fields into alternating current (AC) or vice-versa. (Song, Chin, Liang, & Anyi, 2006). There are two types: the transmitting antenna, which transduces AC power into EM field to be transmitted and receiving antenna, which transduces EM energy into AC power to electronic circuit.

Each antenna is designed to operate in a certain frequency band and reject signals from the other operating band.

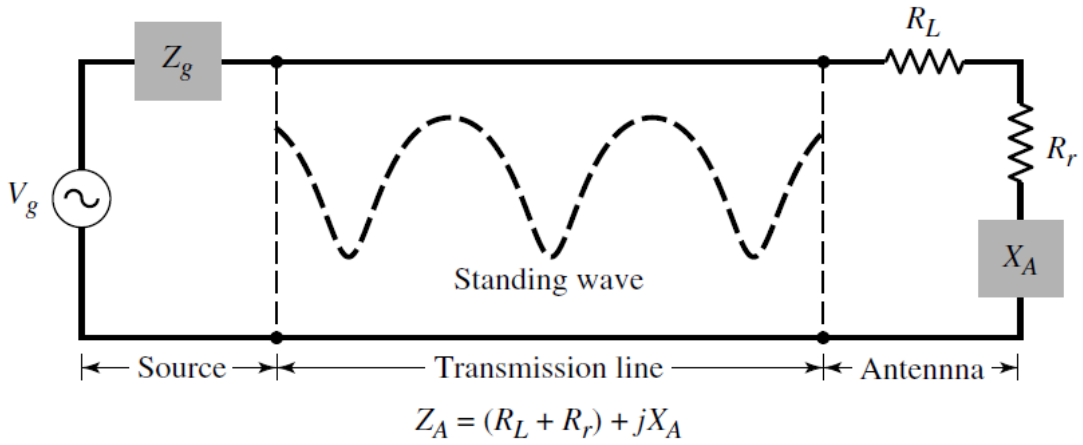

Figure (2.1): Transmission line Thevenin equivalent of antenna in transmitting mode. (Balanis, 2005)

Since the antenna is transceiver device, it can be used as a transmitter or as a receiver. An antenna can be modeled in the equivalent of the antenna system in the transmitting mode as Thevenin equivalent shown in Figure 2.1 where the source is represented with ideal generator, the transmission line can be represented by a line with characteristic impedance Z_c, and the antenna is represented by a load Z_A $[Z_A = (R_L + R_r) + jX_A]$ connected to the transmission line. The resistance of load R_L is used to represent the dielectric and conduction losses set side by side with the antenna structure while R_r , referred to the radiation resistance, is used to represent radiation

by the antenna. The reactance X_A is the imaginary part of the impedance as represent associated with radiation done by the antenna (Balanis, 2005).

The official IEEE definition of an antenna as given by Stutzman and Thiele follows the concept: "That part of a transmitting or receiving system that is designed to radiate or receive electromagnetic waves "as shown in Figure 2.2 (Balanis, 2005).

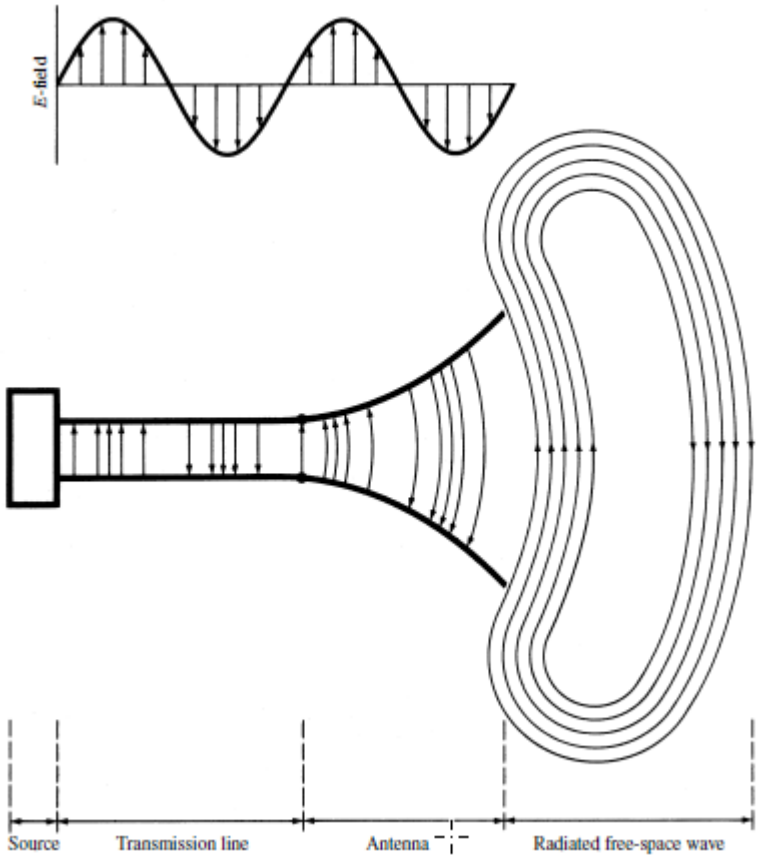

Figure (2.2): Antenna as a transference device.(Balanis, 2005)

2.2 Maxwell's equations

Maxwell's equations are set of four complicated equations that describe the magnetic and electric fields arising from distributions of electric charges and currents, and how those fields varying in time. Maxwell's equations as shown in (table 2.1) are a set of partial differential and integral equations that, simultaneously with force law of the Lorentz, form the foundation of quantum field theory, classical electromagnetism, classical optics, and electric circuits. They Formed the foundation of all magnetic, electric, optical and radio technologies, including power generation,

electrical generators, linear alternators, TV, wireless communication, computers etc. The four equations describe how magnetic and electric fields are produced by currents, charges, and changes of each other. One of the important results of the equations is that they explain how fluctuating electric and magnetic fields propagate at the speed of light. This is known as electromagnetic radiation waves, that waves may arise at various wavelengths to produce a spectrum from radio frequency waves to γ-rays. Referred to the mathematician and physicist James Clerk Maxwell, the equations were named. Maxwell published an early form of the equations between 1861 and 1862, he was the first who proposed that light is an electromagnetic phenomenon (Thidé, 2004).

Table 2.1 : General Forms of Maxwell's Equations (Sadiku, 2014)

Name	Integral equations	Differential equations
Gauss's law	$\nabla . \boldsymbol{D} = \boldsymbol{\rho_v}$	$\oint_{\boldsymbol{S}} \boldsymbol{D}.d\boldsymbol{S} = \oint_{\boldsymbol{v}} \boldsymbol{\rho_v}.d\boldsymbol{v}$
Gauss's law for magnetism	$\nabla . \boldsymbol{B} = 0$	$\oint_{\boldsymbol{S}} \boldsymbol{B}.d\boldsymbol{S} = \mathbf{0}$
Maxwell–Faraday equation	$\nabla \mathbf{x}\, \mathbf{E} = -\frac{\partial \boldsymbol{B}}{\partial t}$	$\oint_{\boldsymbol{L}} \boldsymbol{E}.d\boldsymbol{l} = -\frac{\partial}{\partial t}\int \boldsymbol{B}.d\boldsymbol{S}$
Ampere's circuital law	$\nabla \mathbf{x}\, \mathbf{H} = \mathbf{J} - \frac{\partial \boldsymbol{D}}{\partial t}$	$\oint_{\boldsymbol{L}} \boldsymbol{H}.d\boldsymbol{l} = \int_{s} (\mathbf{J} + \frac{\partial \boldsymbol{D}}{\partial t}).dS$

Maxwell's equations that describe the interrelationship between Electric Field Intensity **E** $(V\ /m)$, magnetic fields Intensity **H** (A/m) , electric charge $\boldsymbol{\rho}$ (charge density,) $(coulomb/m^3)$, and current density **J** $(ampere/m^2)$.

The quantities **D** is electric flux density $(coulomb/m^2)$ and **B** is magnetic flux density $(weber/m^2)$, or $(Tesla)$.

2.3 Fundamental Parameters of Antenna

The performance of an antenna can be described using Antenna parameters when measuring and designing antennas. We can classify antenna parameters into two kinds,

first antenna parameters from the field point of view which include the radiation pattern, beamwidth, directivity, gain, polarization and the bandwidth. The second antenna parameters are based on circuit point of view which include input impedance, radiation resistance, reflection coefficient, return loss, VSWR and bandwidth (Huang & Boyle, 2008).

2.3.1 Radiation Pattern

A radiation pattern of antenna is known as a graphical representation or mathematical function of the radiation properties of the antenna as a function of space coordinates. The radiation pattern is determined mostly in the far field region and explained as a function of the directional coordinates. Radiation properties involve radiation intensity, power flux density, directivity, field strength, polarization.

The most important radiation property is the 2D or 3D spatial distribution of radiated energy as a function of the surface of constant radius or observer's position along a path. An appropriate set of coordinates is shown in Figure 2.3 (Pozar, 2012).

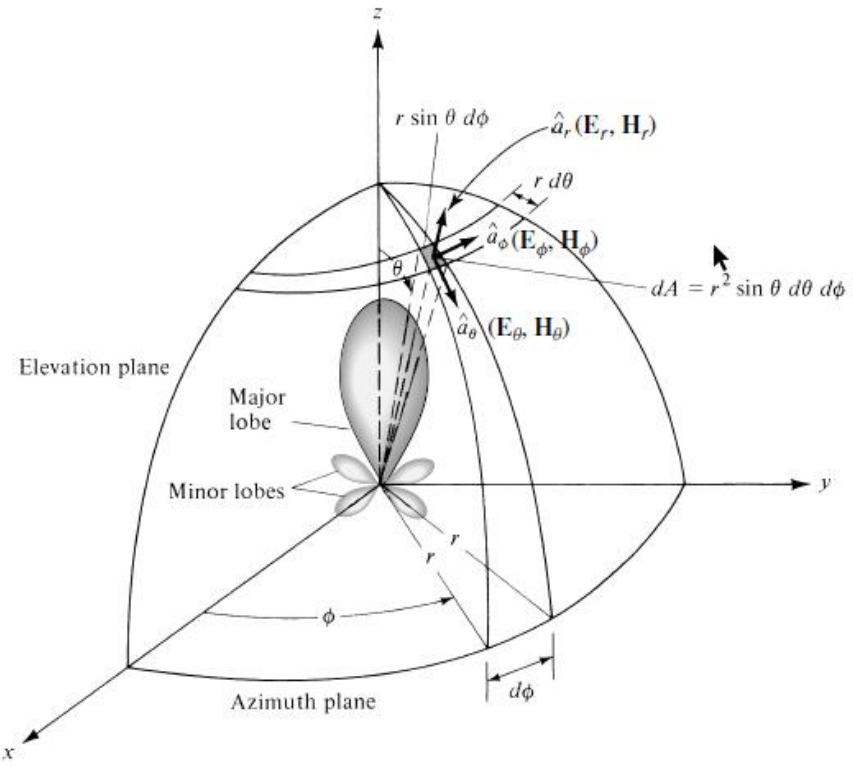

Figure 2.3: coordinate system for antenna analysis (Pozar, 2012).

The amplitude field pattern is trace of the received electric (magnetic) field at a constant radius. Also, amplitude power pattern is a graph of the spatial variation of the power density along a constant radius. Power and field patterns are normalized with respect to their maximum value constantly. The power pattern is usually plotted in decibels (dB) or less commonly on a logarithmic scale. (Pozar, 2012)

2.3.2 Radiation Pattern Lobes

The radiation pattern parts are called lobes, which can be classified into major or minor, main, side, and back lobes.

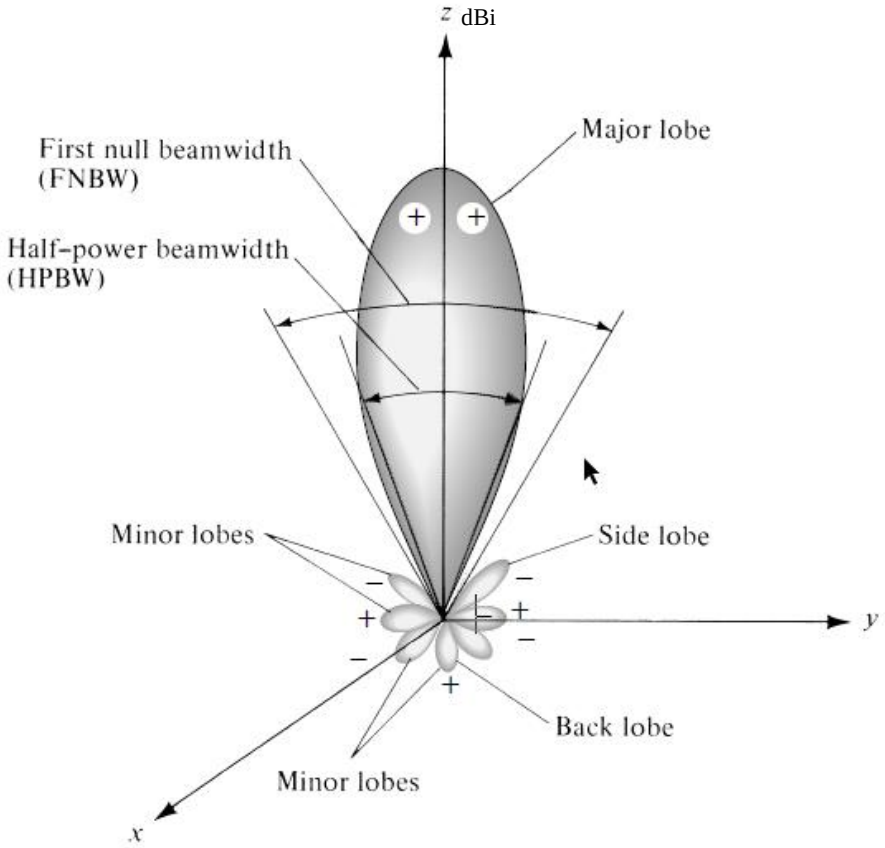

Figure 2.4 : Radiation lobes and beamwidth of an antenna electric field pattern (Pozar, 2012).

Radiation lobes are defined as 'portion of the radiation pattern bounded by regions of relatively weak radiation intensity.' (Balanis, 2005) Figure 2.4 explains a symmetrical 3D polar pattern include a number of radiation lobes with various radiation intensity which may be greater or less than others, but all are known as lobes. As we can see in Figure 2.5, that clarify radiation pattern lobes and beamwidth.

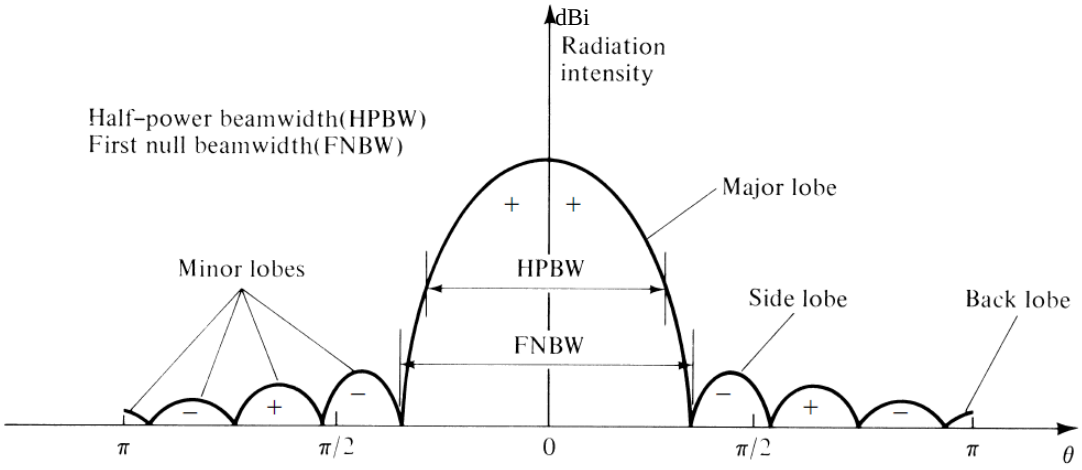

Figure 2.5 : 2D radiation pattern lobes and beamwidth(Pozar, 2012)

2.3.3 Isotropic radiation

It can be described as the radiation from a source, radiating in all directions with same intensity despite the direction of measurement and it can be used to improve the radiation pattern of an antenna. If the radiation is equal in all directions, then it is known as an isotropic radiation.

2.3.4 Beamwidth

The very important antenna parameter is beamwidth of an antenna which is often used as a trade-off between it and the side lobes level. Beamwidth is also used to clarify the resolution capabilities of the antenna to differentiate between two adjacent radiating sources or the radar target (Kumar, Patel, Mittal, & De, 2012).

There are many types of beamwidths in an antenna radiation pattern. The Half-Power Beamwidth (HPBW) is the most important one, which is defined by IEEE as: 'In a plane containing the direction of the maximum of a beam, the angle between the two directions in which the radiation intensity is one-half value of the beam'. The First Null Beamwidth (FNBW) is defined as the angular separation between the first nulls of the pattern. Both of the HPBW and FNBW are shown in Figure (2.4) and in Figure(2.5) that describe 2D radiation pattern lobes and beamwidth (Balanis, 2005).

2.3.5 Directivity of antenna

Directivity of antenna known as 'ratio of the radiation intensity in a given direction from the antenna to the radiation intensity averaged over all directions' as in IEEE Standard for Definitions of Terms for Antennas.

The average radiation intensity is equal to the total radiated power by the antenna divided by 4π. The direction of the radiation intensity if not specified then it is the direction of maximum radiation. Or we can say, the directivity of a non-isotropic source is equal to the ratio of its radiation intensity in a given direction over that of an isotropic source. In mathematical equation form, it can be as:

$$D = \frac{U}{U_0} = \frac{4\pi U}{P_{rad}} \quad \textbf{(2.1)}$$

$$D_{max} = D_0 = \frac{U_{max}}{U_0} = \frac{4\pi U_{max}}{P_{rad}} \quad \textbf{(2.2)}$$

where:

D = directivity (dimensionless)

D_0 =D_{max} =maximum directivity (dimensionless)

U = radiation intensity (W/unit solid angle) can be obtained by multiplying the radiation density (W_{rad}) by the square of the distance (r^2). where $U = r^2 W_{rad}$.

U_{max}= maximum radiation intensity (W/unit solid angle)

U_0= radiation intensity of isotropic source (W/unit solid angle)

P_{rad}= total radiated power (W)

2.3.6 Antenna Efficiency

A number of efficiencies are Associated with an antenna and the equivalent can be defined by using Figure 2.6. The total antenna efficiency (e_0) is used considering the losses at the input terminals and the antenna structure. This losses may be due, referred in Figure 2.7,(Balanis, 2005) to reflections that happened because of mismatch between the antenna and the transmission line, and losses of (dielectric and conduction) which can be calculated by equation: (I^2R).

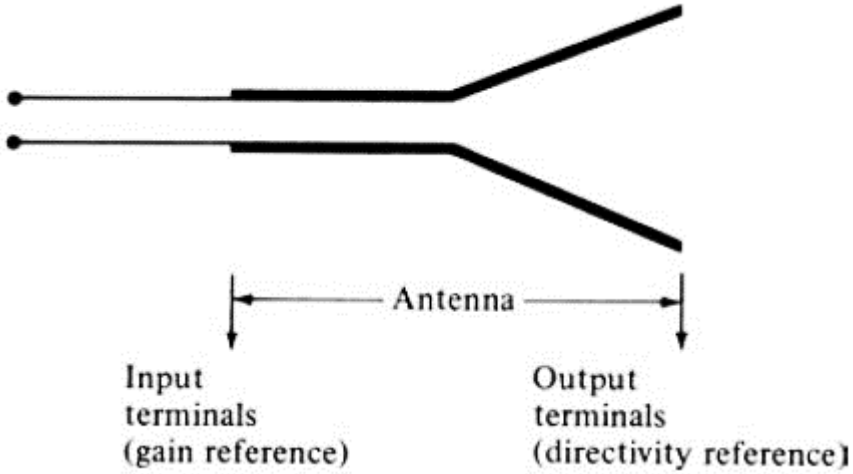

Figure 2.6 : Antenna reference terminals

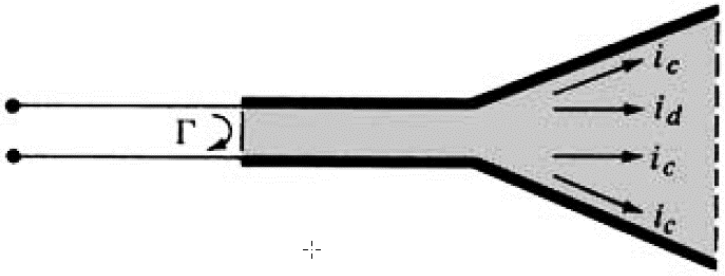

Figure 2.7: losses of an antenna.

The overall efficiency can be expressed as:

$$e_0 = e_r e_c e_d \qquad \textbf{(2.3)}$$

where

e_0 = total efficiency (dimensionless)

e_r = reflection (mismatch) efficiency = $(1-|\Gamma|^2)$dimensionless)

e_c = conduction efficiency (dimensionless)

e_d = dielectric efficiency (dimensionless)

Γ = voltage reflection coefficient at the input terminals of the antenna

$$\Gamma = \frac{Z_{in} - Z_0}{Z_{in} + Z_0} \qquad \textbf{(2.4)}$$

where

Z_{in} = antenna input impedance.

Z_0 = characteristic impedance of the transmission line.

VSWR = voltage standing wave ratio = $\frac{1+|\Gamma|}{1-|\Gamma|}$

Usually e_c and e_d can be computed experimentally because of its difficulty to compute. Even by measurements they cannot be separated, and it is usually more appropriate to write equation (2.3) as in equation (2.5):

$$e_0 = e_r e_{cd} = e_{cd}\,(1-|\Gamma|^2) \qquad \textbf{(2.5)}$$

where $e_{cd} = e_c e_d$ = antenna radiation efficiency, that used to make related between the gain and directivity (Balanis, 2005).

2.3.7 Antenna Gain

Gain is one of the most common measurements stated on antenna specification sheets. Although the gain of the antenna is closely related to the directivity, it is a measure that takes into account the efficiency of the antenna as well as its directional capabilities. Remember that directivity is a measure that describes only the directional properties of the antenna, and it is therefore controlled only by the pattern.

Antenna Gain is defined as "the ratio of the intensity, in a given direction, to the radiation intensity that would be obtained if the power accepted by the antenna were radiated isotopically". (Balanis, 2005). In equation form, this can be shown at equation 2.6:

$$Gain = 4\pi \frac{radiation intensity}{total\ input\ (accepted)\ power} = 4\pi \frac{U(\theta,\phi)}{Pin} \qquad \textbf{(2.6)}$$

The antenna gain can be expressed as the ohmic losses (e_{cd})in the antenna multiplied by the antenna directivity $D\ (\theta, \phi)$ at equation 2.7.

$$G\ (\theta,\phi) = e_{\ cd}\ D\ (\theta,\phi) \qquad \textbf{(2.7)}$$

2.3.8 The Return Loss

The return loss (RL) defined by 'the ratio of the incident power of the antenna P_{inc} to the power reflected back from the antenna of the source P_{ref}'. Return loss tells

us how much of the input signal is reflected. It also can be explained as the difference between the power of a transmitted signal and the power of the signal reflections caused by variations in link and channel impedance.(Huang & Boyle, 2008)

Return loss is the negative of the reflection coefficient expressed in decibels. In terms of the voltage standing wave ratio (VSWR). Return loss can be expressed as: (Huang & Boyle, 2008; Pozar, 2012)

$$RL = 10\log_{10}\frac{Pin}{Pref} = 20\log_{10}\left|\frac{VSWR+1}{VSWR-1}\right| = -20\log_{10}|\Gamma|(dB) \qquad (2.8)$$

2.3.9 Bandwidth

Antenna bandwidth IEEE defined as "the range of frequencies within which the performance of the antenna, with respect to some characteristic, conforms to a specified standard." (Balanis, 2005)

The bandwidth can be considered as the range of frequencies, the bandwidth is the range of frequencies on either side of a center frequency, where acceptable value of the antenna characteristics at the center frequency (such as input beamwidth, pattern, impedance, polarization, gain, side lobe level, radiation efficiency, beam direction). The bandwidth is usually taken at -10 dB in reflection coefficient S11 response as shown in Figure 2.9.

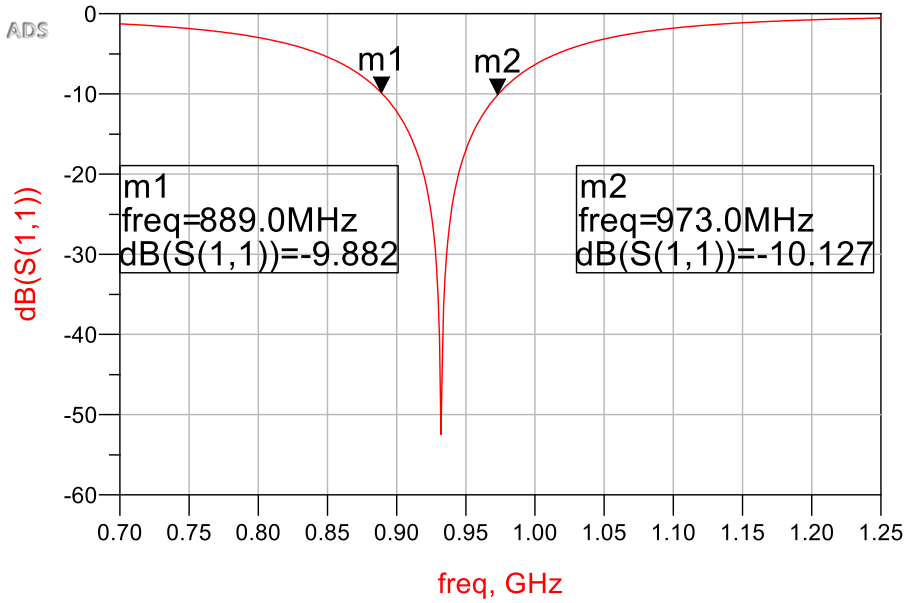

Figure 2.8: The Bandwidth at -10 dB in S11 plot.

2.3.10 Polarization

Polarization of a radiated wave is defined as "that property of an electromagnetic wave describing the time-varying direction and relative magnitude of the electric-field vector"(Balanis, 2005).

Two special cases of elliptical polarization are: linear polarization and circular polarization as shown in Figure 2.8. The initial polarization of a radio wave is determined by the antenna.

Linear polarization: if the vector that describes the electric field at a point in space as a function of time is always directed along a line.

Elliptical polarization: if the electric field traces is an ellipse.

Circular polarization: if the electric field vector remains constant in length but rotates around.

This rotation may be right hand or left hand. Choice of polarization is one of the design choices available to the RF system designer.

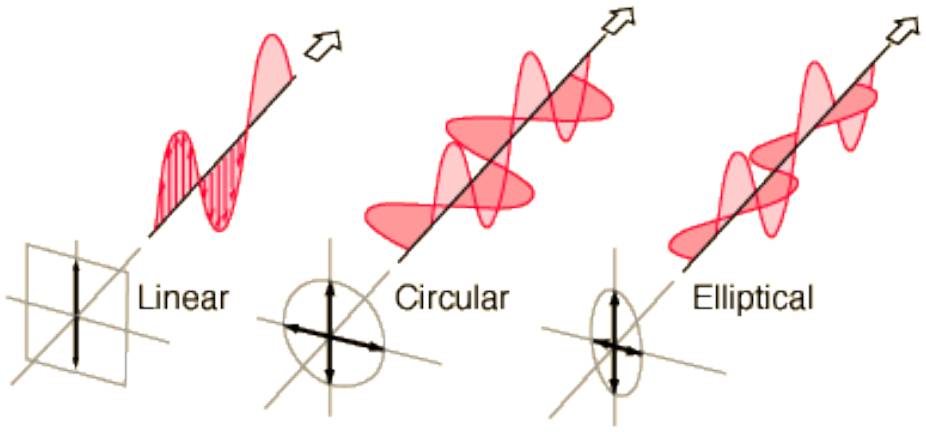

.

Figure 2.9: Three types of antenna polarization as linear, circular, and elliptical

2.4 Antenna types:

Antenna is a transducer device which is designed to transmit or receive the electromagnetic waves. Antenna types can be divided into many types depending on many factors like apertures, frequency, polarization or radiation.

Antenna or aerial refers to an electronic device used for transmission of radio or other electromagnetic waves. It converts electricity into electromagnetic waves.

Some basic types of antenna are (Dipoles and Monopoles- Loop Antenna- Microstrip Antenna - Helical Antenna - Horn Antenna) (Balanis, 2005), in the next section we will discuss Microstrip Antenna type because we use it in this thesis.

2.5 Microstrip Patch Antenna

Microstrip patch antennas have been widely used and research studies, as a widely use in wireless applications, due to their advantages and attractive characteristic. They are lighter in weight, low volume, low cost, low profile, smaller in dimension and ease of fabrication and conformity with integrated circuits.

Also, the microstrip antenna or array suffers from a number of disadvantages such as narrow bandwidth of the antenna, high cross polarization, high feeding network losses, and low power handling capacity. With scientific progress in the field of

microstrip, many of the drawbacks have been solved and overcome, but some still need to be resolved. Using of microstrip antennas increased with the rapid deployment of wireless communication systems in particular personal communication systems, mobile satellite communications, wireless local area networks and intelligent vehicle highway systems, which calls for further work to be developed and find solutions to the existing drawbacks.

A microstrip patch antenna is very useful antenna type and it can be used in array design. At this chapter we will focus on the description of the principle of the microstrip patch antenna that shown in Figure 2.10. Therefore, the necessary basic steps to start design of a microstrip patch antenna have been developed at this chapter and the best feeding mechanisms of the antenna have been considered.

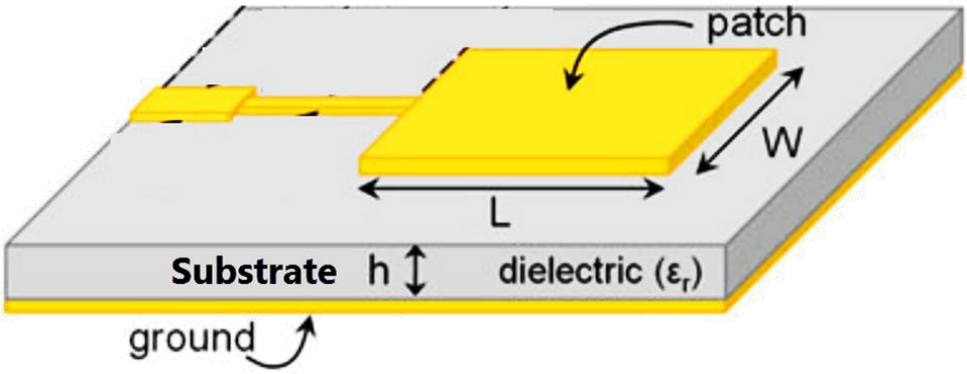

Figure 2.10: Microstrip patch antennas © emtalk.com

Through the results of the microstrip patch antenna we find that the intrinsic drawback is the limited bandwidth. So, at last few decades many efforts and several effective methods have been done to solve these drawbacks, such as using thick substrate with low dielectric constant.

2.5.1 Feeding techniques

Microstrip patch antennas have radiating elements on the upper side of its dielectric substrate. Feeding of this patch is achieved by a microstrip line or a coaxial probe through the ground plane which was used early. After that a number of new

feeding configurations have been improved, such as proximity-coupled microstrip feed and aperture coupled microstrip feed. The antenna feeding techniques that will be discussed on this section are as follows: (Saraswati & Agrawal, 2016)

2.5.1.1 Coaxial-line feeds

The internal main conductor of the coax connector is attached to the radiation side of the patch antenna while the other conductor connector is connected to the ground side as shown in Figure 2.11. The coaxial probe feed is easy to match and fabricate, and it has low losses radiation.

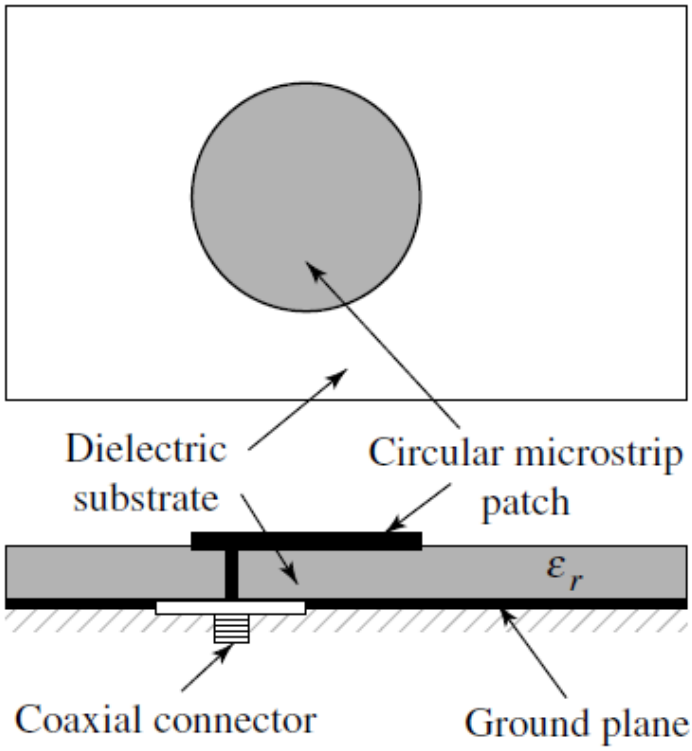

Figure 2.11: Microstrip Probe feed

2.5.1.2 Microstrip (coplanar) feeds:

The microstrip feed line width is usually much smaller compared to the patch. The microstrip-line feed is simple to match by controlling the inset position and rather simple to model. However, as the substrate thickness increases, surface waves and spurious feed radiation increase, which for practical designs limit the bandwidth (typically 2–5%). Microstrip (coplanar) feeds include more than one configuration

such as Inset Feed, Quarter-Wavelength Transmission Line and Coupled (Indirect) Feeds: (Balanis, 2005)

2.5.1.3 Aperture Coupling Feed

Aperture coupling is one of feeding techniques for microstrip patch antenna but it is difficult at fabrication and leads to narrow band width. The structure formed of two substrates separated by a ground plane. a transmission line feeds the bottom side of the substrate and the energy is coupled to the patch through a slot as shown in Figure 2.12.

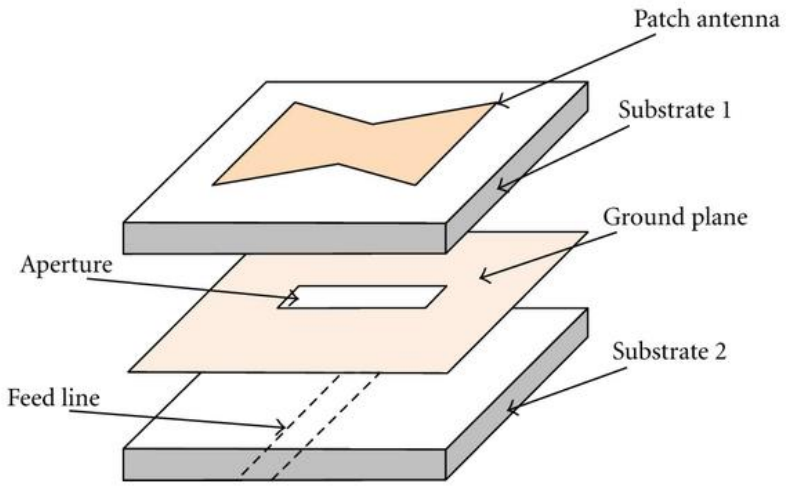

Figure 2.12: Configuration of bow-tie antenna fed by aperture coupled.(Didouh, Abri, & Bendimerad, 2012)

With noting that the top substrate has a low dielectric constant while the substrate on the bottom is a higher material with a no contacting feed. In this type, matching can be performed by controlling of the width of the transmission line or the length of the slot.

2.5.1.4 Inset Feed:

The input impedance of the patch antenna at the edge is high 150–300 ohms. If the feeder is connected at the antenna edge as shown in Figure 2.13 impedance mismatch will occur, so the feeder must be modified. Since the current is low at the ends of a half-wave patch and increases in magnitude toward the center the input

impedance (Z=V/I) could be reduced if the patch was fed closer to the center. One method of doing this is by using an inset feed (a distance D from the end) as shown Figure 2.13. The inset length can be calculated from (Huang & Boyle, Antennas from Theory to Practice, 2008)

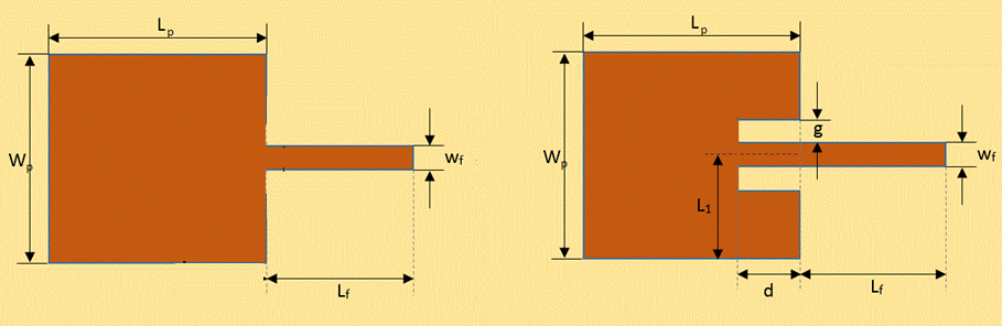

Figure 2.13 : unmatched microstrip antenna & Patch Antenna with an Inset Feed

2.5.1.5 Fed with a Quarter-Wavelength Transmission Line

A quarter-wavelength transmission line with characteristic impedance Z_1 can be used to match microstrip antenna to a transmission line of characteristic impedance Z_0 as shown in Figure 2.14:

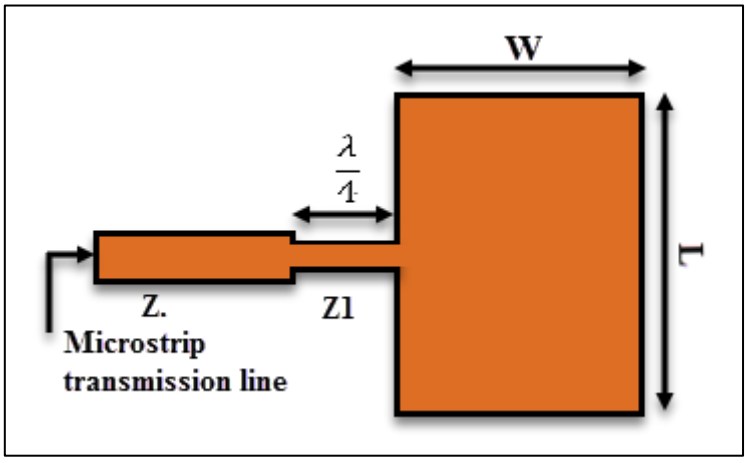

Figure 2.14: Patch antenna with a quarter-wavelength matching section

The target is to match antenna input impedance (Z_A) to the transmission line (Z_0), after transformation the impedance seen from the beginning of the quarter-wavelength line will be (Z_0) which equal to 50 Ω.

2.6 Designing Rectangular Microstrip Antenna

Microstrip antenna works as resonant style so, it must one of its dimensions must be $\lambda_g/2$, where λ_g is a guided wavelength taking into consideration the adjacent environment of the printed patch antenna. The patch conductor shape plays a role in which the resonant dimension depends on it. Also, the substrate properties like dielectric constant ε_r and substrate height play essential role in the patch antenna performance. The main advantage of a microstrip patch antenna is its size which is small compared to other types.

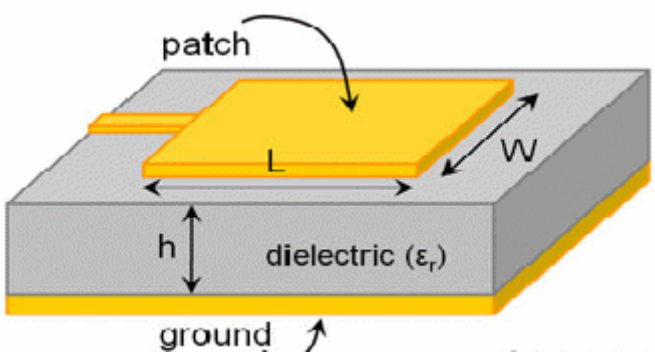

Figure 2.15: Microstrip antenna dimensions.

The first part of the design is to estimate the length (L) and width (W) of the antenna look at Figure 2.15. The length and width of the patch antenna can be calculated using equations as shown below.

$$W = \frac{c}{2f_r}\sqrt{\frac{2}{\epsilon_r + 1}} \qquad \textbf{(2.9)}$$

where c is the free-space velocity of light, ϵ_r is relative permittivity and f_r is resonance frequency.

2.6.1 Effective parameters:

Effective parameters are Effective Length, Resonant Frequency, and Effective Width Because of the fringing effects, electrically the patch of the microstrip antenna looks greater than its physical dimensions. In order to estimate the length of the patch, some parameters must be calculated before such:

$$\epsilon_{r_{eff}} = \frac{\epsilon_r + 1}{2} + \frac{\epsilon_r - 1}{2}\left[1 + 12\frac{h}{W}\right]^{-\frac{1}{2}} \quad \textbf{(2.10)}$$

The extension length ΔL (where it is represented to the increasing in L duo to fringing field) is calculates as:

$$\frac{\Delta L}{h} = 0.412\frac{\left(\epsilon_{r_{eff}} + 0.3\right)\left(\frac{W}{h} + .264\right)}{\left(\epsilon_{r_{eff}} - .258\right)\left(\frac{W}{h} + 0.8\right)} \quad \textbf{(2.11)}$$

By using the above-mentioned equation, we can find the value of actual length of the patch as:

$$L = \frac{c}{2f_r\sqrt{\epsilon_{r_{eff}}}} - 2\Delta L \quad \textbf{(2.12)}$$

The length and the width of the ground plane can be calculated:

$$Lg = 6h + L \quad \textbf{(2.13)}$$

$$Wg = 6h + W \quad \textbf{(2.14)}$$

2.7 Summary

This chapter start with Antenna theory. Generally, Maxwell's equations have been discussed, then antenna parameters are available and discussed in this chapter, firstly antenna parameters from the field point of view which include the radiation pattern, beamwidth, directivity, gain, polarization and the bandwidth. The second antenna parameters are based on circuit point of view which include input impedance, radiation resistance, reflection coefficient, return loss, VSWR and bandwidth.

Chapter 3

Impedance Matching Techniques

Chapter 3

Impedance Matching Techniques

3.1 Introduction

Impedance matching is one of the most important parts for a microwave component or systems. Impedance matching can be simply defined as the process of making one impedance look like another terminal impedance. Often, it is important to make matching between the load impedance and the source or internal impedance.

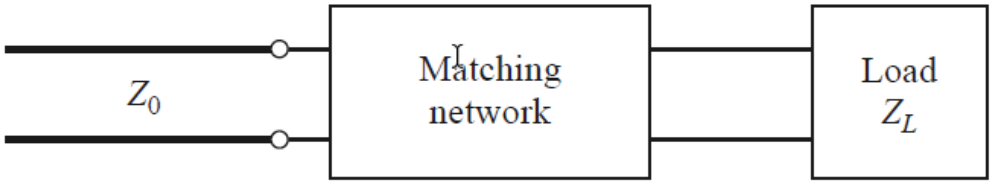

Figure 3.1: Impedance matching network.(Pozar, 2012)

Impedance matching network is placed between a load impedance and a transmission line as shown in Figure 3.1. Impedance matching happens when $Z_0 = Z_L$ which satisfies maximum delivered power at this point as at Figure 3.2. The matching network is ideally lossless, to achieve the maximum delivered power in the network. By using a matching circuit, reflections on transmission line will be eliminated to the left side of the matching network, taking into consideration there will be multi reflections between the load and the matching network. For impedance matching many types of parts and circuits can be used (L. E. Frenzel, 2004). In this chapter we will summarize the most common impedance matching techniques.

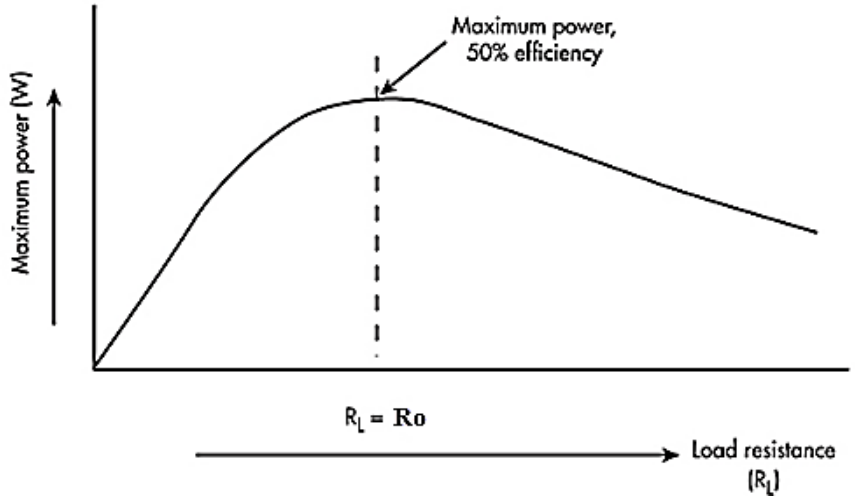

Figure 3.2: Relation between load resistance and delivered power (L. Frenzel, 2011)

3.2 Matching Techniques

3.2.1 Lumped element matching network

The L-section with Lumped elements is the simplest type of impedance matching techniques, which uses two Lumped elements to match any load impedance to a transmission line as shown in Figure 3.3, there are two ways are possible to make matching at this network, the first way when the normalized impedance is, $z_L = Z_L/Z_0$, is inside the $1 + jX$ circle on the Smith chart, then we must use the circuit of Figure 3.3a. and the second way when the load impedance in normalized form is outside the $1 + jX$ on the Smith chart, then we must use the circuit of Figure 3.3b. The resistance circle is $1 + jX$ circle on the Smith chart for which $\gamma = 1$. (where γ is the complex reflection coefficient) The reactive elements are either inductors or capacitors (Pozar, 2012).

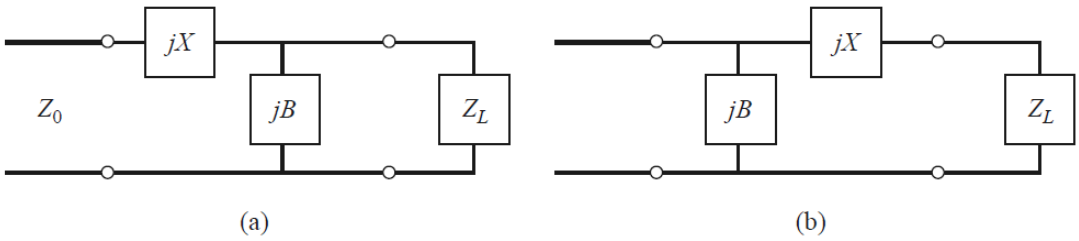

Figure 3.3: L-section matching networks (a) The normalized load impedance, $\boldsymbol{z_L = Z_L/Z_0}$, is inside the circle $\boldsymbol{1 + jX}$ (b) Load impedance in normalized form, $\boldsymbol{z_L = Z_L/Z_0}$, is outside the circle $\boldsymbol{1 + jX}$ (Pozar, 2012).

For the circuit in Figure 3.3 (a), the total impedance of L-section (matching circuit) plus Z_L should equal to Z_0, to satisfy matching, thus:

$$Z_0 = jX + \frac{1}{jB + 1/(R_L + jX_L)} \quad \textbf{(3.1)}$$

After rearranging equation (3.1) and separating into real and imaginary parts gives two equations with two unknowns, X and B:

$$B(XR_L - X_L Z_0) = R_L - Z_0 \quad \textbf{(3.2)}$$

$$X(1 - BX_L) = BZ_0 R_L - X_L \quad \textbf{(3.3)}$$

Solving Equation (3.2) for *X* and substituting into Equation (3.3) gives a quadratic equation for B. Equation (3.4) there are two possible solutions for B and X. we can realize these solutions physically if negative and positive values of X and B are possible (positive value of X means inductor and negative value of X means capacitor, while positive value of B means capacitor and negative value of B means inductor). The both solutions are shown at Equations below:

$$B = X_L \pm \frac{\sqrt{R_L/Z_0}\sqrt{R_L^2 + X_L^2 - Z_0 R_L}}{R_L^2 + X_L^2} \quad (3.4)$$

The series reactance can be found as in Equation (3.5) Since $R_L > Z_0$, then the second square root is always positive.

$$X = \frac{1}{B} + \frac{X_L Z_0}{R_L} - \frac{Z_0}{BR_L} \quad \textbf{(3.5)}$$

If Z_L is outside the circle of $1 + jX$ at Smith chart, then it means that $R_L < Z_0$ we can use circuit in Figure 3.3b, the admittance should equal $1/Z_0$ for an impedance matching condition, followed by the load impedance as shown in equation 3.6:

$$\frac{1}{Z_0} = jB + \frac{1}{R_L + j(X + X_L)} \quad \textbf{(3.6)}$$

After arranging equation 3.6 and make separation into imaginary and real it gives two equations with two unknowns, B and X:

$$BZ_0(X + X_L) = Z_0 - R_L \quad (3.7)$$

$$(X + X_L) = BZ_0R_L\,. \quad (3.8)$$

Solving equations for X and B gives:

$$X = \pm\sqrt{R_L(Z_0 - R_L)} - X_L\,, \quad (3.9)$$

$$B = \pm\frac{\sqrt{(Z_0 - R_L)/R_L}}{Z_0} \quad (3.10)$$

The square roots are usually positive due to value of $R_L < Z_0$. Note the two solutions are possible. To make matching of the load to the line with characteristic impedance Z_0, the imaginary part must be zero, while the real part of the input impedance to the matching network is equal to Z_0. This means that a general matching network must have at least two solutions; in the L-section matching circuit the both solutions can be provided by the two reactive components inductor or capacitor. (Pozar, 2012)

3.2.2 Matching with Quarter Wave Transformer

This is a simple matching techniques type; the quarter wave transformer is a transmission line with quarter wavelength length with characteristic impedance Z_1 that yields a matched system when it placed between a real load impedance $R_L$and a transmission line of characteristic impedance Z_0.

To find value of Z_1required for matching we use lossless Equation 3.11:

$$Z_{in} = Z_1 + \frac{R_L + jZ_1 \tan \beta l}{Z_1 + jR_L \tan \beta l} \quad (3.11)$$

But $\beta l = \left(\frac{2\pi}{\lambda}\right)\left(\frac{\lambda}{4}\right) = \frac{\pi}{2}$ then $\tan \beta l = \infty$ so $Z_{in} = \frac{Z_1^2}{R_L}$.

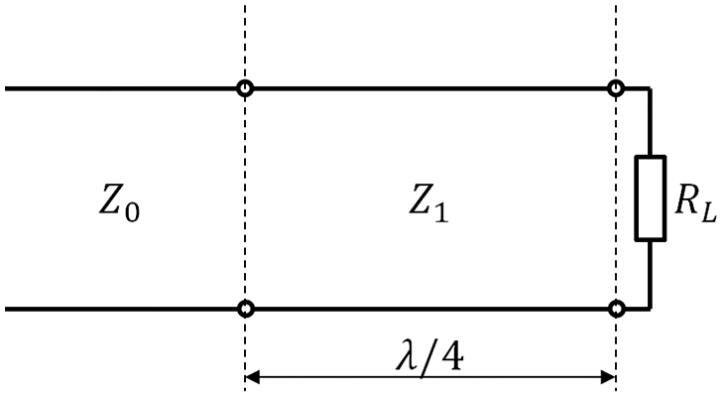

Figure 3.4 : Quarter-Wave Transformer Impedance Matching

For a matched system, $\boldsymbol{Z_{in}}$ must equal $\boldsymbol{Z_0}$, Hence**:**

$$\boldsymbol{Z_{in} = \frac{Z_1^2}{R_L} = Z_0 \Rightarrow Z_1 = \sqrt{Z_0 R_L}} \quad (3.12)$$

3.2.3 Single-Stub Tuning

At the complex load Stub matching is widely used to matches with a transmission line. The stub included of shorted or opened section of the line, which connected at appropriate point in the line from the load in parallel or in series. Shorted stubs are usually used in coaxial cable or two-wire line applications, because opened stubs may work as antenna from their opened ends. The most widely matching circuit are used is the single stub match which can match any load.

The value of reactance or susceptance resulted by the stub that represented by stub length and width, and the distance from the stub position to the load, d, in single stub tuning are the two adjustable parameters. The variance in lengths of a short or open-circuited stub is wavelength by (λ/4) which is for a given susceptance or reactance.

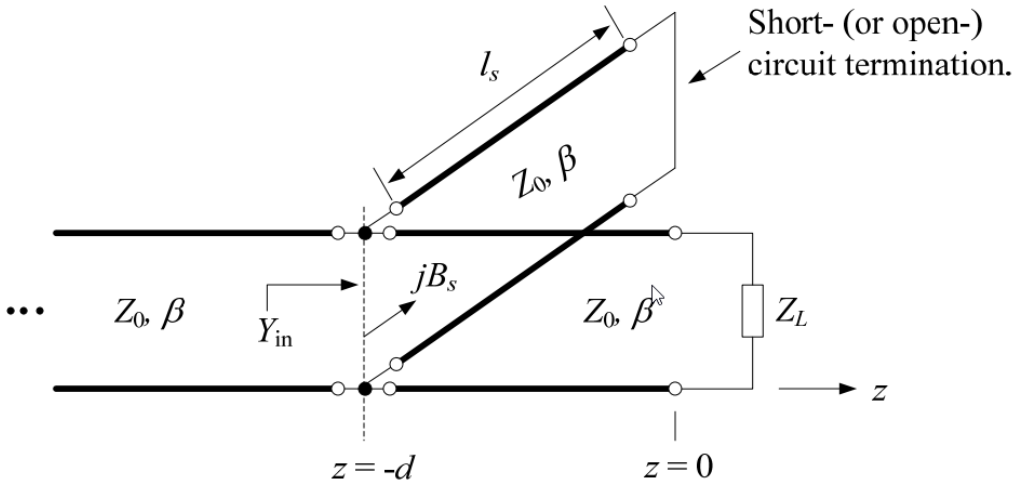

Figure 3.5: Single stub tuner (Pozar, 2012)

3.2.3.1 Shunt Stub matching

For the shunt-stub case the first step is to select d length that satisfy the admittance value, Y_0 seen looking into the line at distance d from the load is of the form $Y_0 + j\,B$. as shown in Figure 3.6, Then the stub susceptance is chosen as $-j\,B$, resulting in a matched condition.

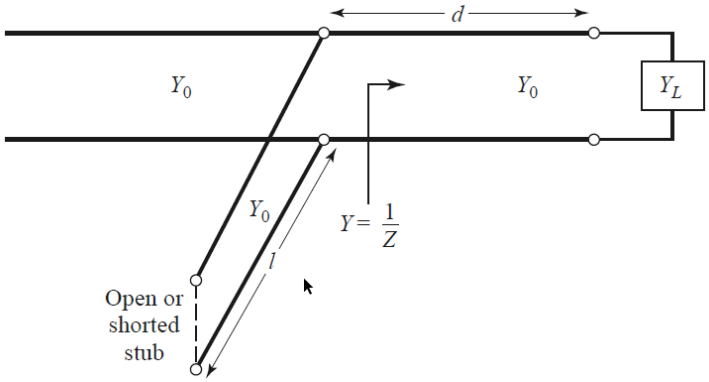

Figure 3.6: Shunt single-stub tuning circuits.(Pozar, 2012)

To obtain formulas for parameters d and l, the load impedance can be written as $Z_L = 1/Y_L = R_L + jX_L$. Then the impedance Z at down of length d at line from the load can be obtained as below:

$$Z = Z_0 \frac{(R_L + jX_L) + \mathrm{j}Z_0 \tan \beta d}{Z_0 + j(R_L + jX_L) \tan \beta d} \tag{3.13}$$

$$Y = G + jB = \frac{1}{Z} \tag{3.14}$$

$$G = \frac{R_L\,(1+(\tan\beta d)^2)}{R_L^2 + (X_L + Z_0 \tan\beta d)^2} \tag{3.15}$$

$$B = \frac{R_L^2 \tan\beta d - (Z_0 - X_L \tan\beta d)\,(X_L + Z_0 \tan\beta d)}{Z_0\left[\left[R_L^2 + (X_L + Z_0 \tan\beta d)^2\right]\right.} \tag{3.16}$$

If $R_L = Z_0$, then $\tan\beta d = -X_L/2Z_0$. So, the two solutions for d are:

$$\frac{d}{\lambda} = \begin{cases} \frac{1}{2\pi}\tan^{-1}\tan\beta d\,, & \tan\beta d \geq 0 \\ \frac{1}{2\pi}(\pi + \tan^{-1}\tan\beta d)\,, & \tan\beta d < 0 \end{cases} \tag{3.17}$$

To find the required stub lengths, find the stub susceptance, $Bs = -B$. Then, for an open-circuited stub,

$$\frac{l_0}{\lambda} = \frac{-1}{2\pi}\tan^{-1}\frac{B}{Y_0} \tag{3.18}$$

and for a short-circuited stub,

$$\frac{l_s}{\lambda} = \frac{1}{2\pi}\tan^{-1}\frac{Y_0}{B} \tag{3.19}$$

If the length given by Equation (3.18) or Equation (3.19) is negative value, then we can add λ/2 to be positive results.

3.2.3.2 Series stub matching

For the case of series stub matching which shown in Figure 3.7, the distance d is selected at which the impedance, Z, at this distance from the load equal to $Z_0 + jX$. Then to eliminate the reactance we use series stub with opposite value equal to $-jX$, that will obtain matching condition.

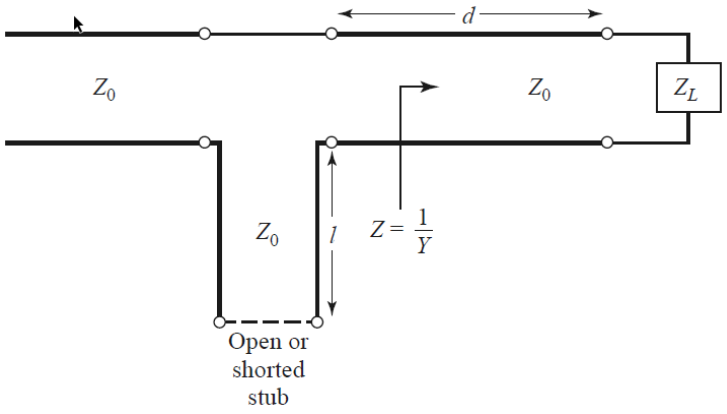

Figure 3.7: Series stub tuning circuit.(Pozar, 2012)

To obtain formulas for parameters d and l for series stub impedance tuning, the load admittance can be written as $Y_L = 1/Z_L = G_L + jB_L$. So, the admittance Y before a length d of line from the load can be as below:

$$Y = Y_0 \frac{(G_L + jB_L) + jY_0 \tan \beta d}{Y_0 + j(G_L + jB_L) \tan \beta d} \tag{3.20}$$

$$Z = R + jX = \frac{1}{Y} \tag{3.21}$$

$$R = \frac{G_L (1 + (\tan \beta d)^2)}{G_L^2 + (B_L + Y_0 \tan \beta d)^2} \tag{3.22}$$

$$X = \frac{G_L^2 \tan \beta d - (Y_0 - B_L \tan \beta d)(B_L + Y_0 \tan \beta d)}{Y_0 \left[[G_L^2 + (B_L + Y_0 \tan \beta d)^2 \right]} \tag{3.23}$$

If $G_L = Y_0$, then $\tan \beta d = -B_L/2Y_0$. Thus, the two prime solutions for d are:

$$\frac{d}{\lambda} = \begin{cases} \frac{1}{2\pi} \tan^{-1} \tan \beta d, & \tan \beta d \geq 0 \\ \frac{1}{2\pi} (\pi + \tan^{-1} \tan \beta d), & \tan \beta d < 0 \end{cases} \tag{3.24}$$

To compute the stub lengths that required, we first find the value of reactance X. The reactance must be equal the negative of the required stub reactance, Xs and same for a short-circuited stub.

$$\frac{l_s}{\lambda} = \frac{-1}{2\pi}\tan^{-1}\frac{X}{Z_0} \tag{3.25}$$

and for open-circuited stub,

$$\frac{l_0}{\lambda} = \frac{1}{2\pi}\tan^{-1}\frac{Z_0}{X} \tag{3.26}$$

When the length by Equation (3.25) or Equation (3.26) is negative value, then we can add λ/2 for length to give a positive result (Pozar, 2012).

3.2.4 Tapered line impedance matching

A tapered line transformer is one of the most important broadband matching techniques, it consists of continuously varying characteristic impedance along its length. which obtains lower reflection coefficients than at frequencies exceeding a minimum value as we see at Figure 3.8 that show A tapered impedance matching network.

Multi sections transmission lines transformer can make Impedance matching in any bandwidth. The change of impedance between each section will decrease When the number of sections increases. therefore, a tapered transmission line satisfied when infinity number of sections reached, So, we can consider Multi sections transmission lines transformer tapered transmission line. Infinite number of multi-section transformers is impossible so we use tapered transmission line as infinite number of multi section transmission lines (Zheng & Li, 2011).

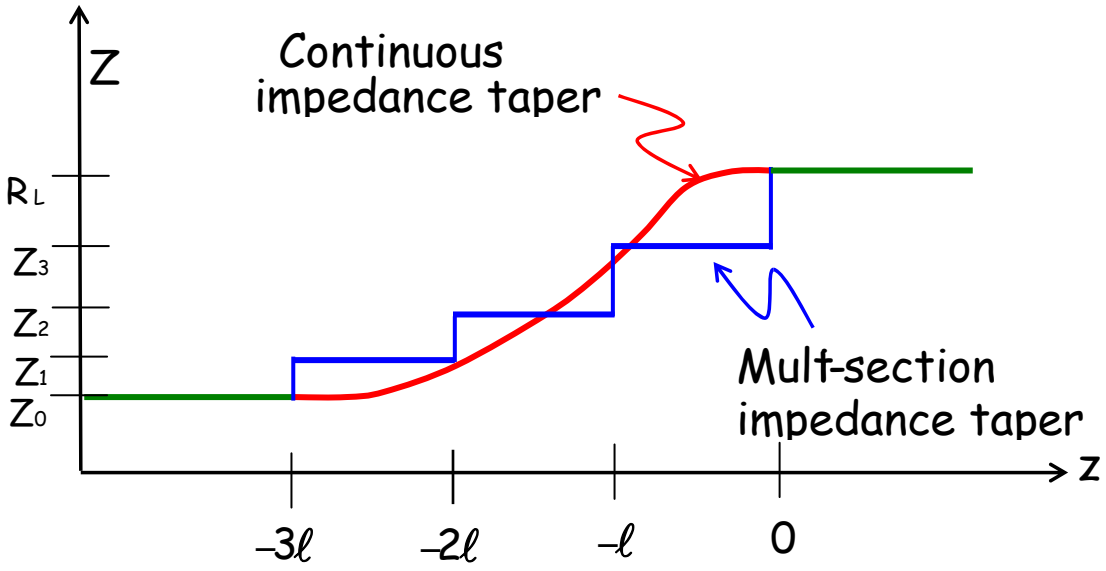

Figure 3.8: A tapered impedance matching network.(Stiles, 2010)

There are many types of taper designs, the main types are raised-cosine impedance profiles, linear taper, and exponential taper as. due to Klopfenstein the optimal design which involves cavity of the impedance at the end of transformer as shown below at Figure 3.9. (Stiles, 2010)

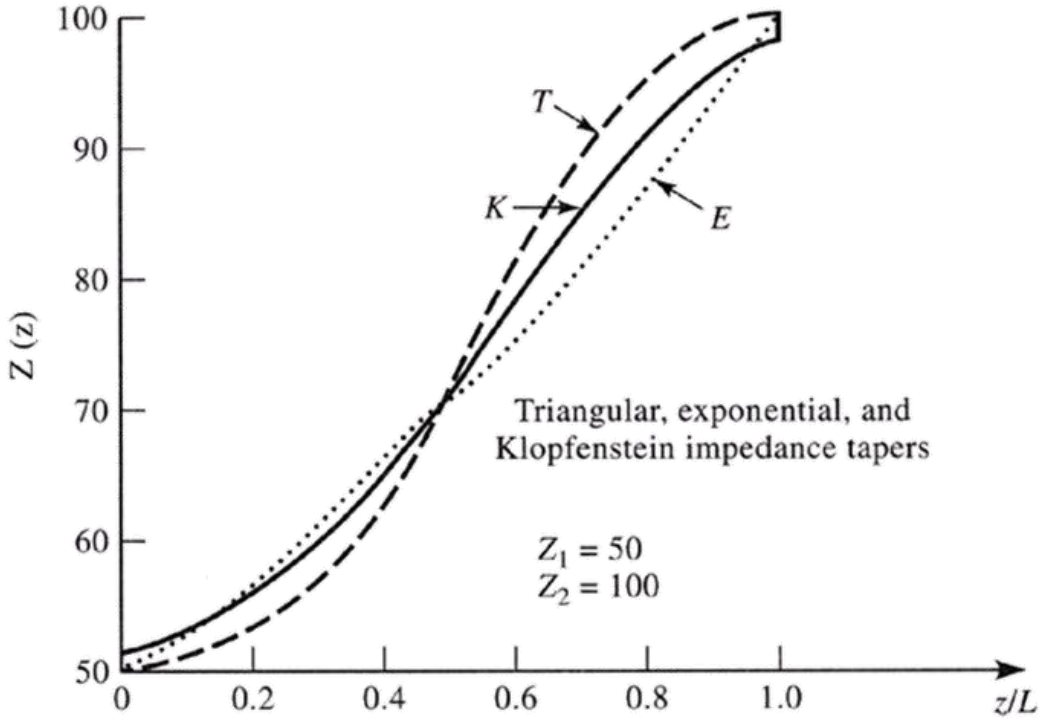

Figure 3.9: Relation of Impedance variations for various types of tapers (Pozar, 2012).

The relation of Impedance variations for various types of tapers as shown in Figure 3.9 and Figure 3.10 which describes the relation between frequency and reflection coefficient magnitude for the three types of tapers of (Figure 3.9).

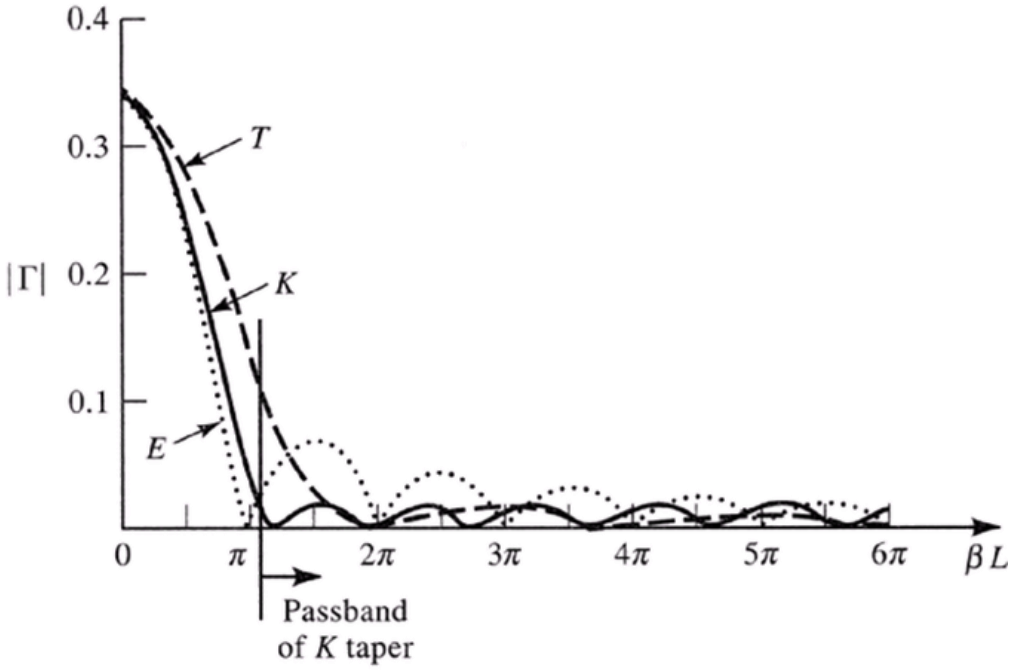

Figure 3.10: The relation between frequency and reflection coefficient magnitude for the three types of tapers of (Figure 3.9).

Tapered lines matching networks have the characteristic impedance of a transmission line changing continuously with position Z belong to L length changing, as shown in Figure 3.11a.

Two main characteristics can realize a tapered impedance matching network, that taper Length L and its function $Z(z)$ as shown in Figure 3.11.

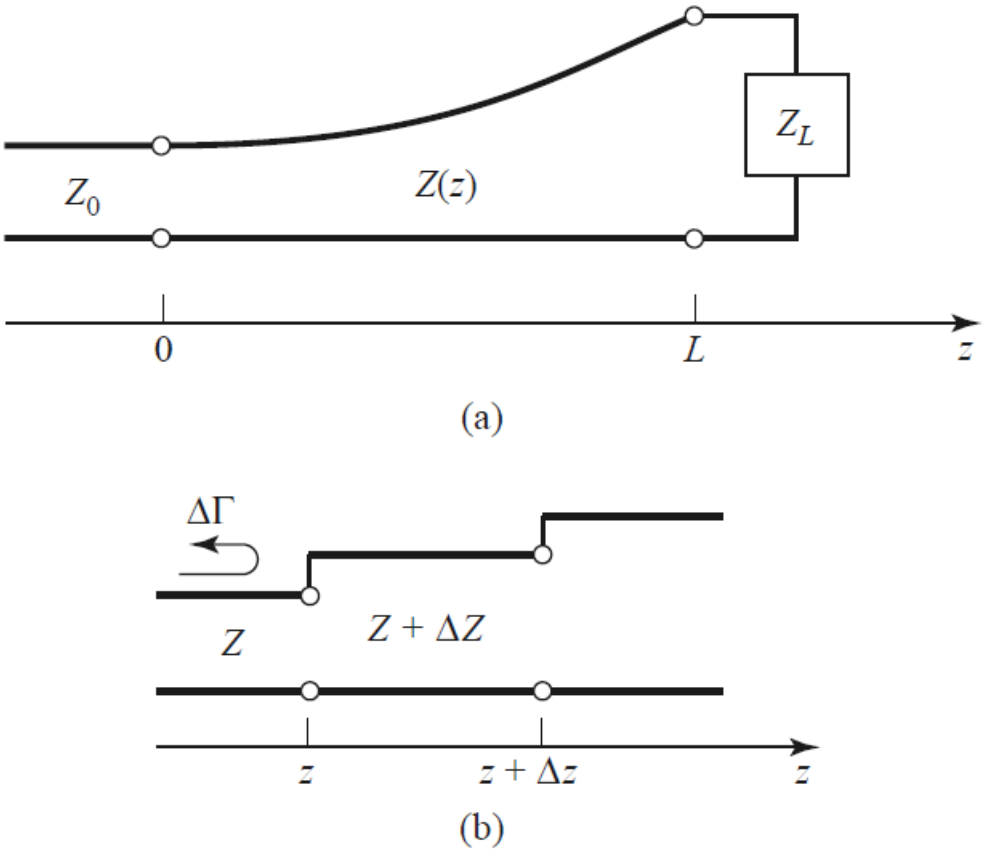

Figure 3.11: A tapered transmission line matching section (a) A tapered transmission line matching section which impedance change with position Z. (b) The model for an incremental length of tapered line.

Taper function Z(z) can be defined as shown in equation 3.27 for a triangular taper (Pozar, 2012),

$$Z(z) = \begin{cases} Z_0\, e^{2(z/L)^2 \ln Z_L / Z_0}, & \text{for } 0 \le z \le L/2 \\ Z_0\, e^{2(4z/L - 2z^2/L^2 - 1)\ln Z_L / Z_0}, & \text{for } L/2 \le z \le L \end{cases} \tag{3.27}$$

The derivative for a triangular taper for $d\ ln\ (Z/Z0)\ /dz$, (Pozar, 2012), is triangular in form:

$$\frac{d\ ln\ (Z/Z0)}{dz} = \begin{cases} 4z/L^2 \ln Z_L / Z_0, & \text{for } 0 \le z \le L/2 \\ (4/L - 4z/L^2)\ln Z_L / Z_0, & \text{for } L/2 \le z \le L \end{cases} \tag{3.28}$$

At Figure 3.12 show taper function Z(z) that a triangular taper matching section for derivative $d(ln\ Z/Z0)/dz$. At (a) Impedance differences. And at (b) The results of reflection coefficient magnitude.

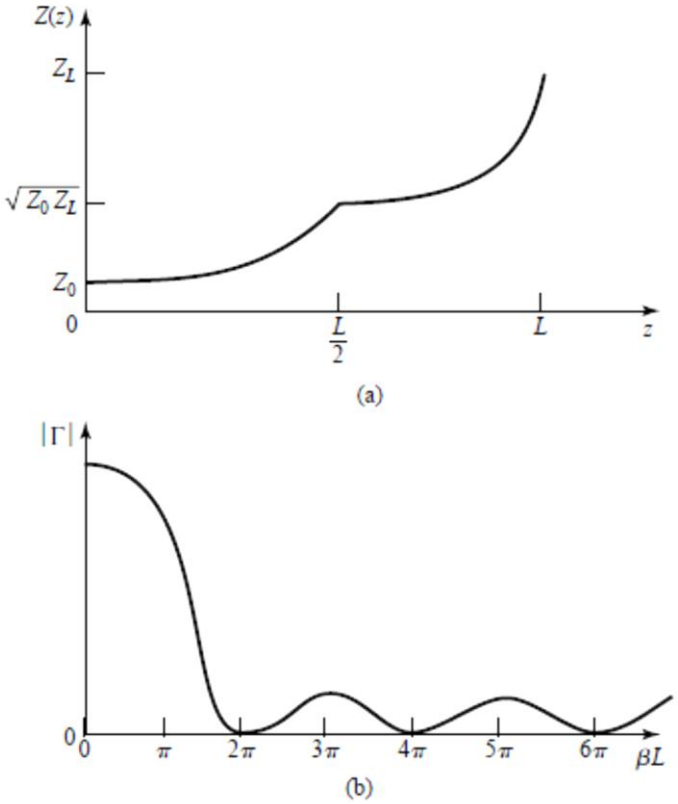

Figure 3.12: Taper function Z(z) that a triangular taper matching section for derivative $\boldsymbol{d(ln\ Z/Z0)/dz}$. At (a) Impedance differences. And at (b) The results of reflection coefficient magnitude.

3.3 Summary

This chapter start with the principles of impedance matching describe. Generally, various types of the matching techniques are available and discussed in this chapter, like lumped elements matching, matching with stubs transmission lines and tapered transmission lines matching. To clarify and the imagine the matching network design process, simple equations and an analytical approach discussed and used for calculation of the parameters of the matching circuits.

Chapter 4

Ultra-wideband Antenna Design

Chapter 4
Ultra-wideband Antenna Design

4.1 Introduction

Recently, RF energy harvesting is increasingly attracting researchers as an alternative solution to short-life batteries. Harvesting of ambient energy available in RF signals enables empowering low-power devices such as wireless sensors and medical implants. An energy harvesting system is mainly formed of an antenna, a matching circuit and a rectifier circuit to convert the AC signal into a DC signal. There has been extensive research reported in literature on designing antennas to scavenge the electromagnetic waves for harvesting applications. The vast majority of proposed antennas are based on microstrip technology and they are designed with various objectives. Some antennas are reported for multi-band operation to increase the amount of harvested power while other researches focused on increasing gain by employing array structures. Some antennas have been reported for single band operation (Zheng & Li, 2011), (Khan & Deng, 2016) and others working on dual-bands have also been proposed (Saad-Bin-Alam & Moury, 2014; Sarma & Akhtar, 2016). Increasing energy harvesting capacity can be achieved with multi-band operation and hence several works targeted to enhance antenna bandwidth for wideband/multi-band operation (Arrawatia, Baghini, & Kumar, 2016), (Zhou, Liao, Zhang, Han, & Chen, 2016). In (Arrawatia et al., 2016), a bent triangular antenna operating within the frequency range 850 MHz to 1.94 GHz with antenna gain of 2 dBi is presented. In (Wen et al., 2016), a collar-shaped antenna is proposed and it works from 1.7 GHz to 3.6 GHz. The antenna consists of two folded diploes laid on circular FR-4 substrate. Moreover, a broadband antenna is reported for harvesting over frequency range of 900 MHz to 3 GHz (X. Wang, Zhao, Chen, & He, 2014). In (Zainuddin et al., 2013), a wideband antenna with ice-cream cone structure is proposed and it operates within the range from 2.17 GHz to 4.2 GHz. However, this frequency range does not include many mobile signals. A triple band antenna is also reported in (Pham & Pham, 2013) for energy harvesting and it operates at 900 MHz, 1900 MHz and 2.4 GHz. In (Maher, Tammam, Galal, & Hamed, 2016), another broadband antenna operating over the frequency band from 2.1 GHz to 7 GHz has been presented.

This antenna also does not operate at GSM signals. Other researches were focused on increasing antenna gain to capture more energy by implementing an antenna array configuration (Mathur, Agarwal, Singh, & Bhatnagar, 2016), (Tawk, Ayoub, Christodoulou, & Costantine, 2015). This leads to larger antenna structures as a trade-off with higher gain. Moreover, circularly polarized antennas have been proposed for energy harvesting applications (Jie, Karim, Bin, Chin, & Ong, 2016). A recent interesting design of an antenna matched to the input impedance of the rectifier has been proposed to eliminate the need for a matching circuit (Song et al., 2006).

A novel microstrip antenna is proposed for RF energy harvesting over Ultra-wideband frequency range from 790 MHz to 3.4 GHz. This range includes variety of wireless applications and it incorporates not only mobile and WiFi signals as in (Arrawatia et al., 2016), (Zhou et al., 2016) but also some digital terrestrial TV signals. The broad bandwidth covered by the proposed antenna in addition to its reasonable size makes it an excellent candidate for harvesting applications. The standard wireless applications operating within the aforementioned frequency range are: digital terrestrial TV (portion of 700 MHz band and all 800 MHz band), GSM-900 (890 MHz-960 MHz), GSM-1800 (1710 MHz-1880 MHz), UMTS (1920 MHz-2170 MHz), LTE (bands 1-8, others), WiFi 2.45 GHz and WiMAX 2.3 GHz and 2.5 GHz.

4.2 Antenna Structure

The proposed antenna structure is depicted in Figure 4.1. The metallic surface consists of star-shaped microstrip patch. Crescent and rectangular slots are cut onto the patch element to broaden the operating frequency range of the antenna. The substrate used is FR-4 with dielectric constant of 4.3 and thickness of 1.6 mm. The substrate length is 140 mm, and its width is 60 mm and the microstrip feed line is designed such that the characteristic impedance is 50 Ω with width of 3.1 mm. The ground plane is cut beneath the star-shaped patch to widen the antenna bandwidth and the length of ground plane from the port to inside is 81 mm. Figure 4.2 presents a clear top view of the star-shaped patch along with its dimensional parameters. The antenna parameters have been optimized using CST simulation software and the final dimensions of the antenna are listed in Table 4.1. The main goal in optimization is matching input impedance of the antenna to 50 Ω over wide operating frequency range.

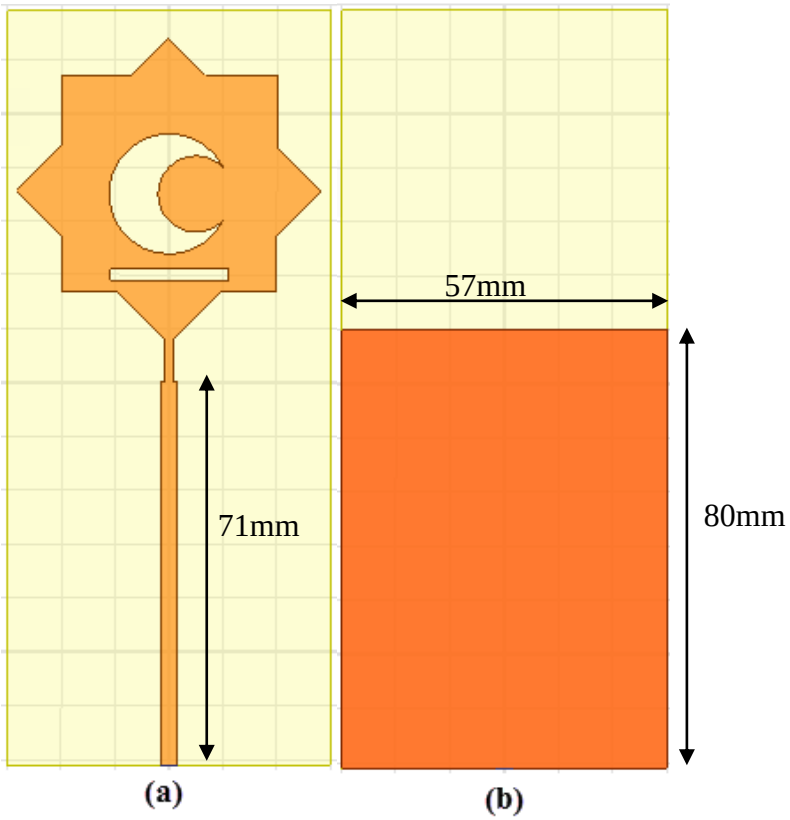

Figure 4.1: Proposed antenna structure (a) Top view (b) bottom view.

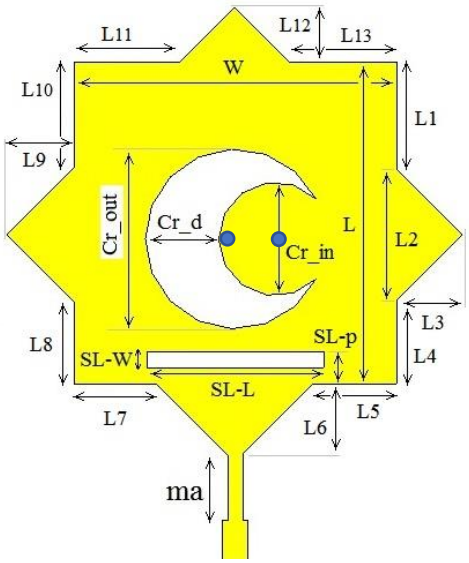

Figure 4.2: Parameters of star-shaped patch

Table 4.1: Optimized parameters of the antenna

Parameter	Value (mm)	Parameter	Value (mm)
L	40.0	L10	13.074
W	40.0	L11	13.074
L1	13.287	L12	6.819
L2	16.355	L13	13.287
L3	8.178	Cr_out	22.360
L4	10.357	Cr_in	14.142
L5	10.358	Cr_d	9.109
L6	8.849	SL-L	22.0
L7	10.145	SL-W	2.0
L8	10.145	SL-p	4.0
L9	8.390	Ma	8.045
GND	80	Feeder width	3.1

4.3 Simulation Results

The simulation results of the return loss S_{11} of the antenna is presented in Figure (4.3) and it can be noticed that the return loss is below 10-dB from 774 MHz to 3.1 GHz. This broad 10-dB bandwidth of the proposed antenna makes it convenient for energy harvesting of signals of many standard wireless systems.

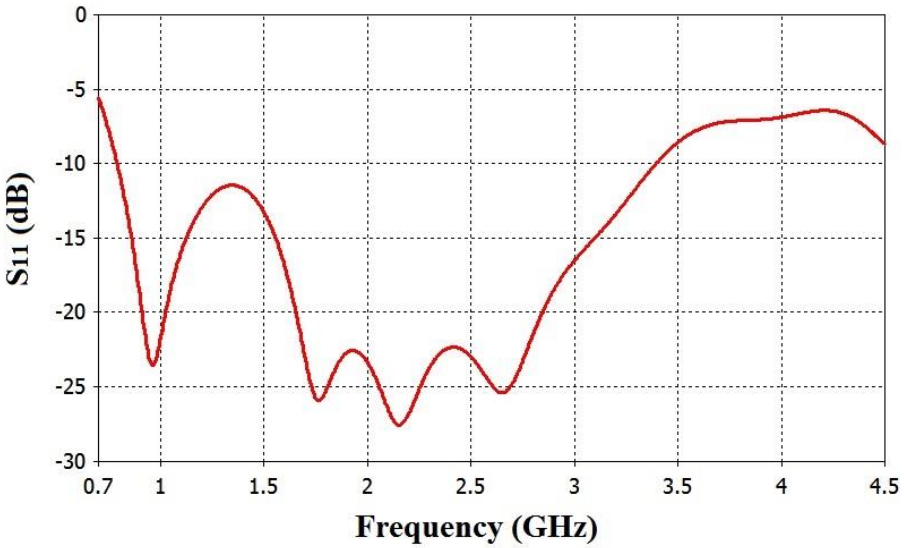

Figure 4.3: Simulated return loss of the antenna.

Figure 4.4 (a) exhibits the three-dimensional simulated radiation pattern at 900 MHz and it shows an omni-directional pattern with a maximum directivity of 2.33 dBi. The simulated radiation patterns in both xz-plane (ϕ=0) and yz-plane (ϕ=90) are shown in Figure 4.4 (b) and Figure 4.4 (c), respectively. Viewing the radiation pattern at 900 MHz in yz-plane, a null is observed at θ=90 and maximum radiation is noticed in broadside direction at θ=0 and θ=180. The three-dimensional radiation patterns are also simulated at other frequencies of interest for standard wireless applications and they are shown in Figure 4.5 (a) to Figure 4.5 (f) for the frequencies 800 MHz, 950 MHz, 1.83 GHz, 2.12 GHz, 2.45 GHz and 2.62 GHz. The realized gains at those frequencies are 0.902 dBi, 1.79 dBi, 3.65 dBi, 2.31 dBi, 1.7 dBi and 2.83 dBi, respectively. It can be noticed that the radiation patterns in Figure 4.5 at the given operating frequencies also exhibit omni-directional characteristics. In the proposed design with cut in ground plane the bandwidth is broadened, however, it is traded-off against the gain. This explains the relatively low values of gain when compared to full-grounded standard patch antennas in addition to the high loss tangent of the FR-4 substrate (tan δ=0.02) that contributed to decreasing antenna gain. Nevertheless, the broad bandwidth of the antenna in addition to its omni-directional radiation patterns makes the proposed antenna an excellent candidate for RF energy harvesting.

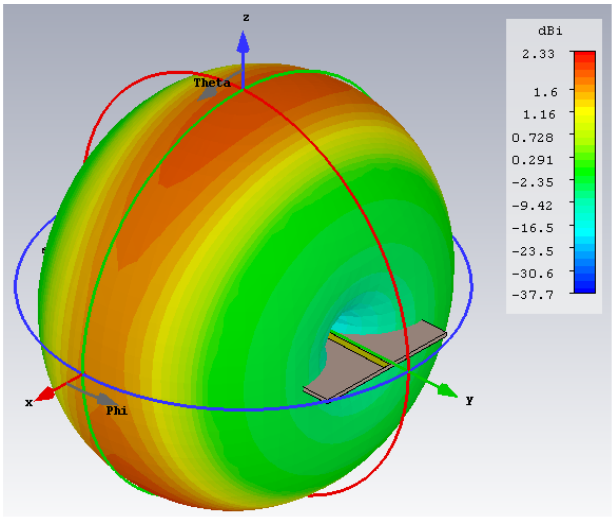

(a)

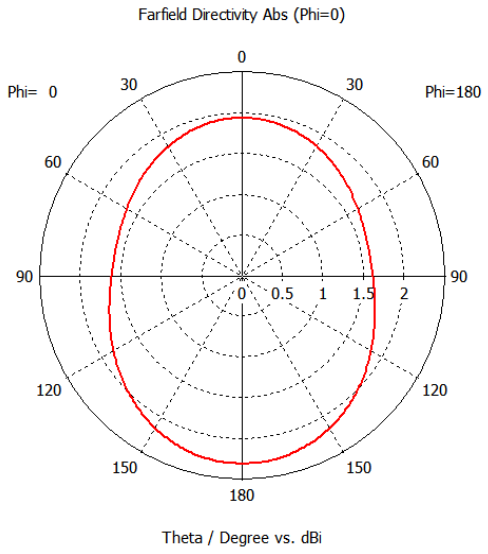

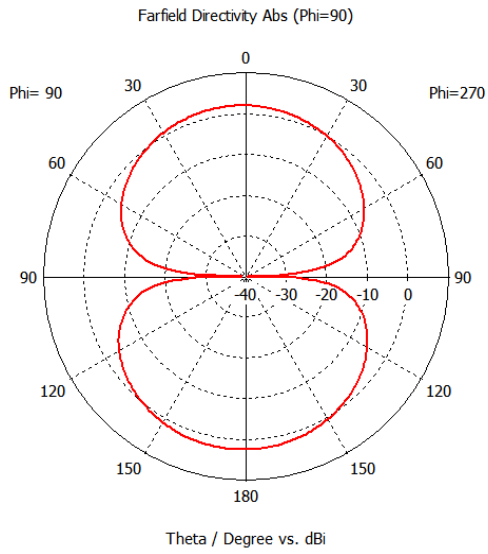

(b) **(c)**

Figure 4.4: Simulated radiation pattern of the antenna (a) 3D pattern, (b) xz-plane, (c) yz-plane.

The simulated radiation patterns are also shown in the yz-plane (θ=90) in Figure 4.6 for the aforementioned frequencies of interest where nulls are observed at θ=90.

To give a good insight about the performance of the antenna over wide frequency range, the simulated peak realized gain is depicted in Figure 4.7 over the frequency range from 750 MHz to 3.25 GHz. It can be noticed that the antenna has satisfactory gain over wide frequency range and the gain is above 1.6 dBi within the range 900

MHz to 3.25 GHz. It can also be noticed that the maximum gain reaches 3.93 dBi at frequency 1.7 GHz.

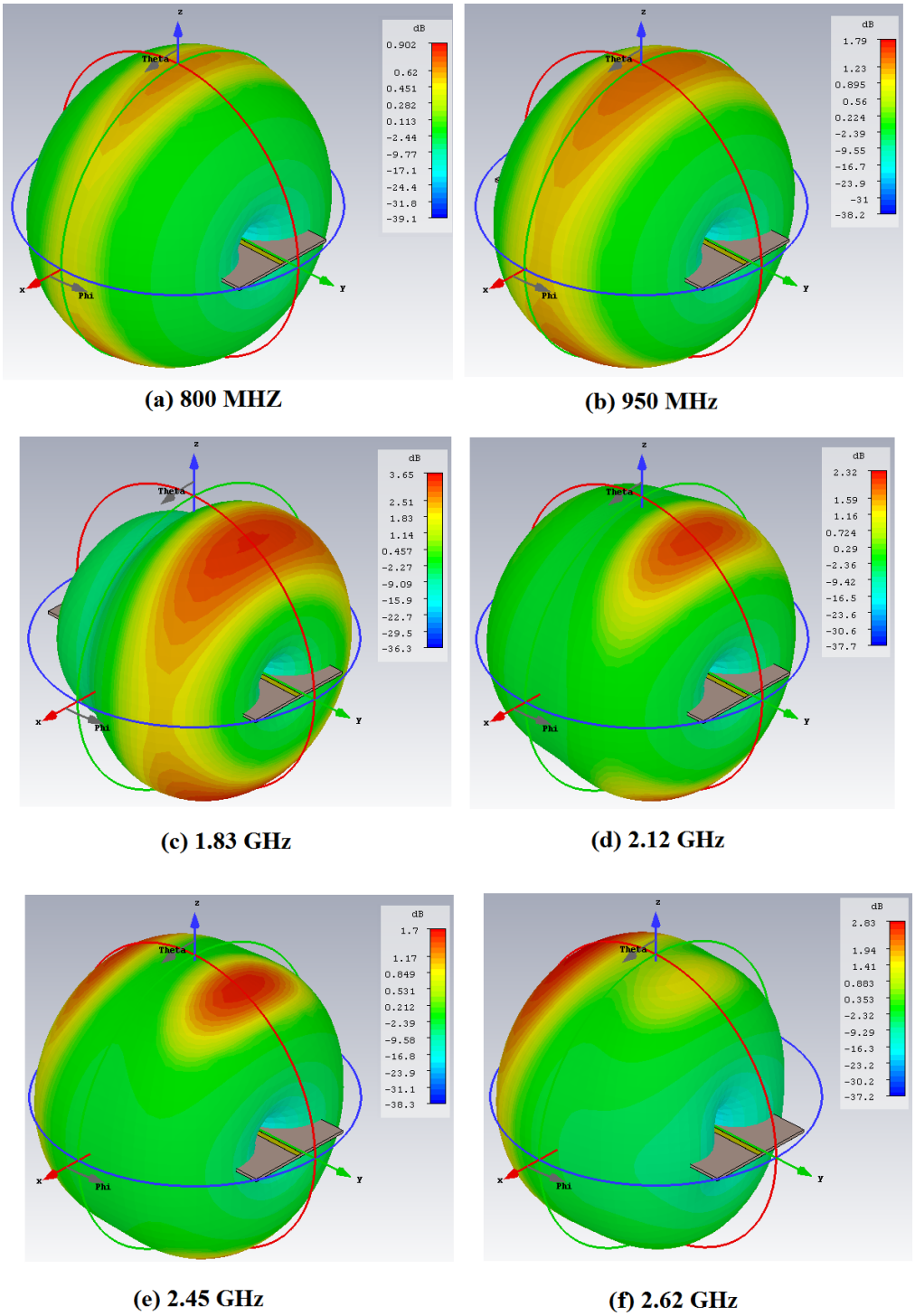

(a) 800 MHZ **(b) 950 MHz**

(c) 1.83 GHz **(d) 2.12 GHz**

(e) 2.45 GHz **(f) 2.62 GHz**

Figure 4.5 : 3D radiation patterns of the antenna at (a) 800 MHz, (b) 950 MHz, (c) 1.83 GHz, (d) 2.12 GHz, (e) 2.45 GHz, (f) 2.62 GHz.

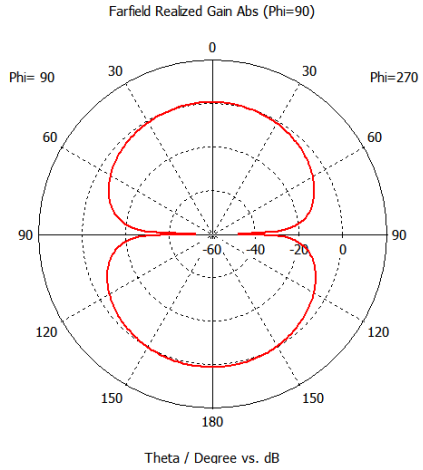

(a) 800 MHz

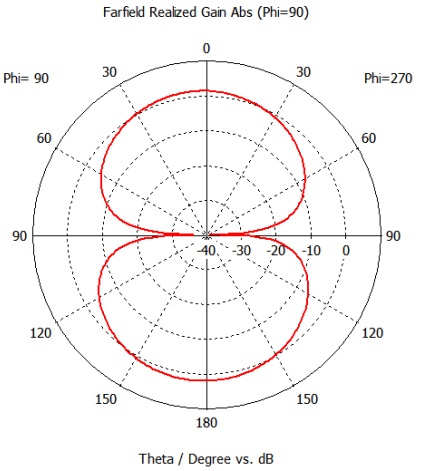

(b) 950 MHz

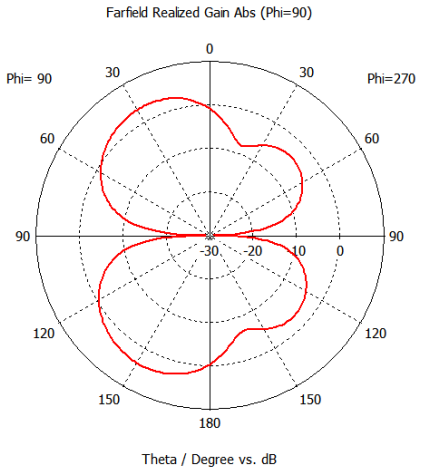

(c) 1.83 GHz

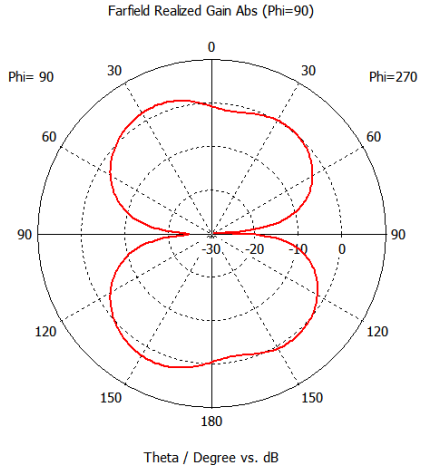

(d) 2.12 GHz

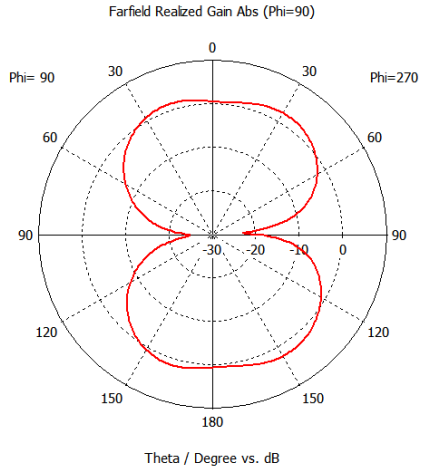

(e) 2.45 GHz

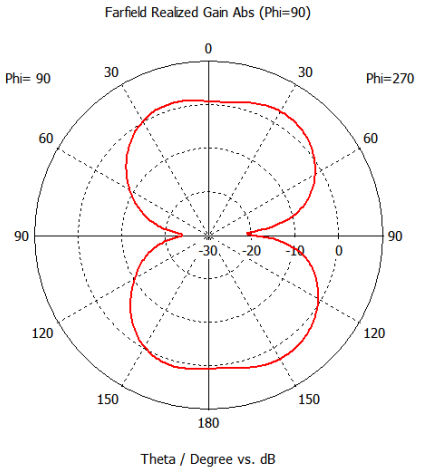

(f) 2.62 GHz

Figure 4.6: 2D radiation patterns of the antenna in yz-plane at (a) 800 MHz, (b)950 MHz, (c) 1.83 GHz, (d) 2.12 GHz, (e) 2.45 GHz, (f) 2.62 GHz**.**

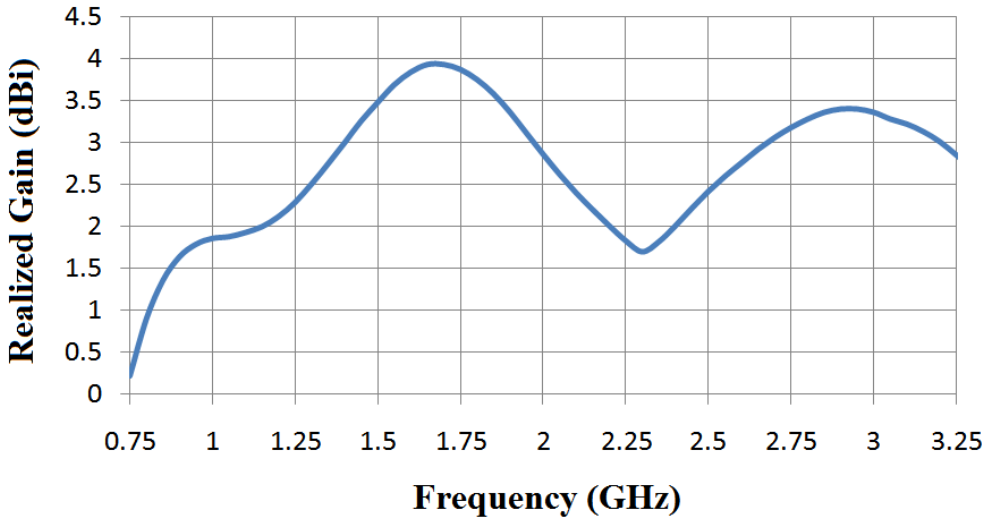

Figure 4.7: Simulated peak realized gain of the antenna

4.4 Fabrication results of Ultra-wideband patch antenna

The Ultra-wideband patch antenna was designed and fabricated on FR-4 substrate and the same property of the rectifier circuit, as shown in Figure 4.9.

The measurement results of the return loss S11 of the antenna is presented in Figure 4.8 and it can be noticed that the return loss is below 10-dB from 940 MHz to more than 3.5 GHz. This broad 10-dB bandwidth of the proposed antenna makes it convenient for energy harvesting of signals of many standard wireless systems the fabrication of top and bottom of antenna shown in Figure 4.9.

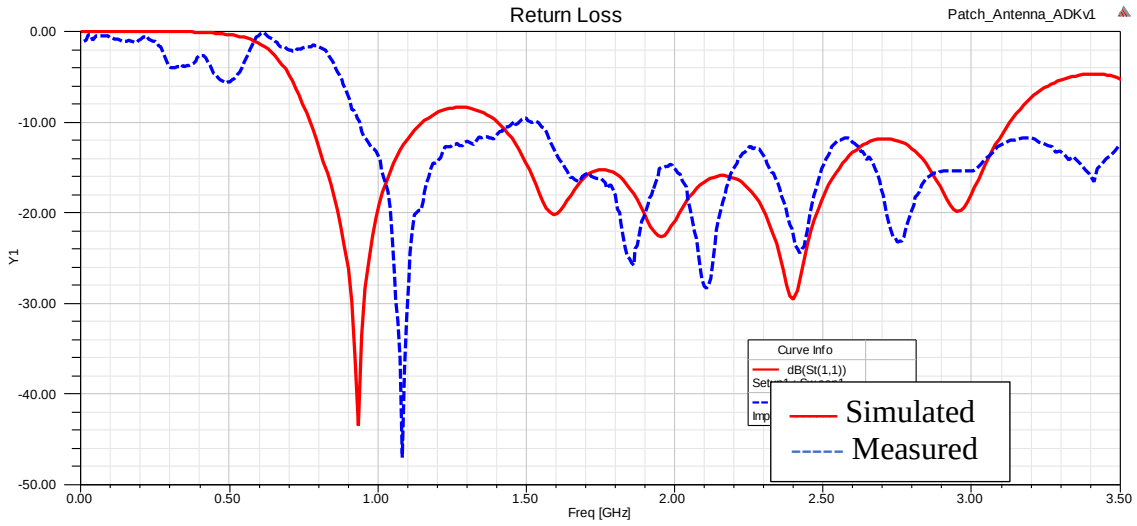

Figure 4.8 : Simulated and measured S11 for Ultra-wideband patch antenna design

The simulated and measured results at S11 can be compared in Figure 4.9 it can be noticed that the return loss is shifted about 150 MHz at the beginning of plot but this does not affect other bands, the reason behind this may be due to the uncertainty of substrate parameters such as dielectric constant and also may be due to fabrication errors.

On the other hand, the result of broad band star patch antenna is covered other bands as GSM1800, UMTS, LTE and WiFi and other applications which it works on frequencies located in antenna range from 940MHz to 3500MHz.

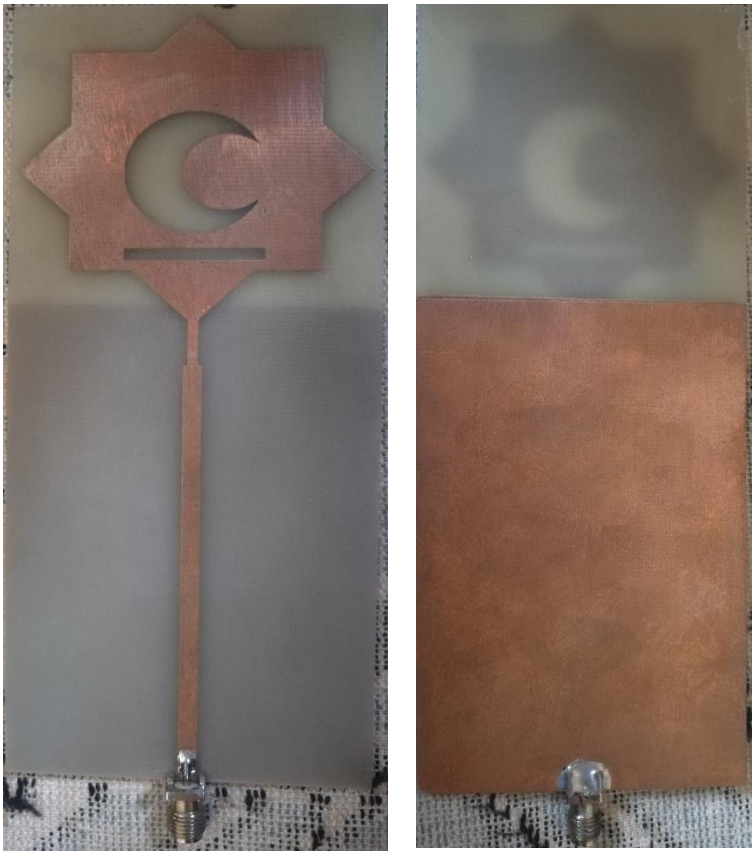

Figure 4.9: Ultra-wideband patch antenna fabrication on FR4

4.5 Summary

In this Chapter an Ultra-wideband microstrip antenna is proposed for energy harvesting applications. The patch element is star-shaped conductor with two slots in the form of a crescent and a rectangle. The ground plane is cut underneath the patch to extend the bandwidth and thus enabling antenna to harvest more energy. The proposed antenna operates within the frequency range 790 MHz to 3.4 GHz and this range incorporates various wireless communications systems such as GSM, UMTS, LTE and WiFi. The realized gain is simulated over wide range and it reaches 3.93 dBi at 1.7 GHz and it is above 1.6 dBi within the range 900 MHz to 3.25 GHz. The radiation patterns are simulated at the operating frequencies of the given wireless systems and omni-directional patterns are obtained. The good performance of the antenna in terms of broad bandwidth, omni-directional radiation pattern and acceptable realized gain makes it a good candidate for energy harvesting.

Chapter 5

Rectifier Design and Implementation

Chapter 5
Rectifier Design and Implementation

5.1 Introduction

Rectifier circuit is the third important part of the energy harvesting system, which is used to transform AC voltage into DC voltage. The rectenna circuit can harvest RF energy and it consists of the combination of antenna, matching circuit and voltage rectifier.

Many applications are using rectenna as a voltage converter as example radio frequency identification (RFID) systems, wireless power transmission systems, wireless sensor systems, space solar systems, and power detector systems. The efficiency of the energy harvesting system depends on the efficiency of the antenna and the rectifier, also the good matching of the connection between the antenna and the rectifier circuit. The good matching can be determined by source-pull technique that provides the optimal impedance for the input impedance and the diode impedance (Khansalee, Zhao, & Nuanyai, 2015).

Simply the rectifier circuit is an electrical device consists of one or more diodes that transforms (AC) alternating current into (DC) direct current as shown in Figure 5.1. In Half-Wave rectifier, a diode works as one-way valve that allow current to flow in only one direction (look at Figure 5.1). This process is called rectification (Ren & Chang, 2006).

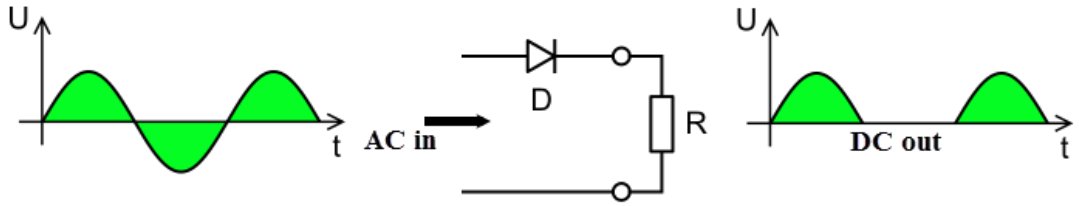

Figure 5.1: Transforms (AC) alternating current into (DC) direct current.

5.1.1 Half-wave rectifier

At half-wave rectifier, either the negative or positive half of the AC wave is passed throw the circuit as shown in Figure 5.1 and in Figure 5.2, while the other half is not allowed to pass. At this case only, one-half wave of the input can reach the output, so that it is half efficient power transformer.

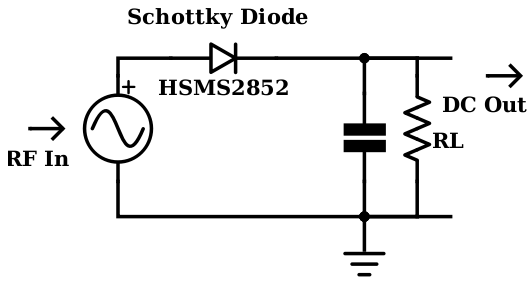

Figure 5.2: RF Half-wave rectifier.

5.1.2 Full-wave rectifier

A full-wave rectifier allows both the positive and negative of input waves to enter to the output as we see at Figure 5.3. By using two diodes which work as two valves, that let us using both halves of the AC waveform to reach full-wave rectification which is more efficient than half wave.

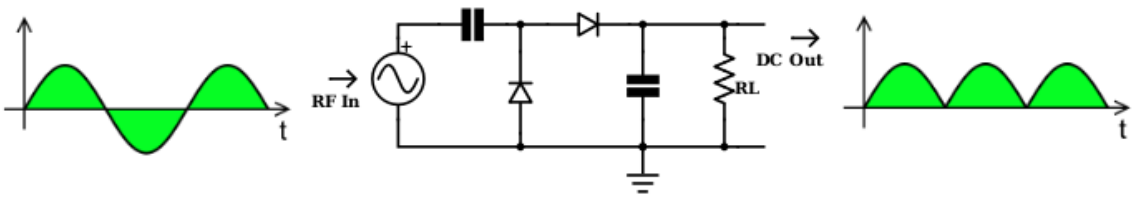

Figure 5.3: Full-wave rectification

5.2 Voltage doubler rectifier

The voltage doubler rectifier consists of two diodes and two capacitors. Look at Figure 5.4 to see the two diodes are connected as presented, so that forward current can pass only from the ground to the positive output voltage terminal $Vout$ by using D2 then D1. Thus, the capacitor C1 blocked the DC current from passing toward the

source. Capacitor C1 stores the charge and allows the high frequency currents to pass. But the other capacitor at this case stores the resulting charge for output voltage $Vout$ smoothing. Basically, the circuit works as a charge-pump design. The capacitor C1 and diode D2 make up a dc-level shifter, and the capacitor C2 and diode D1 form a peak detector.(J. Wang, Gao, Yu, Wang, & Jin, 2012)

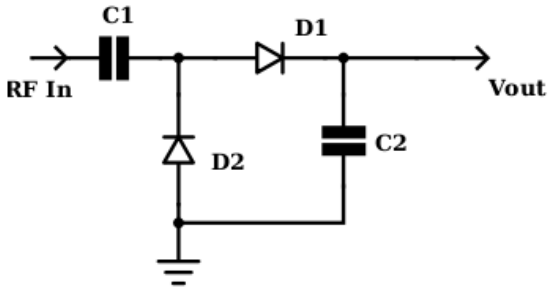

Figure 5.4: Voltage doubler rectifier

When the RF signal is positive and larger than required voltage for diode D1 turn-on, at this moment the diode D2 work as open switch and the diode D1 as turns on switch as shown in Figure 5.5.

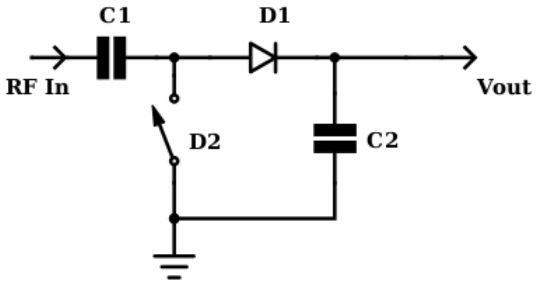

Figure 5.5: Rectifier when RF signal is positive

Second case When the RF signal is negative and larger than required voltage for diode D2 turn-on, the current passes from the ground by using the diode D2 and results storing charge on capacitor C1.

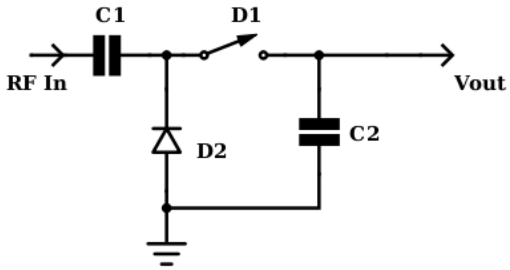

Figure 5.6: Rectifier RF signal is negative

The voltage on the capacitor C1 can be the difference between the negative peak voltage Vpk and the turn-on voltage of the diode Von at the negative peak as shown at Equation (5.1).

$$V_1 = Vpk - Von \tag{5.1}$$

From the equivalent model at Figure 5.5 of positive case part of the RF cycle, we can calculate the peak voltage on diode D1 by the next equation:

$$Vout = V_1 + Vpk - Von \tag{5.2}$$

$$Vout = 2(Vpk - Von) \tag{5.3}$$

The output voltage $Vout$ can be calculated as summation of the voltage on the capacitor C1 and the positive RF voltage, then subtract the turn-on voltage Von.

5.3 Multistage rectifier

One stage of rectifier does not produce enough voltage to trigger harvesting application needed, as the produced voltage is $2(Vpk - Von)$.

Thus, many of voltage doubler rectifiers can be used to reach multistage rectifier. Four stage rectifiers are proposed to reach the required voltage. To compute the DC output voltage for N-stage multistage rectifier Equation (5.4) can be used as shown below: (J. Wang et al., 2012).

$$Vout = 2N(Vpk - Von) \tag{5.4}$$

The N-stage multistage rectifier can be designed as in Figure 5.7 which describe the cascaded rectifier stages.

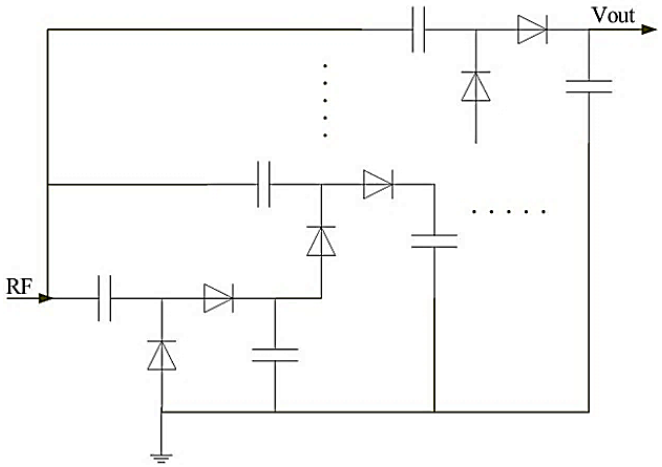

Figure 5.7: N-stage multistage rectifier.(J. Wang et al., 2012)

5.4 Schottky diode

After looking on equation 5.3, the best diode choice can be realized by which is the zero bias schottky diode, because the output voltage *Vout* increased, by let the voltage of the diode *Von* to be the lowest as possible.

The output voltage *Vout* can doubled the peak voltage of the RF signal when *Von* is very low and can be ignored as in theory, which the circuit voltage doubler rectifier derives its name from it in fact. Note, the output voltage *Vout* must be less than the theoretical value, because we cannot ignore the load resistance, and the circuit cannot be able to withdraw out all the current and charge that stored in the capacitors (J. Wang et al., 2012).

5.4.1 Diode Modeling

We chose schottky diode HSMS2852 zero bias in our rectifier structure, the equivalent circuit for the schottky diode can be clarify as in Figure 5.8. We chose this Schottky diode because of its attractive features as very fast switching and low substrate losses. This diode is commonly used at the energy harvesting circuits and modeled of two diode configurations.

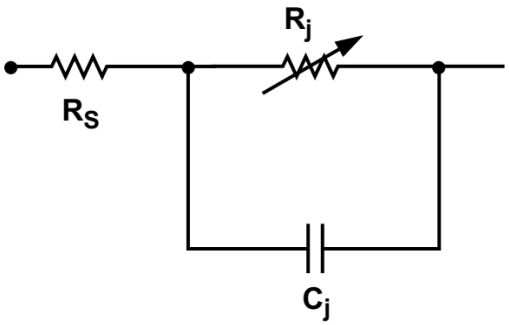

Figure 5.8: Equivalent Linear Circuit Model HSMS-285x chip

where Rs and Cj are constants and the frequency of operation (w) is the only variable parameter. when frequency increased, we can neglect the value of Z with compared to the diode series resistance RS. The function of the schottky diode can be considered independent of the frequency of operation.

The junction resistance Rj is given by the Equation 5.5 and Rs is the series resistance of the circuit (Technologies, 1999).

$$R_j = \frac{8.33*10^{-5} * N * T}{I_b * I_S} \tag{5.5}$$

R_S = series resistance
C_j = junction capacitance
where
I_b = externally applied bias current in amps
I_S = saturation current
T = temperature, °K
N= ideality factor

The modeling parameters for schottky diode HSMS2852 is given at table 5.1. These parameters are used in Multisim for its own modeling purposes.

The total impedance Z_T is given by Equation (5.6):

$$Z_T = R_S + \frac{R_j}{jwc_j + 1} \tag{5.6}$$

Table 5.1: Diode SPICE modeling parameters.

Parameters	Units	HSMS 2850
B_V	V	3.8
C_{J0}	pF	0.18
E_G	eV	0.69
I_{BV}	A	3E–4
I_S	A	3E–6
N	No unite	1.06
R_S	Ω	25
$P_B(V_J)$	V	0.35
$P_T(XTI)$	No units	2
M	No units	0.5

5.5 Efficiency

The conversion efficiency is defined in (Curty, Joehl, Dehollain, & Declercq, 2005) at equation 5.7 and 5.8,

$$\eta_C = \frac{DC\ Output\ Power}{Incident\ RF\ Power - \text{Re}\ flected\ RF\ Power} \tag{5.7}$$

whereas, the overall efficiency is given by:

$$\eta_C = \frac{DC\ Output\ Power}{Incident\ RF\ Power} \tag{5.8}$$

at our case we use equation 5.9 to compute efficiency as below:

$$\eta_C = \frac{Vout^2 / R_L}{Pin} * 100\% \tag{5.9}$$

Where

η_C is the overall efficiency.

Pin is incident RF power (w).

R_L is Load impedance.

$Vout$ Output Voltage (V).

5.6 Voltage doubler rectifier design

The voltage doubler rectifier designed in this section by using many matching impedance techniques, at first, we start at single band with different models to reach the efficient model, then multi band with lumped element and Taper matching designed. Single and multi-band fabricated and compered with simulated results.

5.6.1 Single band four stages voltage doubler rectifier design

The single band RF rectifier circuit was designed to operate at 935 Mhz. The input impedance of the voltage doubler rectifier was matched to 50 ohms of the RF source by lumped element matching using T-matching technique that transforms the input impedance (*Zin*) of the rectifier circuit to 50 ohms as shown in Figure 5.9. The T-matching circuit consists of three inductors and their values are tuned to provide the optimal efficiency for the circuit. The simulation schematic of the rectifier consists 50 ohms of RF source, the impedance matching, the voltage doubler rectifier and RL, as shown in Figure 5.9.

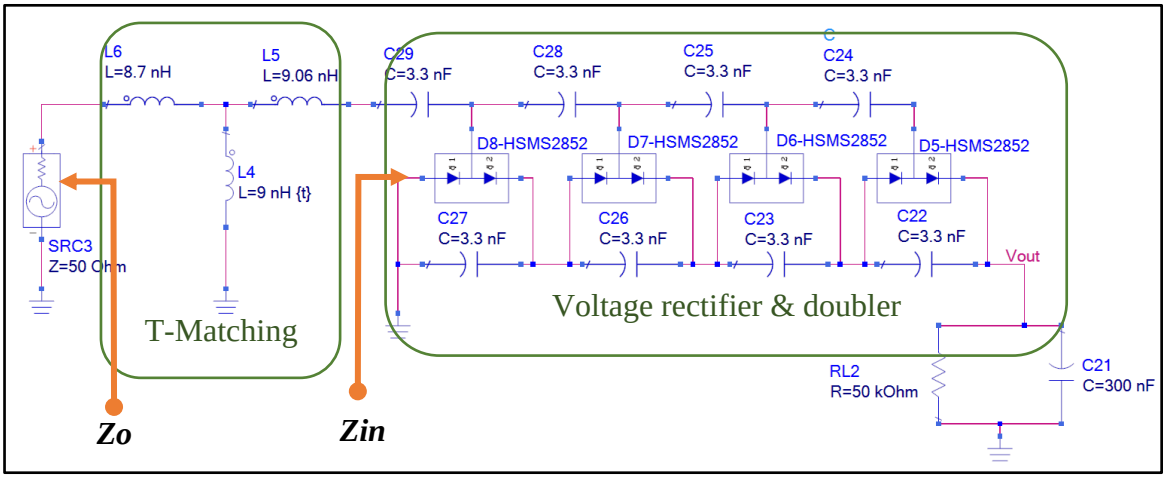

Figure 5.9: Four stage voltage doubler rectifier design by ADS.

5.6.1.1 T-matching circuit

For matching *Zin* must be equal *Zo* 50 Ω so we firstly determine *Zin* the input impedance for rectifier circuit at certain frequency 935 MHz, and then we use equations at chapter 3 to compute matching circuit which convert *Zin* to be equal to

Zo, as shown at Figure 5.10 below, it can be shown from the results that the input impedance of the rectifier circuit is 7.4-j80.2.

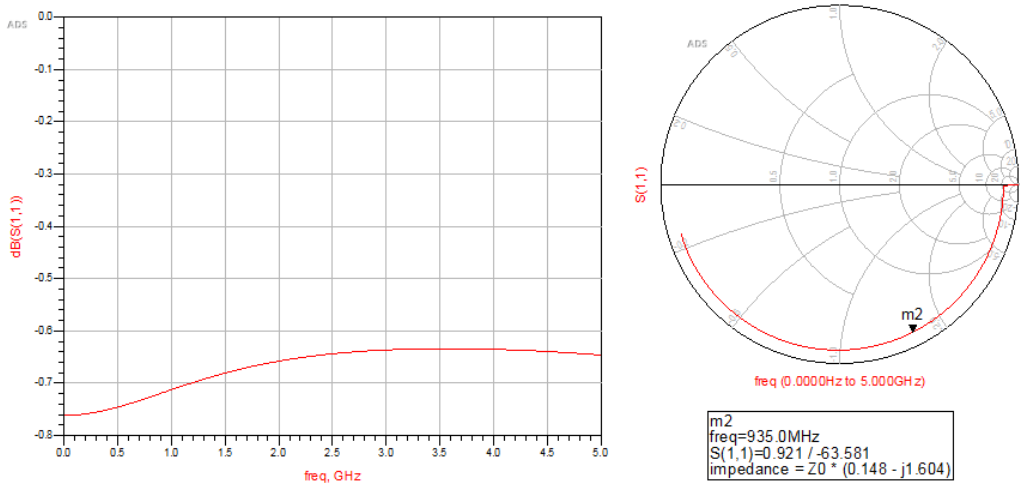

Figure 5.10: S11 and input impedance for rectifier voltage doubler before matching

Also, we use smith chart v3 program for tuning T-matching circuit as shown in Figure 5.11. We found the best values for lumped elements parameters is to use three inductors as shown in circuit 9.1nH, 7nH and 9nH that make matching at frequency of 935 MHz.

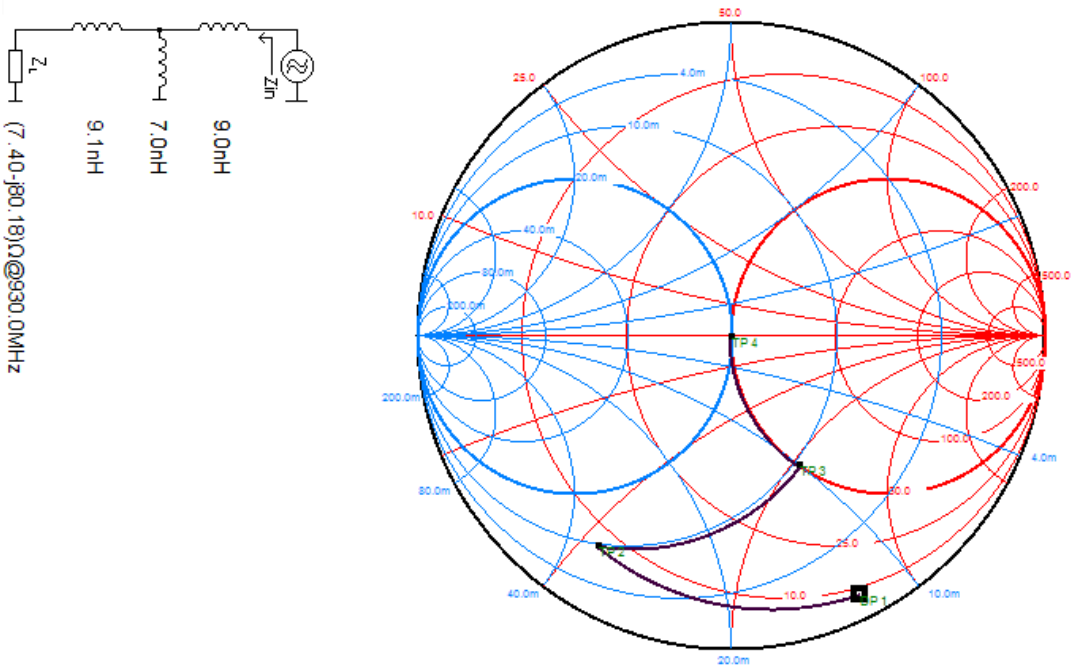

Figure 5.11: T-matching using smith v3.1.

At Figure 5.12 we can see the results after using T-matching circuit and impedance matching on smith chart *Zin* = 50 Ω =*Zo* at frequency 935 MHz.

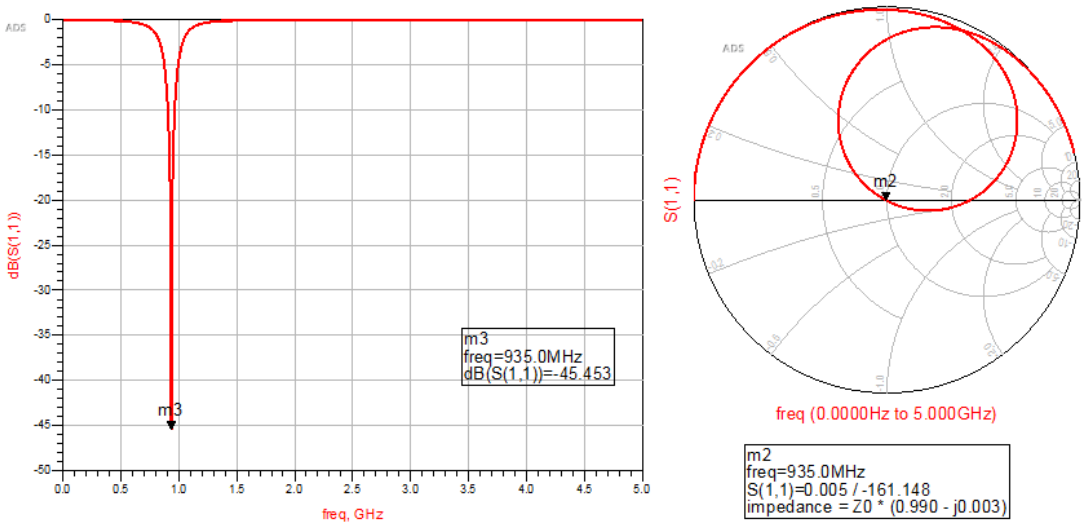

Figure 5.12: S11 after adding T-matching to the rectifier voltage doubler.

5.6.1.2 The Effect of number of rectifier stages

The major effect on the output voltage of the energy harvesting circuit depends on number of rectifier stages. Every stage here which arranged in series works as modified voltage doubler. The number of rectifier stages in proportion with the output voltage of the energy harvesting circuits the Figure 5.14 explain the relation between number of rectifier stages and the harvesting output voltage. Efficiency is inversely proportional to the increase in the number of stages because of the constituent capacitors effect in every stage(Le et al., 2008). Figure 5.13 explain the relation between number of rectifier stages and the efficiency, Figure 5.14 explain the relation between number of rectifier stages and the harvesting output voltage. Agilent ADS with parameters sweep from -40 to 40 dBm have been used for the input RF power and tuned the matching circuit for each case. Also, varied number of circuit stages from one to four stages have been used and tuned the matching circuit for each case to clarify the relation between the number of stages and the output voltage. We can include that the circuit reaches higher voltage as the number of stages increases in direct correlation as shown in Figure 5.14 but efficiency decreases at low input RF power (below -20 dBm).

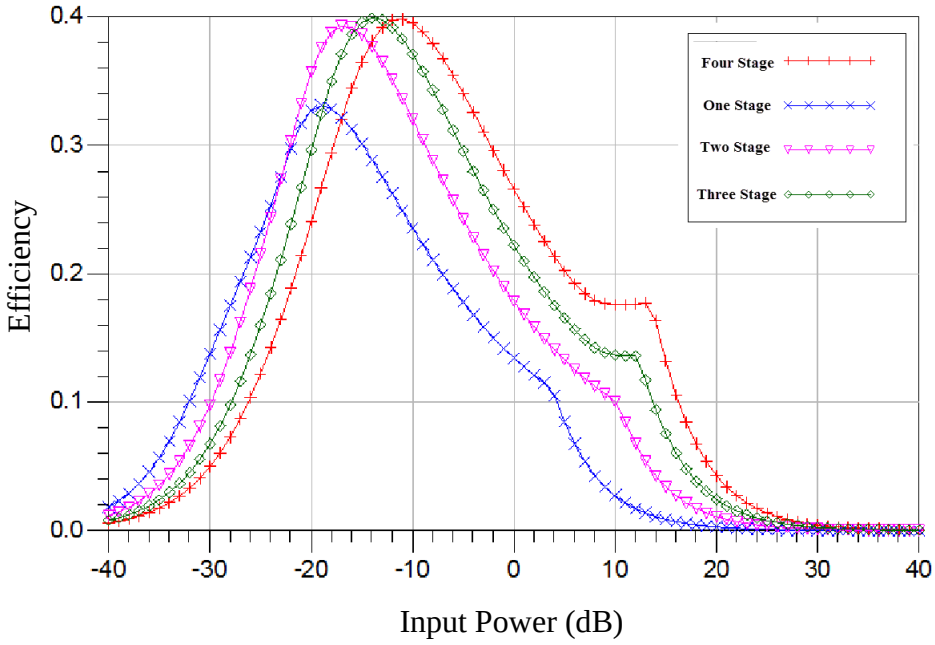

Figure 5.13: The relation between number of rectifier stages and the efficiency.

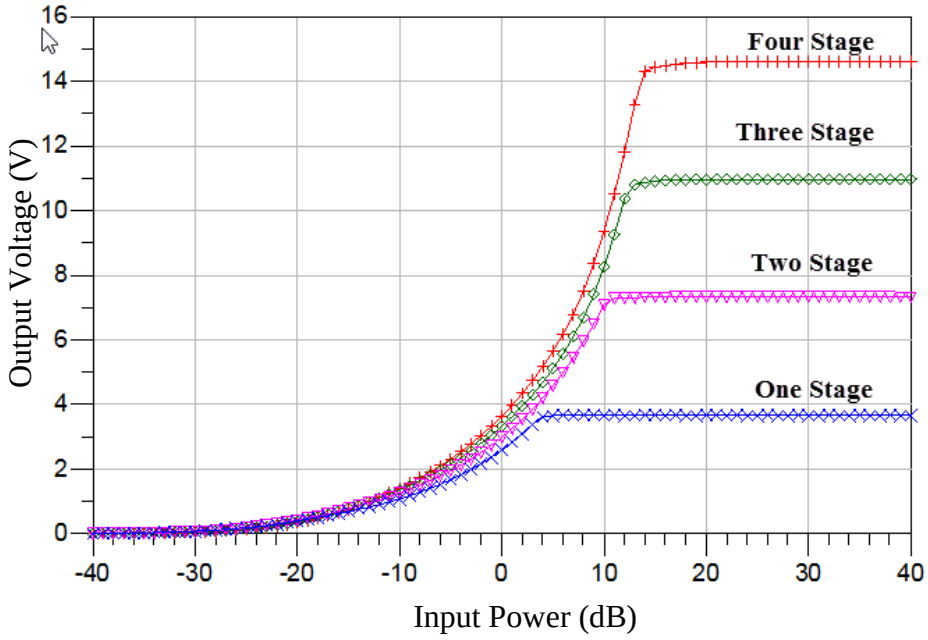

Figure 5.14: The relation between number of rectifier stages and the harvesting output voltage.

By the way, when we cascade the voltage doubler rectifier to form multistage rectifier the efficiency of output voltage will decrease because of losses in diodes,

capacitors and transmission lines, so when rectifier stages increase the efficiency will be decreased as we see at Figure 5.13.

5.6.1.3 Load Impedance Effect on efficiency

Select impedance for energy harvesting circuit is most important and must be selected carefully, that we can see the impedance performance impact in Figure 5.15. To study the effect of the impedance we did a simulation using Agilent ADS2016 to see the efficiency of the energy harvesting circuit. The parameters used for input power sweep from −40 dBm to 40 dBm and 10KΩ to 75KΩ for the load impedance.

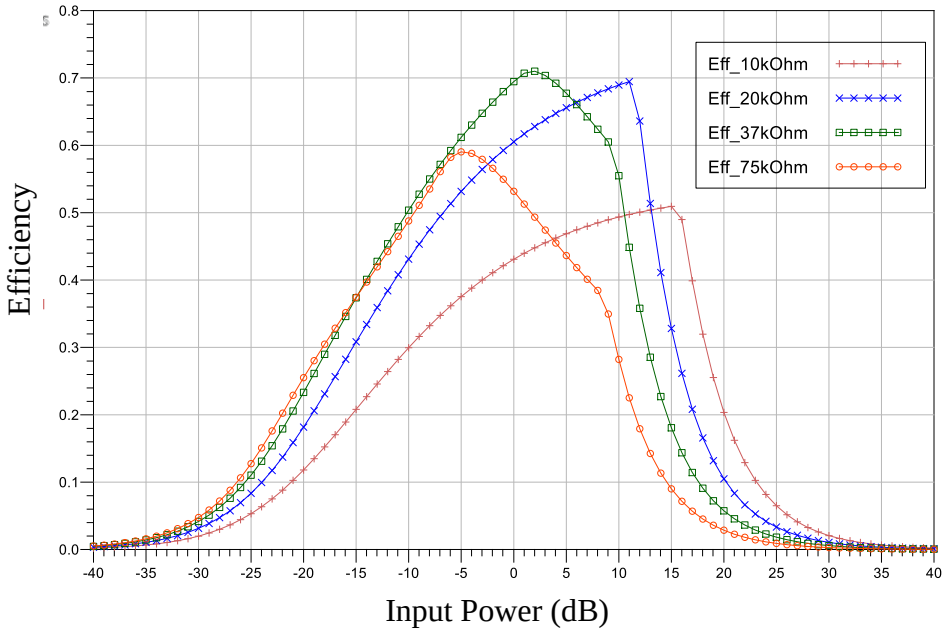

Figure 5.15: Value of load impedance effect on efficiency

After using ADS2016 for simulation, We note that the optimal load impedance Value is 37kΩ, which give the best efficacy, but on other load impedance values efficiency will decreased. We use four stage rectifiers in energy harvesting circuit at simulation, each stage consists of two schottky diodes of HSMS-2852, worked as is a modified voltage multiplier and rectifier.

The main aim of this optimization is to reached to maximum efficiency of the energy harvesting circuit at the required load and input power.

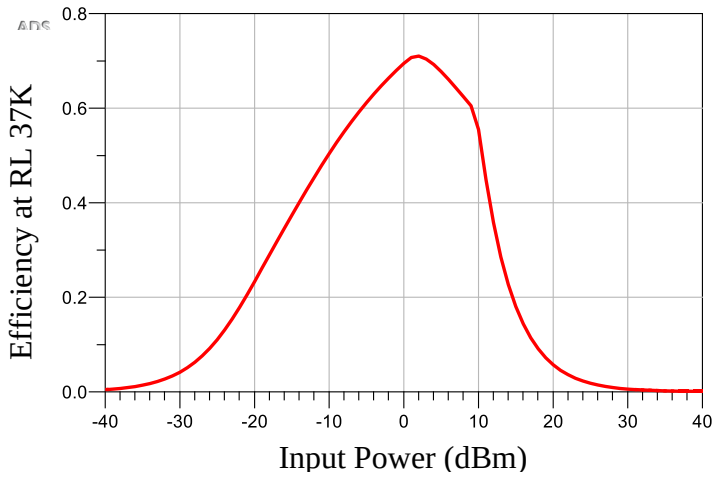

Figure 5.16: Efficiency at 37KΩ load impedance.

Also, we can see the output voltage by using ADS at the load we chose as shown in Figure 5.17.

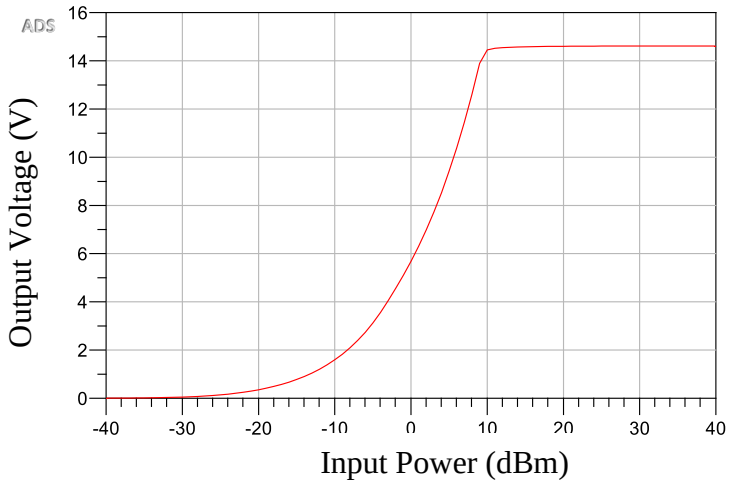

Figure 5.17: Relation between output voltage and input power for impedance load of 37KΩ.

We use frequency sweep to see the relation of efficiency versus frequency, it is noticed that that the highest efficiency is obtained at 935 MHz which reached 71.5% as shown at Figure 5.18.

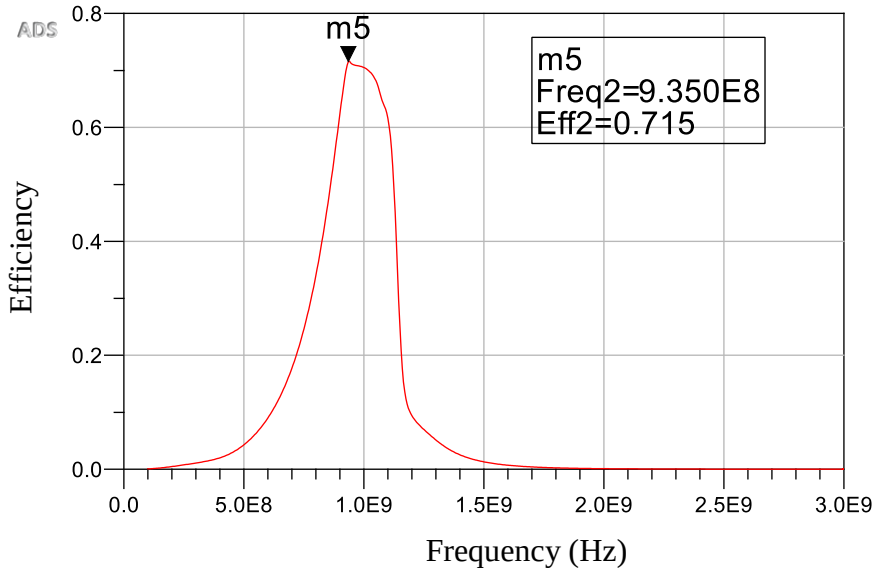

Figure 5.18: Efficiency versus frequency with load 37KΩ

The output voltage versus frequency is presented in Figure 5.19 which shows highest voltage is obtained at frequency 935 MHz where matching circuit is tuned.

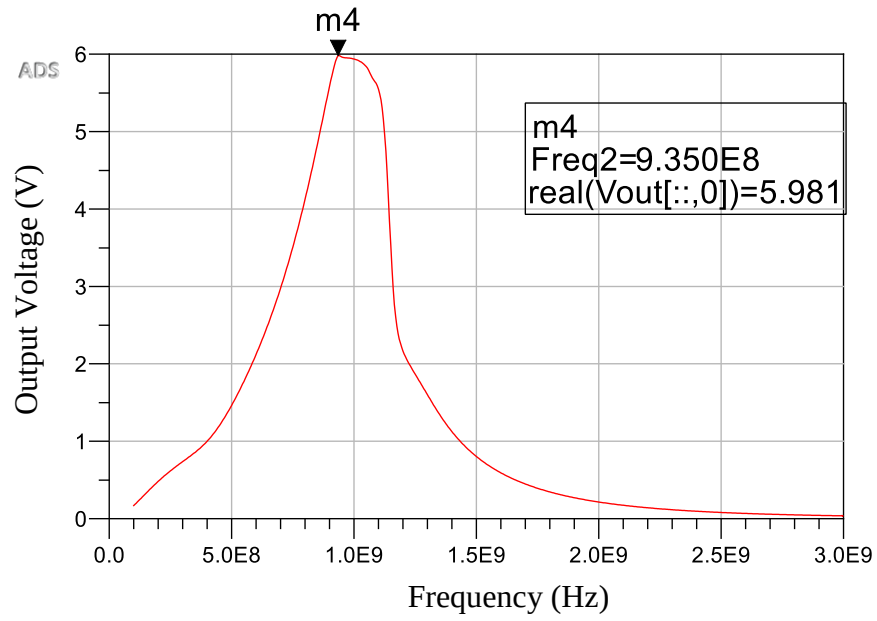

Figure 5.19: It demonstrates the output voltage with frequency change.

5.6.1.4 Fabrication of single band Lumped element matching

Fabrication of single band lumped element matching is shown in Figure 5.20 by using FR4 epoxy substrate with substrate thickness of 1.6mm, The simulated and measured results of S11 are shown graphically in Figure 5.21 for single band with four

stage voltage doubler at 0dBm. From graph in figure 5.21, the fabricated measured and simulated results are agreed with each other considerably.

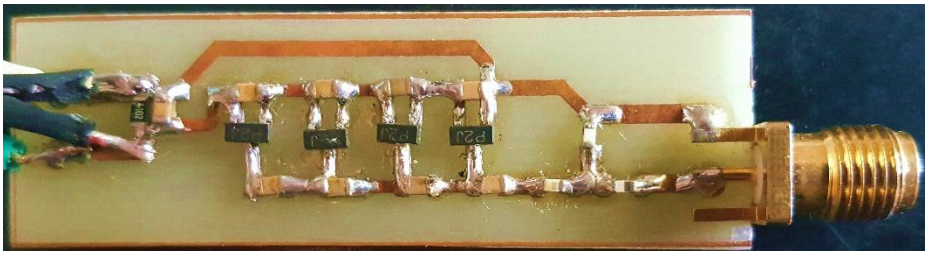

Figure 5.20: Fabrication of single band Lumped element matching.

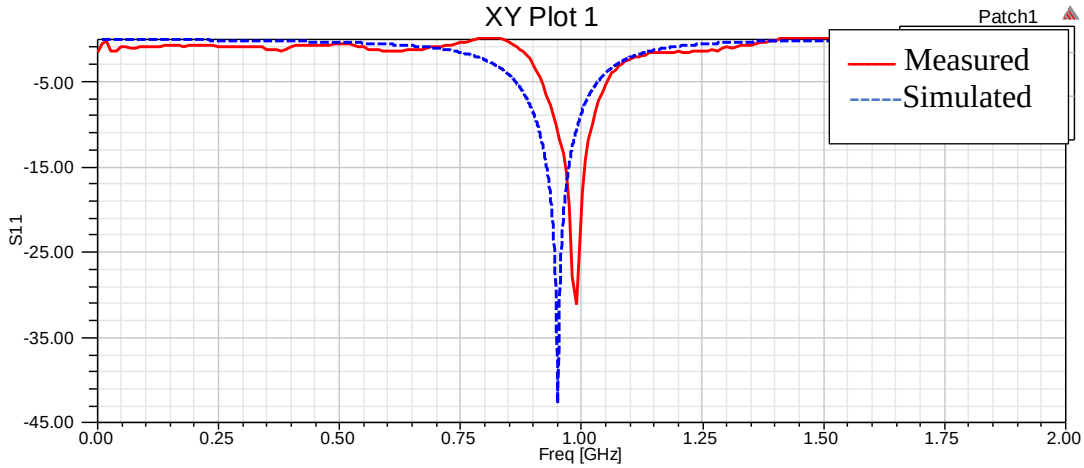

Figure 5.21: S11 for simulated and measured results of single band rectifier.

The output voltage for simulated and measured results of voltage doubler rectifier circuit which shown in Figure 5.22. We can note that, the fabricated measured and simulated results are agreed with each other considerably. In this work, the output DC voltage gained from circuit by measurement at 0 dBm is 6.34 V. This result is comparatively better than simulted results. The reason because of uncertainty at substrate parameters or may be due to the uncertainty in resistance value of the diode from SPICE parameters at table 5.1. This differnce at values of parameters case changes at values of output voltage and shiftting on measured S11.

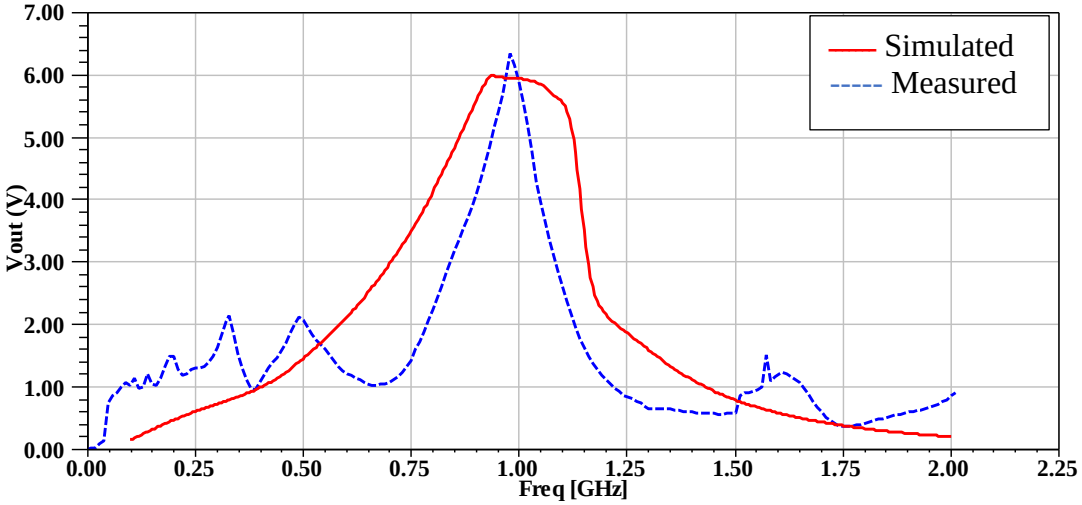

Figure 5.22: Results of the measured and simulated output voltage.

From the results in Figure 5.23, we note that the measured and simulated results of rectifier efficacy for single band with four stage voltage doubler rectifier at 0dBm input power, results agreed with simulation results.

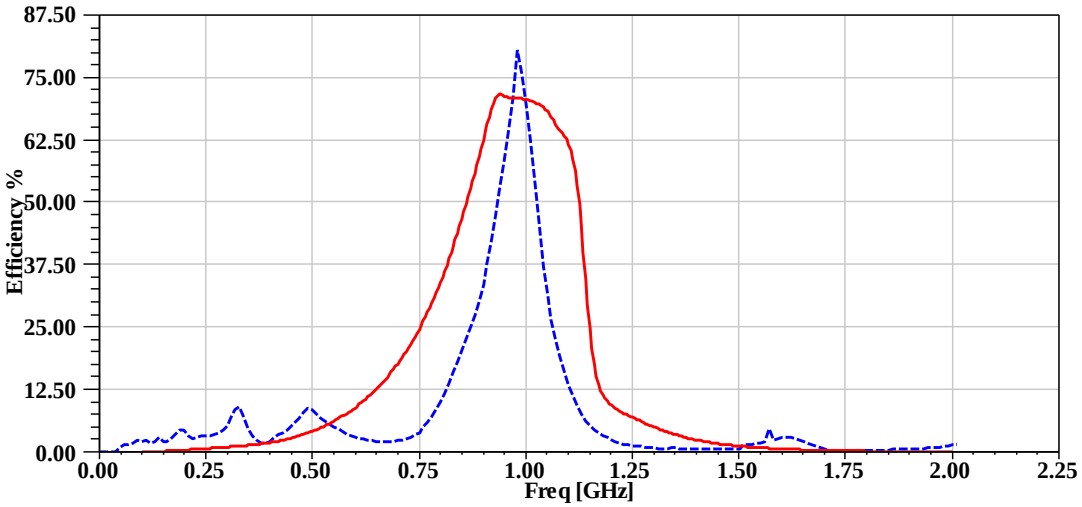

Figure 5.23: The simulated and measured results of rectifier efficacy

5.6.2 Multi-band four stages voltage doubler rectifier design

We prefer the use of voltage doubler rectifier circuit that operate at multi-bands rectifier with Ultra-wideband antenna. Thus, because of number of rectennas used on system the harvested energy can be increased. Block diagram in Figure 5.24 shows Multi-band voltage doubler rectifier design. Each rectifier combines its own signal, a

single broad band antenna is connected to the matching networks and voltage multiplier for all bands.

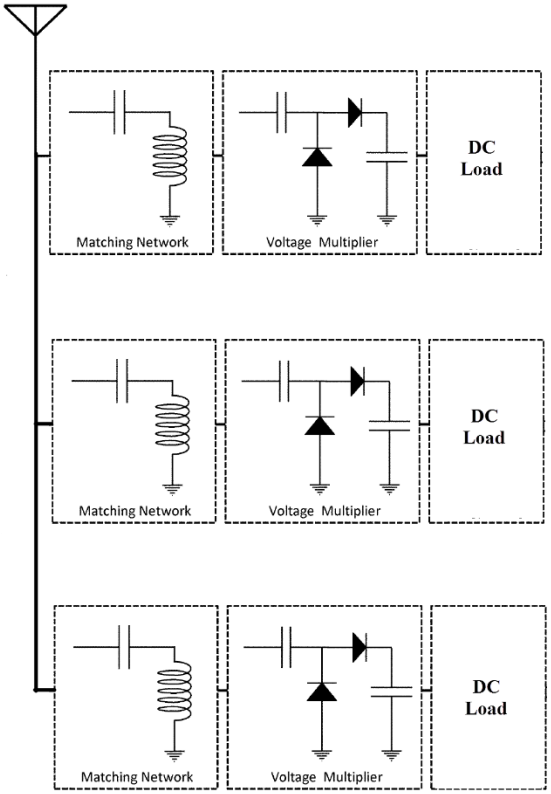

Figure 5.24: Multi-band voltage doubler rectifier design

The multi band rectifier is designed by using Agilent ADS simulation program as shown at Figure 5.25. The system harvests energy from GSM900, GSM1800, and WiFi bands simultaneously.

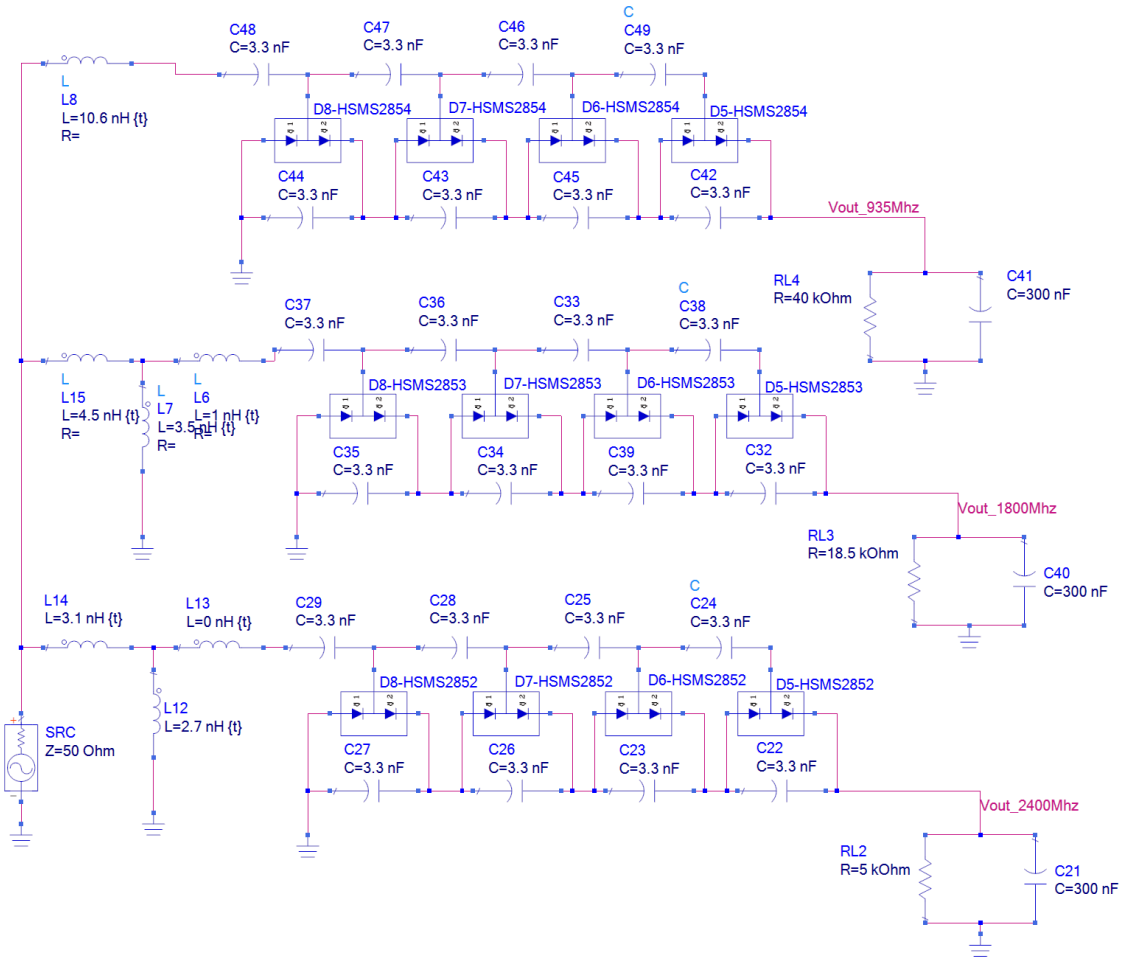

Figure 5.25: Multi-band four stages voltage doubler rectifier design with matching

Lumped element matching circuits are used and tuned in the design. The simulated result of S11 for the design is shown in Figure 5.26 which is -28dB at 928 MHz with 10-dB bandwidth from 890 MHz to 970 MHz, while S11 at GSM1800 (1830 MHz) is -66 dB with 10-dB bandwidth from 1778 MHz to 1878 MHz and S11 at WiFi (2.47 GHz) is -48dBwith 10-dB bandwidth from 2411 MHz to 2550 MHz.

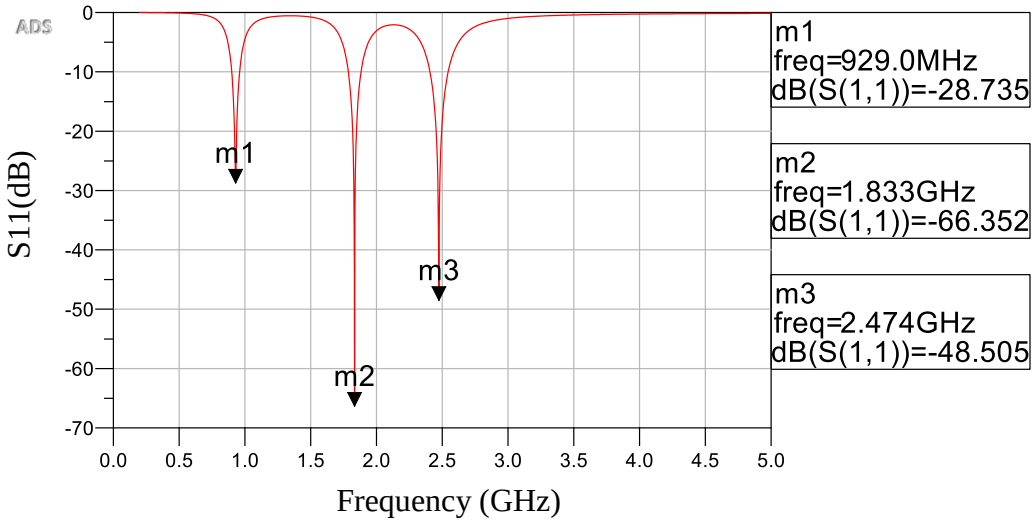

Figure 5.26:S11 for multi-band voltage doubler rectifier

The output voltage of the multi-band energy harvesting system is increased, the output voltage for GSM900 at 0 dBm is 4V, and for GSM1800 it is 0.7V and for WiFi it is 0.5V. But the voltage gradually increases at all bands reach 14 V at input power of 40 dBm, as shown at Figure 5.27.

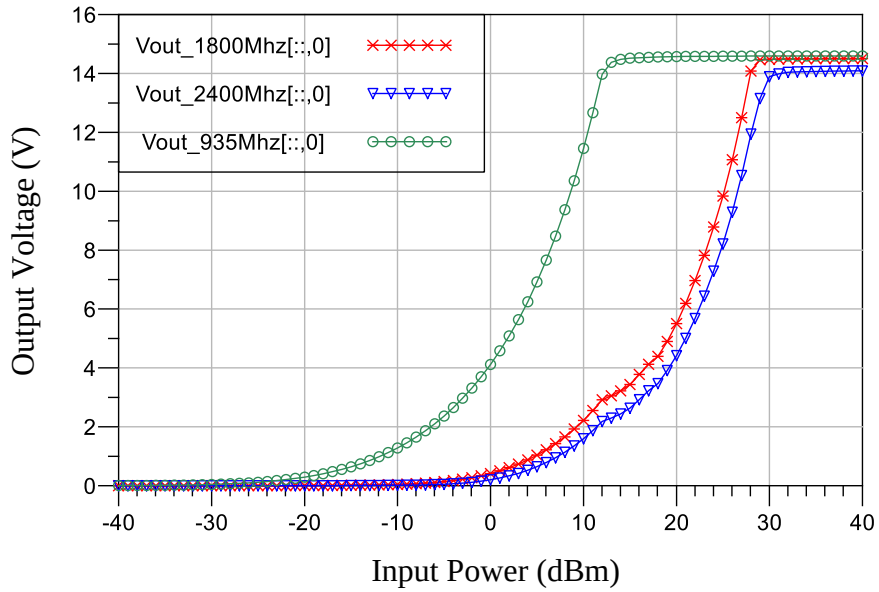

Figure 5.27: Multi-Band Energy harvesting output voltage.

Figure 5.28, describes multi-band rectifier efficiency versus input power from -40 dBm to 40 dBm. Figure 5.28 (a)shows the efficiency at 935MHz which is 43% at -10dBm and Figure 5.28 (b) shows the efficiency at 1800MHz which is 46% at 0dBm and Figure 5.28 (c) presents the efficiency at 2400MHz which is 30% at 18dBm.

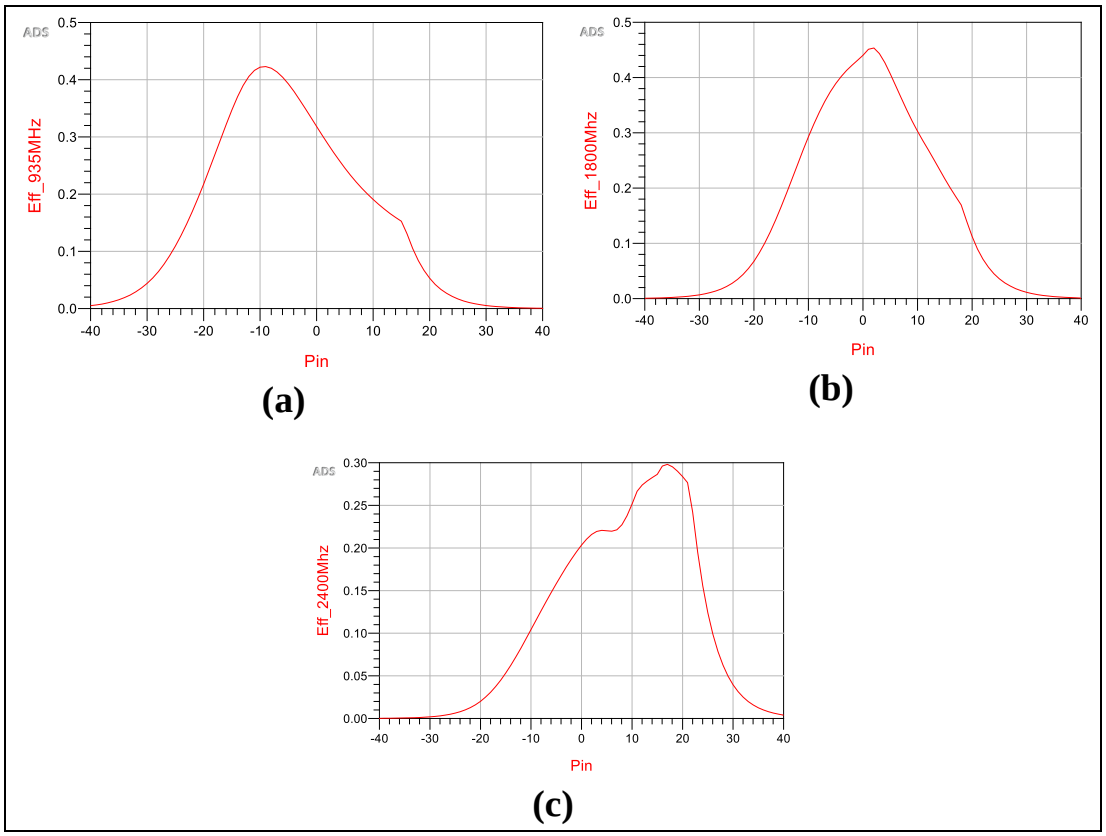

Figure 5.28: Multi-Band rectifier efficiency (a) efficiency at 935MHz (b) efficiency at 1800MHz (c) efficiency at 2400MHz

5.6.3 Multi-Band with Tapered matching

The tapered matching network aims at transforming the complex input impedance of the rectifier circuit into 50 ohms. Taper continuously varying characteristic impedance along its length. The multi-port rectifier system shows excellent harvesting capabilities with an increased output DC voltage.

5.6.3.1 Multi-Band four stages voltage doubler rectifiers

The energy harvesting system circuits are simulated using Agilent Advanced Design System 2016 (ADS2016) software. We use the harmonic balanced at analysis in this work it is a frequency domain method. Taper matching technique used at this design is shown in Figure 5.29 which describes multi-band four stages voltage doubler rectifiers, the load impedance that gave highest efficiency for this system is 30 KOhm.

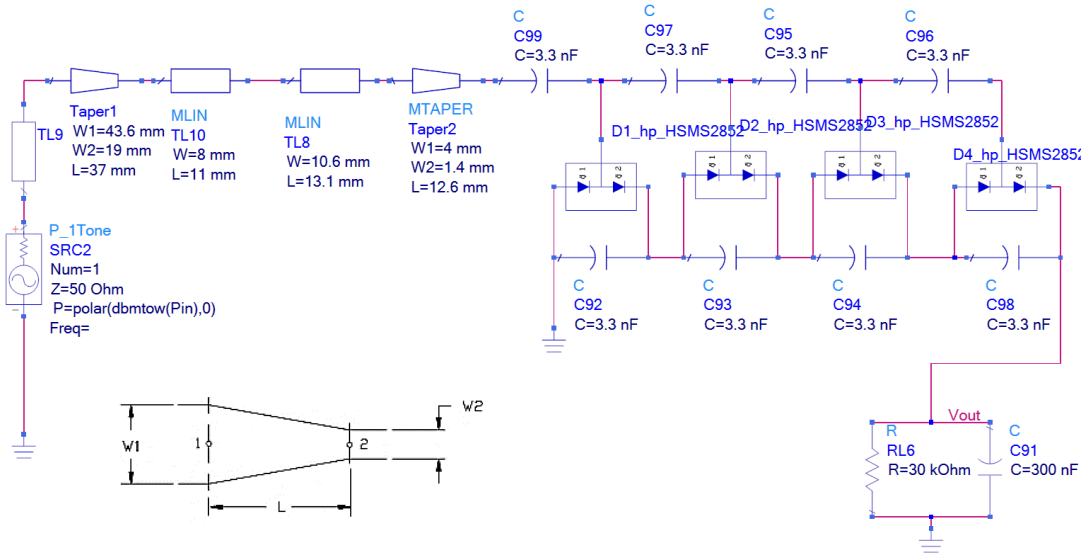

Figure 5.29: Multi-band four stages voltage doubler rectifiers.

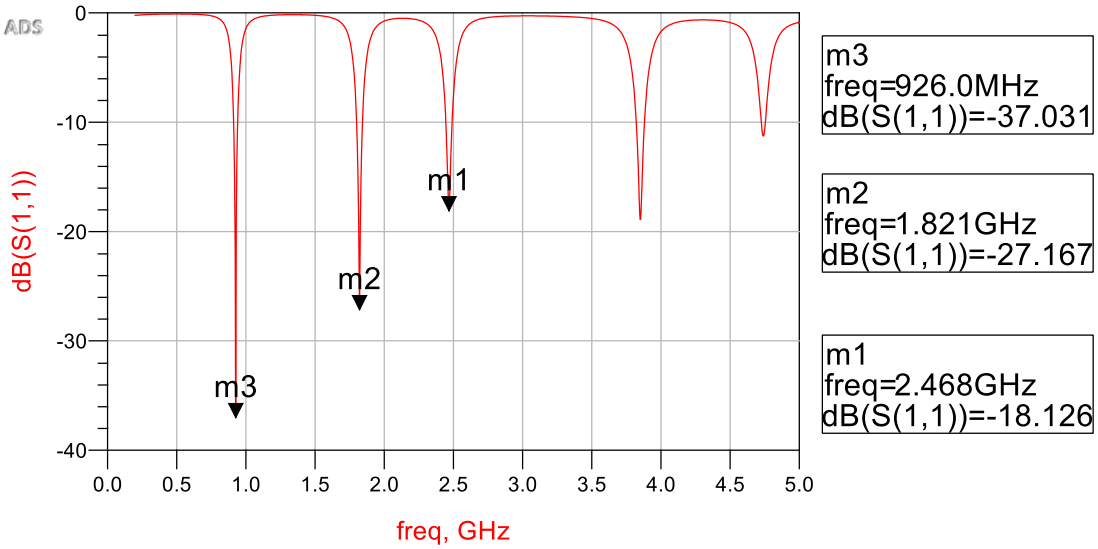

Figure 5.30: S_{11} for Multi-band four-stage rectifier with tapered matching

Results in Figure 5.30 describe S11 for Multi-band four stages voltage doubler rectifiers using the tapered matching. It is evident from the results that matching is achieved at the required frequency bands but with narrow bands.

We use frequency sweep to see the relation of efficiency for Multi-band four stages voltage doubler rectifiers. The results show that efficiency at the certain frequencies bands reached 60% at GSM900, 45% at GSM1800 and 22% at WiFi as shown at Figure 5.31.

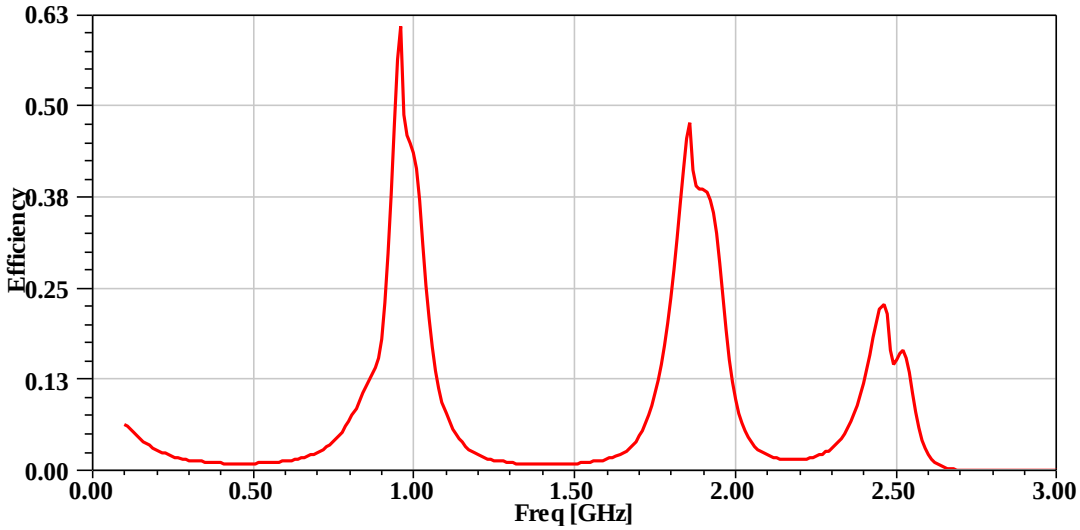

Figure 5.31: Efficiency for Multi-Band four stages voltage doubler rectifiers with tapered matching

The output voltage versus frequency is demonstrated at Figure 5.32 which shows the output voltage for the bands GSM900, GSM1800, UMTS, and WiFi. The output voltage for input power 0 dBm is 4.8v at GSM900, 4.2 at GSM1800 and 2.8 at WiFi band.

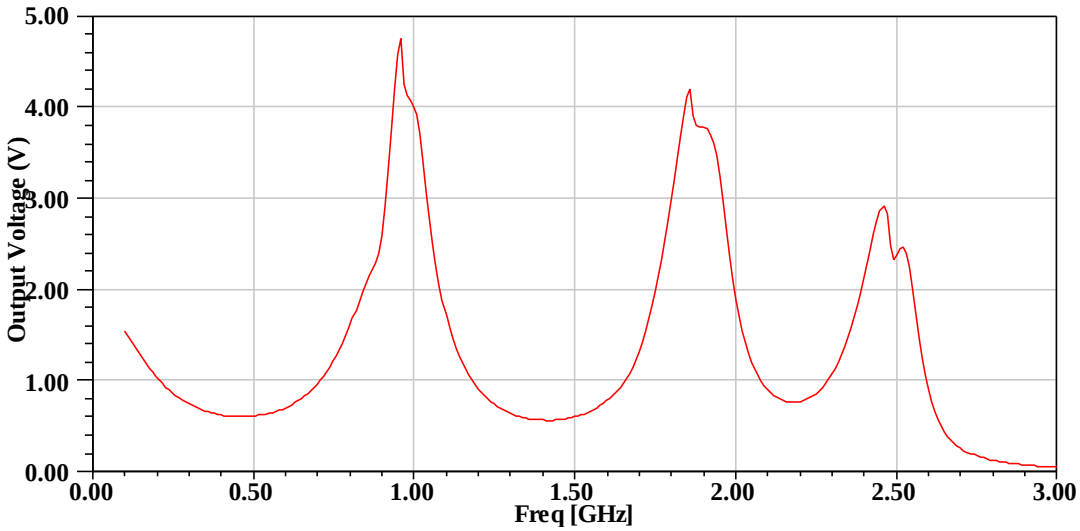

Figure 5.32: The output voltage for Multi-Band four-stage rectifier with tapered matching

Taking into consideration the effect of cupper lines connecting the diodes especially at high frequencies which they act as a capacitors and coils, so the next design is proposed.

5.6.3.2 Multi-Band two stages voltage doubler rectifiers

The design in Figure 5.33 considers all connections between the diodes as a transmission lines. Moreover, the number of stages is reduced to two stages so that the overall loss in diodes is reduced and hence increasing efficiency.

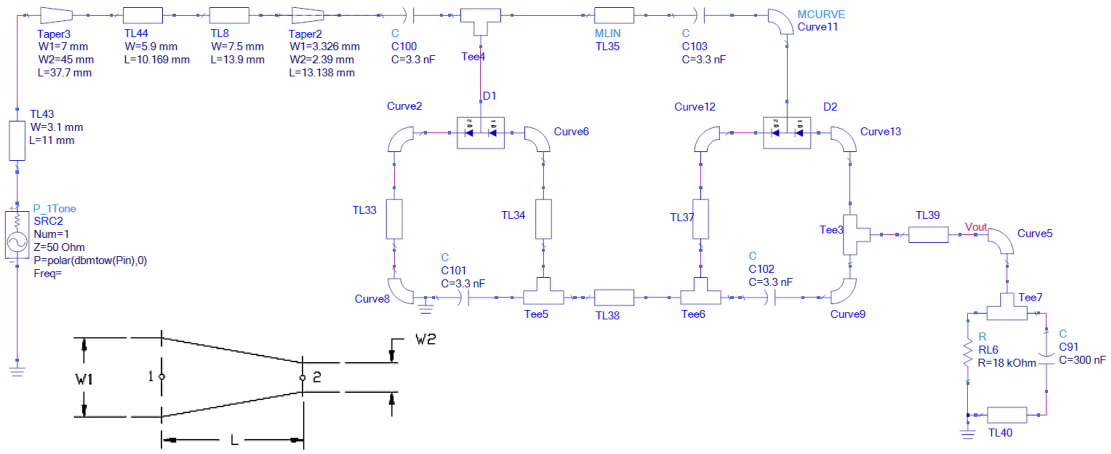

Figure 5.33: Multi-Band two-stages rectifier with taper matching

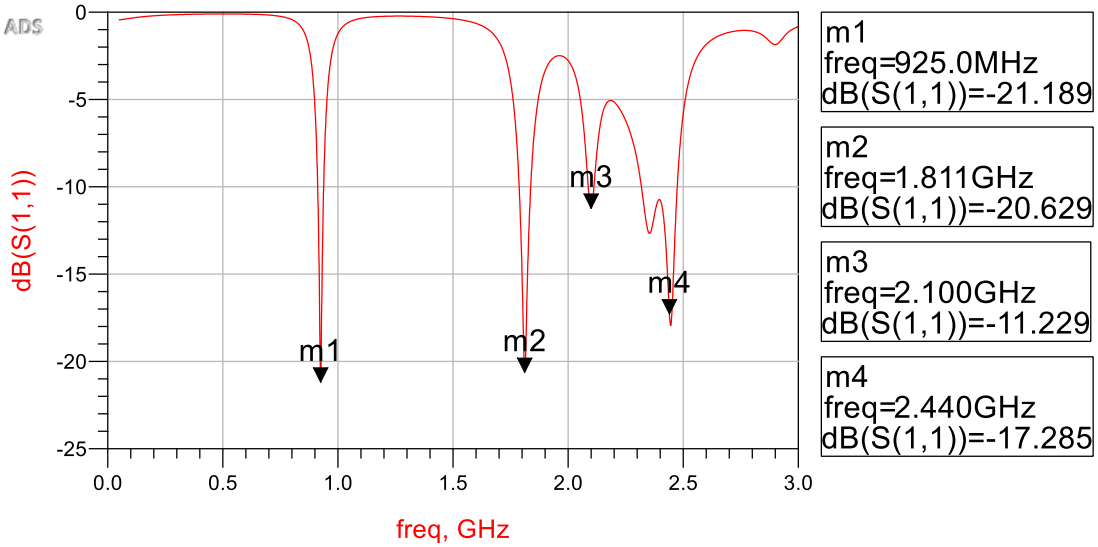

Figure 5.34: S_{11} for Multi-Band two-stage rectifier with taper matching

The simulated S11 for multi-band two-stage voltage doubler rectifier design is shown in Figure 5.34 which covered all required bands as shown with good bandwidth.

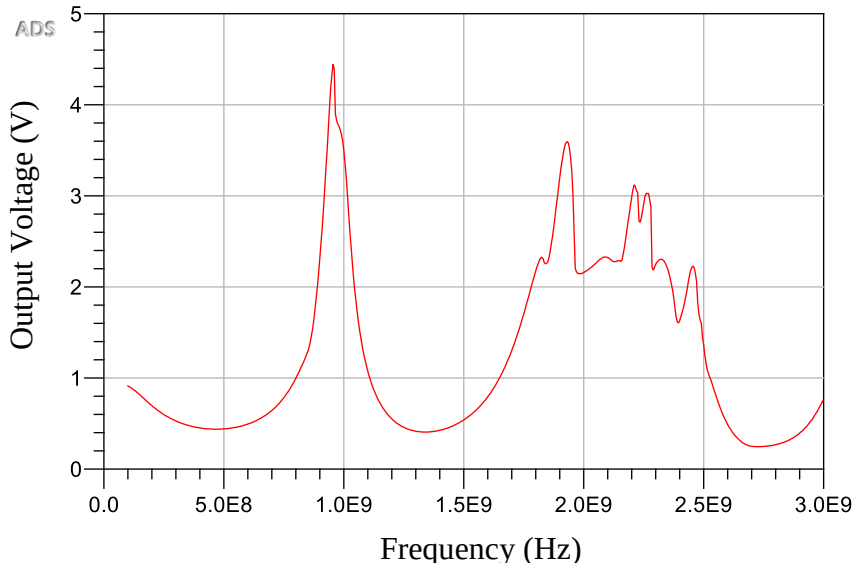

Figure 5.35: The output voltage for Multi-Band two-stage rectifier with taper matching

The output voltage versus frequency is demonstrated in Figure 5.35 which shows the output voltage for the bands GSM900, GSM1800, UMTS, and WiFi. The output voltage at 0dBm input power is 4.5V at GSM900, 3.8V at GSM1800, 3.2V at UMTS and 2.2V at WiFi band. Moreover, the efficiency is presented in Figure 5.36 and it is 67% at GSM900, 45% at GSM1800, 33% at UMTS and 18% at WiFi.

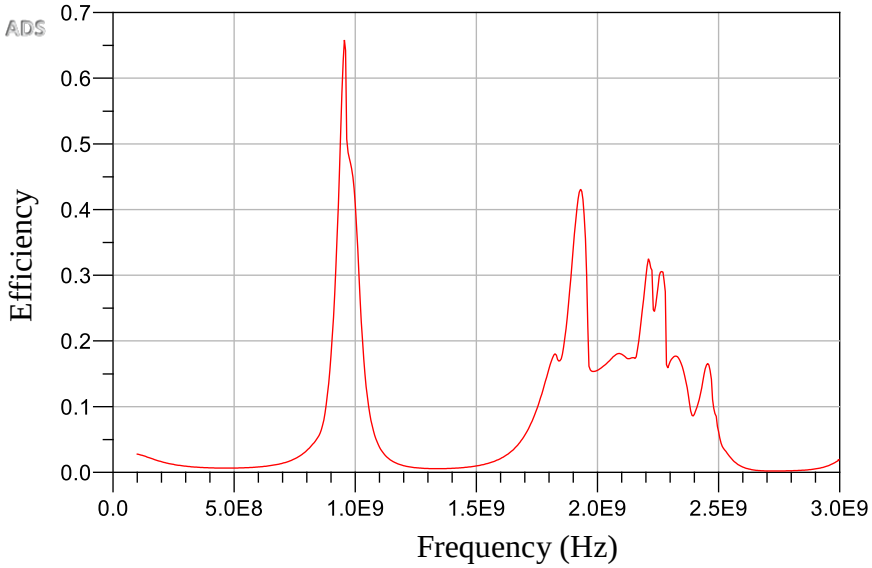

Figure 5.36: Efficiency for Multi-band two-stages rectifier with taper matching

5.6.3.3 Multi-Band rectifier with taper impedance matching

As in the previous design, the energy harvesting system circuits are simulated using Agilent Advanced Design System 2016 (ADS2016) software. Taper matching technique used at this design is shown in Figure 5.37 which describes multi-band four stages voltage doubler rectifiers, the load impedance that gave highest efficiency for this system is 16 KOhm.

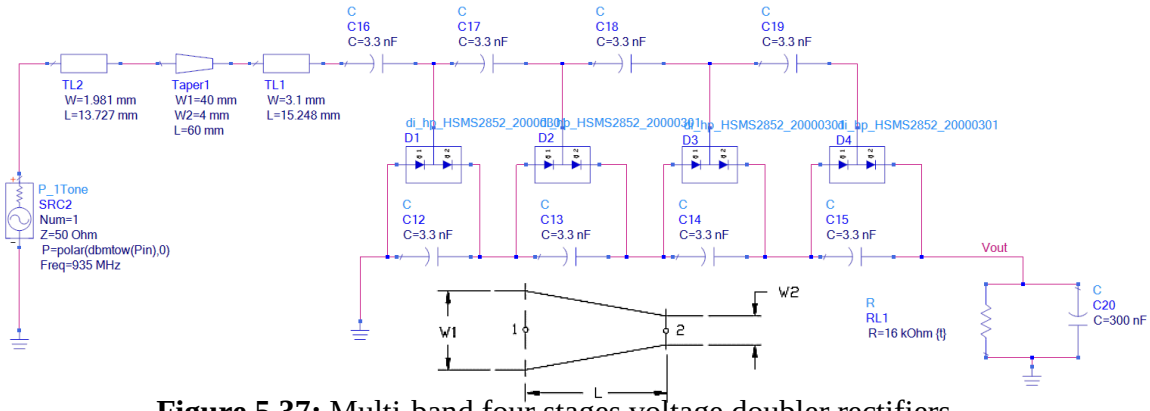

Figure 5.37: Multi-band four stages voltage doubler rectifiers.

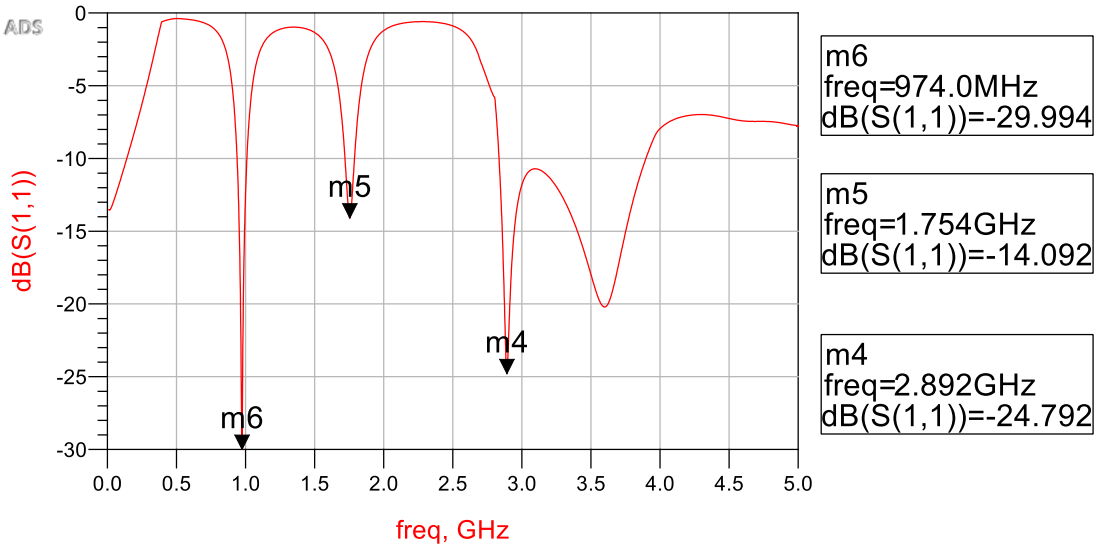

Figure 5.38: S_{11} for Multi-band four-stage rectifier with tapered matching

Results in Figure 5.38 describe S11 for Multi-band four stages voltage doubler rectifiers using the tapered matching. It is evident from the results that matching is achieved at the required frequency bands.

We use frequency sweep to see the relation of efficiency for Multi-band four stages voltage doubler rectifiers. The results show that efficiency at the certain frequencies bands reached 63% at GSM900, 38% at 1700MHz and 15% at WiFi as shown at Figure 5.39.

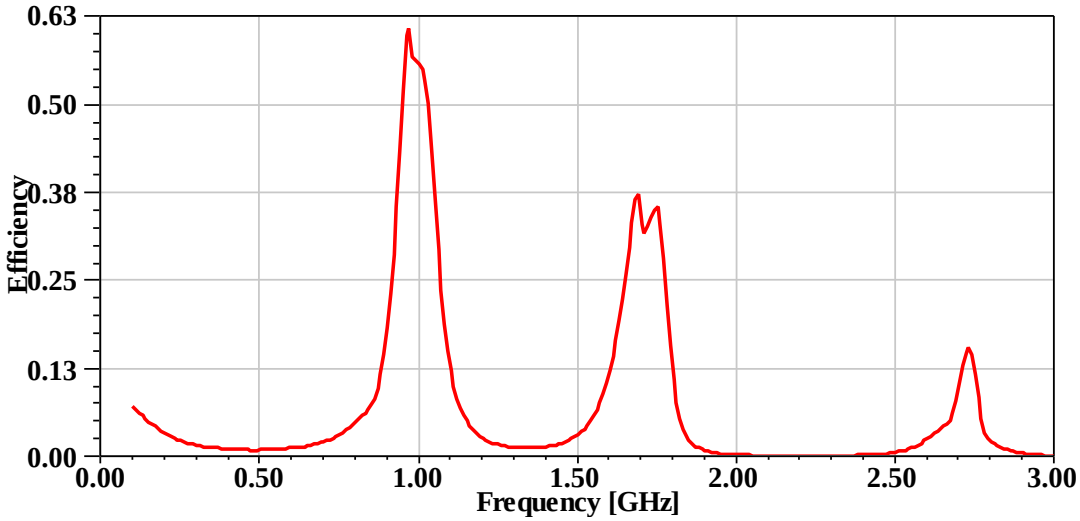

Figure 5.39: Efficiency for Multi-Band four stages voltage doubler rectifiers with tapered matching

The output voltage versus frequency is demonstrated at Figure 5.40 which shows the output voltage for the bands GSM900, GSM1800, and WiFi. The output voltage for input power 0 dBm is 4.7 v at GSM900, 3.4 at GSM1800 and 2.3 at WiFi band.

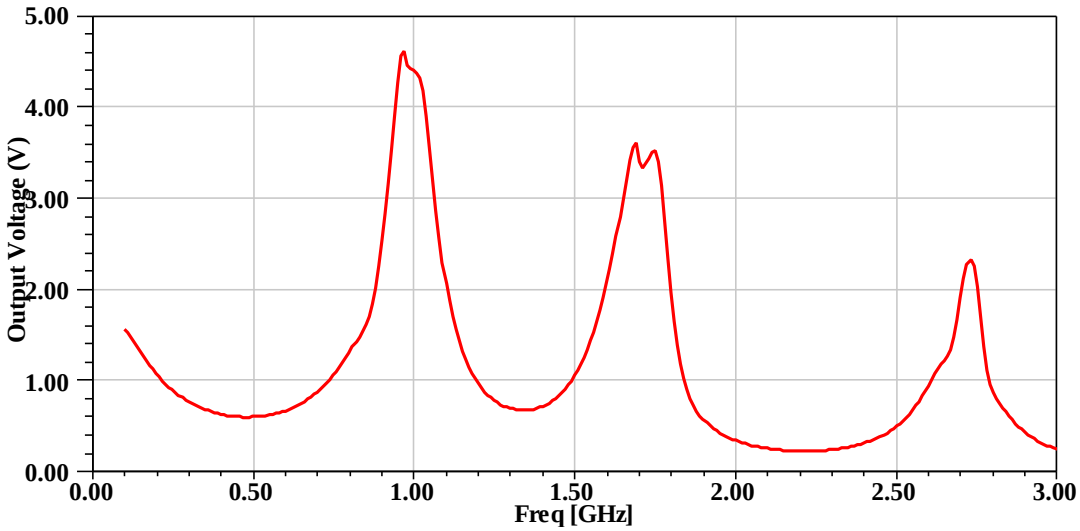

Figure 5.40: The output voltage for Multi-Band four-stage rectifier with tapered matching

5.6.3.4 Fabrication of Multi-Band rectifier with taper impedance matching

Multi-Band circuit with Tapered matching was designed using Agilent Advanced Design System (ADS) software and the circuit layout is depicted in Figure 5.41. The circuit was printed on FR-4 substrate and a photo of the fabricated circuits shown in Figure 5.42. The values of the parameters and the dimensions of the design are shown in table 5.2.

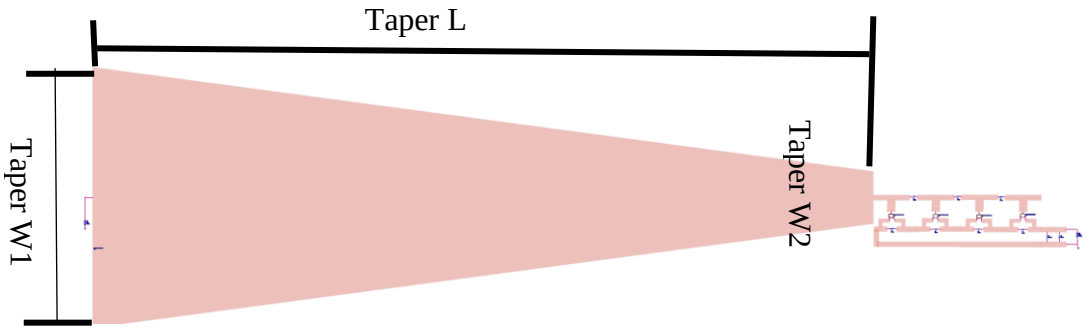

Figure 5.41: Layout of multi-band with Tapered matching designed using Agilent Advanced Design

Table 5.2: Multi-Band with Tapered matching parameters

Parameter	Value	Parameter	Value (mm)
C	33pF	RL	30 KΩ
Diode	HSMS2852	CL	300 nF
Taper L	43 mm	Pin	0 dBm
Taper w1	18 mm	Stages	4
Taper w2	5 mm	Zo	50Ω

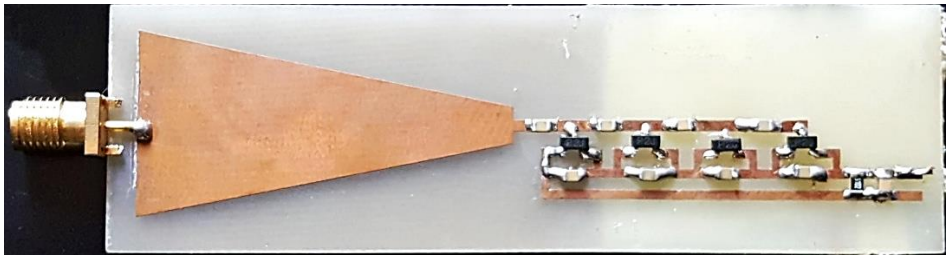

Figure 5.42: Fabricated of Multi-Band with Tapered matching

The simulated and measured results of S11 for Multi-Band rectifier with taper impedance matching compared as shown in Figure 5.43 with step of 5 MHz.

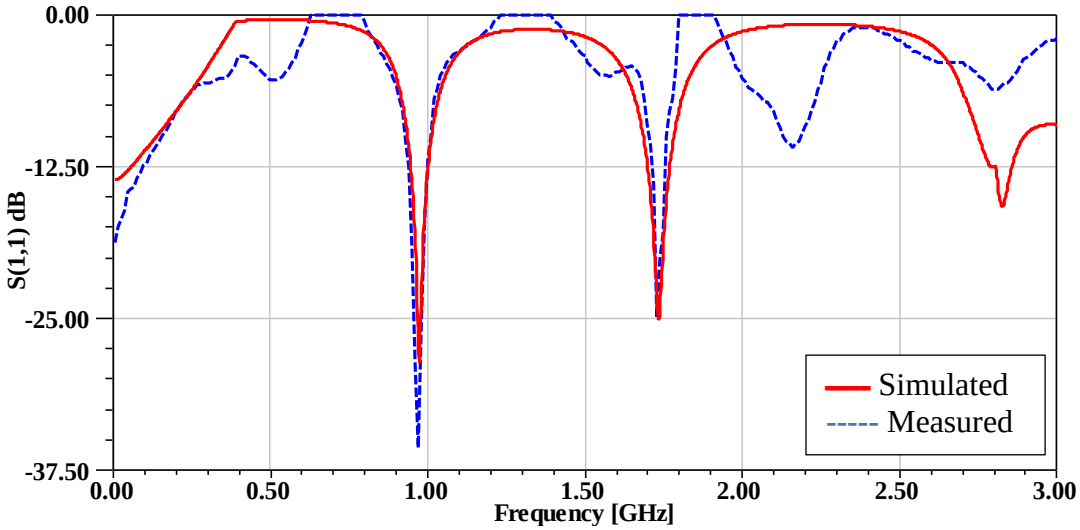

Figure 5.43: The simulated and measured results of S11 for Multi-Band rectifier with taper impedance matching

The output voltage at 0dBm was measured and it is shown in Figure 5.44 and compared with simulation results in Figure 5.45.

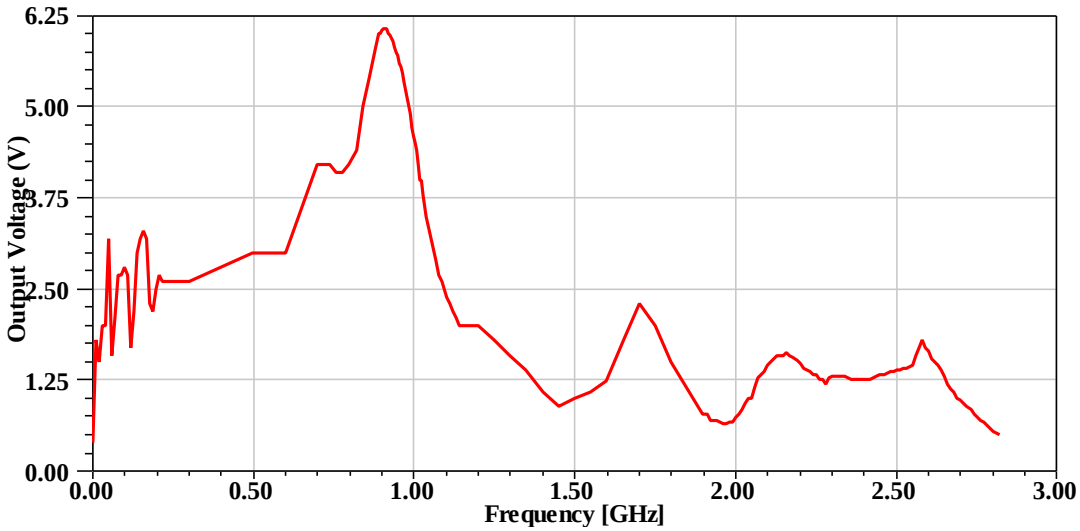

Figure 5.44: Measured output voltage at 0dBm for taper matching circuit

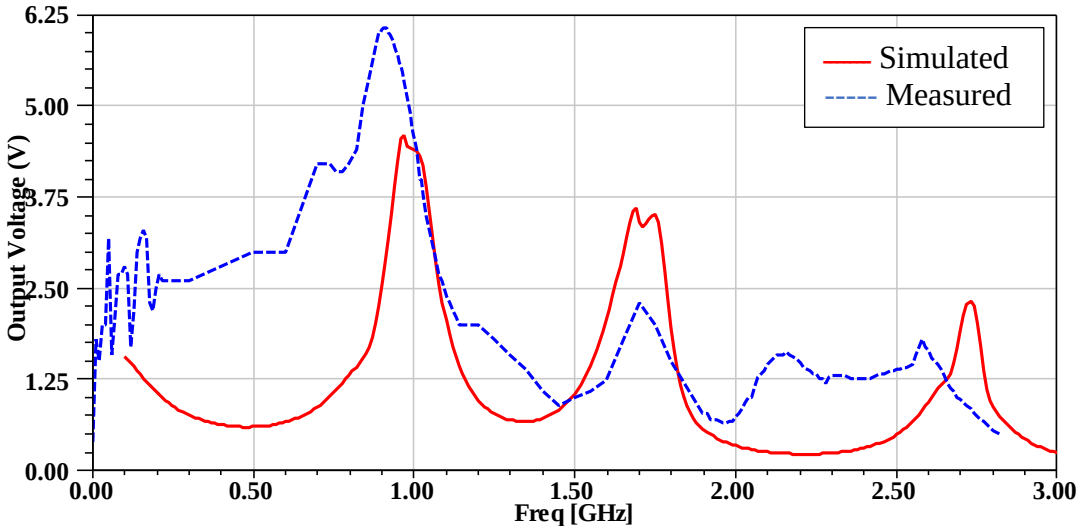

Figure 5.45: Measured output voltage compared with simulation results

From the plot in Figure 5.45 we can notice that the output voltage GSM900 is larger than simulation and the measurements show that output voltage at higher frequencies is smaller than simulated results. The output voltage is varying from 6.2V to 1V when we use 0dBm input power.

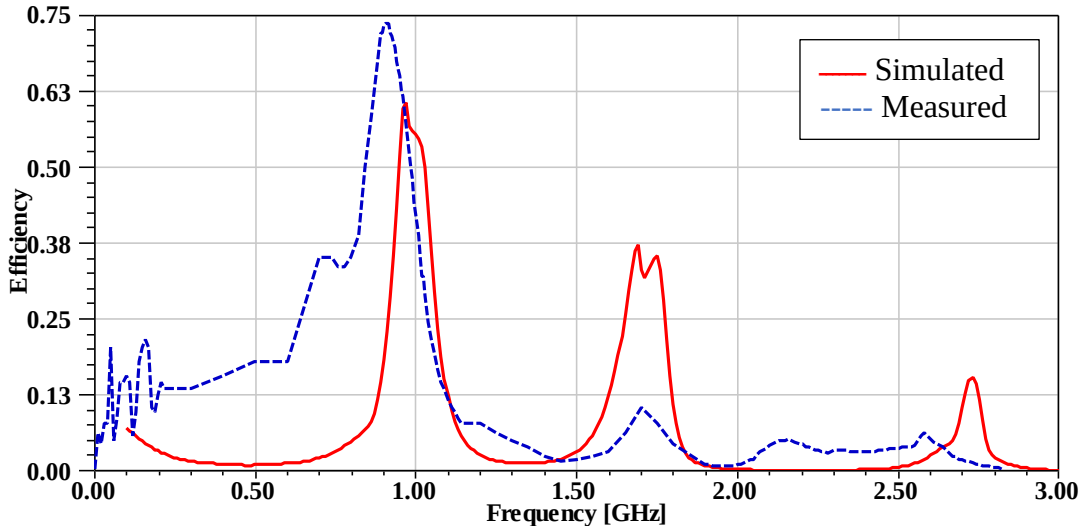

Figure 5.46: Measured efficiency compared with simulation results

We use frequency sweep to see the relation of efficiency for simulated and measured results of Multi-Band rectifier with taper impedance matching. The results show that efficiency at the certain frequencies bands reached 75% at GSM900, 13% at 1700MHz and 8% at WiFi as shown at Figure 5.46.

Chapter 6

Conclusions and Future Work

Chapter 6
Conclusions and Future Work

6.1 Conclusions

Multi-Band RF energy harvesting system has been designed for low power applications, which consists of three parts are Ultra-wideband antenna, Voltage doubler and rectifier connected into the load.

A broadband microstrip antenna is proposed for energy harvesting applications. The patch element is star-shaped conductor with two slots in the form of a crescent and a rectangle. The ground plane is cut underneath the patch to extend the bandwidth and thus enabling antenna to harvest more energy. The proposed antenna operates within the frequency range 790 MHz to 3.4 GHz and this range incorporates various wireless communications systems such as GSM, UMTS, LTE and WiFi. The realized gain is simulated over wide range and it reaches 3.93 dBi at 1.7 GHz and it is above 1.6 dBi within the range 900 MHz to 3.25 GHz. The radiation patterns are simulated at the operating frequencies of the given wireless systems and omni-directional patterns are obtained. The good performance of the antenna in terms of broad bandwidth, omni-directional radiation pattern and acceptable realized gain makes it a good candidate for energy harvesting.

A Multi-band voltage doubler rectifier have been designed for RF energy harvesting. With perfect matching circuit Tuned at design and fabricated for single and multi-band rectifier. Single band rectifier at GSM900 and Two new architectures have been designed covering the GSM900, GSM1800, UMTS, and WiFi bands. The fabricated prototype shows a 70% of RF-to-dc conversion efficiency at 0-dBm input power set on the RF branches. At rectifier circuit many matching techniques used, the first design L and T-Lumped element matching used for single band and multi-band rectifiers, and on the second design Taper matching technique used, taper matching technique is less costly and more efficient than Lumped element matching because it need only one stuff of four stage rectifiers but the other need three.

6.2 Future Work

In the future, it is good to focus on one type of rectifiers matching and make studies about DC combiner to collect highest voltage from all bands.

Moreover, it is important to design the energy harvesting system for the realized energy required for physical devices.

Rectennas for multi-band can be designed and fabricated by using flexible substrates like paper and textile. These give us more flexibility and wide at use.

Finally, Indoor measurements must be done to experiment the system range of work.

The Reference List

Arrawatia, M., Baghini, M. S., & Kumar, G. (2016). Broadband bent triangular omnidirectional antenna for RF energy harvesting. *IEEE Antennas and Wireless Propagation Letters, 15*(1), 36-39.

Balanis, C. A. (2005). Antenna Theory, Hoboken. *New Jersey: John Wiley & Sons, Inc, 8*(1), 21-31.

Barnett, R., Lazar, S., & Liu, J. (2006). *Design of multistage rectifiers with low-cost impedance matching for passive RFID tags.* Paper presented at the Radio Frequency Integrated Circuits (RFIC) Symposium, 2006 IEEE.

Belo, D., & Carvalho, N. B. (2014). *Behavior of multi-band RF-DC converters in presence of modulated signals for space based wireless sensors.* Paper presented at the Microwave Conference (APMC), 2014 Asia-Pacific.

Borges, L. M., Barroca, N., Saraiva, H. M., Tavares, J., Gouveia, P. T., Velez, F. J., . . . Gonçalves, R. (2014). *Design and evaluation of multi-band RF energy harvesting circuits and antennas for WSNs.* Paper presented at the Telecommunications (ICT), 2014 21st International Conference on.

Bouchouicha, D., Dupont, F., Latrach, M., & Ventura, L. (2010). *Ambient RF energy harvesting.* Paper presented at the International Conference on Renewable Energies and Power Quality.

Curty, J.-P., Joehl, N., Dehollain, C., & Declercq, M. J. (2005). Remotely powered addressable UHF RFID integrated system. *IEEE Journal of Solid-State Circuits, 40*(11), 2193-2202.

Didouh, S., Abri, M., & Bendimerad, F. (2012). Corporate-feed multilayer bow-tie antenna array design using a simple transmission line model. *Modelling and Simulation in Engineering, 2012*(1), 41.

Frenzel, L. (2011). Back to Basics: Impedance Matching (Part 1). *Consulté le, 1*(2016), 06.

Frenzel, L. E. (2004). *RF Power for Industrial Applications*: Pearson/Prentice Hall.

Gaur, S. M., Zwolinski, M., Laxmi, V., Boolchandani, D., Sing, V., & Singh, A. (2013). *VLSI Design and Test: 17th International Symposium, VDAT 2013, Jaipur, India, July 27-30, 2013, Proceedings* (Vol. 382): Springer.

Hoang, M. H., Phan, H. P., Van Hoang, T. Q., & Vuong, T.-P. (2014). *Efficient compact dual-band antennas for GSM and Wi-Fi energy harvesting.* Paper presented at the Advanced Technologies for Communications (ATC), 2014 International Conference on.

Huang, Y., & Boyle, K. (2008). *Antennas: from theory to practice* (1 ed.): John Wiley & Sons.

Huurdeman, A. A. (2003). *The worldwide history of telecommunications* (1 ed.): John wiley & sons.

Jie, A. M., Karim, M. F., Bin, L., Chin, F., & Ong, M. (2016). *A proximity-coupled circularly polarized slotted-circular patch antenna for RF energy harvesting applications.* Paper presented at the Region 10 Conference (TENCON), 2016 IEEE.

Keyrouz, S., Visser, H., & Tijhuis, A. (2013). *Multi-band simultaneous radio frequency energy harvesting.* Paper presented at the Antennas and Propagation (EuCAP), 2013 7th European Conference on.

Khan, M. S., & Deng, H. (2016). *Design and implementation of a highly efficient UHF energy harvesting antenna.* Paper presented at the Antennas and Propagation (APSURSI), 2016 IEEE International Symposium on.

Khansalee, E., Zhao, Y., Leelarasmee, E., & Nuanyai, K. (2014). *A dual-band rectifier for RF energy harvesting systems.* Paper presented at the Electrical Engineering/Electronics, Computer, Telecommunications and Information Technology (ECTI-CON), 2014 11th International Conference on.

Khansalee, E., Zhao, Y., & Nuanyai, K. (2015). *High frequency rectifier for RF energy harvesting systems.* Paper presented at the Information Technology and Electrical Engineering (ICITEE), 2015 7th International Conference on.

Khonsari, Z., Björninen, T., Tentzeris, M. M., Sydänheimo, L., & Ukkonen, L. (2015). *2.4 GHz inkjet-printed RF energy harvester on bulk cardboard substrate.* Paper presented at the Radio and Wireless Symposium (RWS), 2015 IEEE.

Kitazawa, S., Ban, H., & Kobayashi, K. (2012). *Energy harvesting from ambient RF sources.* Paper presented at the Microwave Workshop Series on Innovative Wireless Power Transmission: Technologies, Systems, and Applications (IMWS), 2012 IEEE MTT-S International.

Kuhn, V., Lahuec, C., Seguin, F., & Person, C. (2015). A multi-band stacked RF energy harvester with RF-to-DC efficiency up to 84%. *IEEE Transactions on Microwave Theory and Techniques, 63*(5), 1768-1778.

Kumar, S. V., Patel, P., Mittal, A., & De, A. (2012). *Design, analysis and fabrication of rectenna for wireless power transmission-Virtual battery.* Paper presented at the Communications (NCC), 2012 National Conference on.

Le, T., Mayaram, K., & Fiez, T. (2008). Efficient far-field radio frequency energy harvesting for passively powered sensor networks. *IEEE Journal of Solid-State Circuits, 43*(5), 1287-1302.

Maher, R., Tammam, E., Galal, A. I., & Hamed, H. F. (2016). *Design of a broadband planar antenna for RF energy harvesting.* Paper presented at the Electrical, Electronics, and Optimization Techniques (ICEEOT), International Conference on.

Mathur, M., Agarwal, A., Singh, G., & Bhatnagar, S. (2016). *The array structure of 2× 2 coplanar monopole antenna with Wilkinson power combiner for RF energy harvesting application.* Paper presented at the Recent Advances and Innovations in Engineering (ICRAIE), 2016 International Conference on.

Mitcheson, P. D., Yeatman, E. M., Rao, G. K., Holmes, A. S., & Green, T. C. (2008). Energy harvesting from human and machine motion for wireless electronic devices. *Proceedings of the IEEE, 96*(9), 1457-1486.

Paradiso, J. A., & Starner, T. (2005). Energy scavenging for mobile and wireless electronics. *IEEE Pervasive computing, 4*(1), 18-27.

Pham, B. L., & Pham, A.-V. (2013). *Triple bands antenna and high efficiency rectifier design for RF energy harvesting at 900, 1900 and 2400 MHz.* Paper presented at the Microwave Symposium Digest (IMS), 2013 IEEE MTT-S International.

Poranki, K. R., Perwej, Y., & Perwej, A. (2015). The Level of Customer Satisfaction related to GSM in India. *Research Journal of Science & IT Management, 4*(3), 30-36.

Pozar, D. M. (2012). Microwave Engineering. 4th (4 ed.): Wiley.

Prittopaul, P., & Shankarram, N. Trust Aware Secure Routing for Cluster-based Wireless Sensor Networks-A Comparative Study. (1).
Raina, V. K. (2017). *NFC Payment Systems and the New Era of Transaction Processing* (1 ed.): IGI Global.
Ren, Y.-J., & Chang, K. (2006). 5.8-GHz circularly polarized dual-diode rectenna and rectenna array for microwave power transmission. *IEEE Transactions on Microwave Theory and Techniques, 54*(4), 1495-1502.
Saad-Bin-Alam, M., & Moury, S. (2014). *Multiple-band antenna coupled rectifier circuit for ambient RF energy harvesting for WSN.* Paper presented at the Informatics, Electronics & Vision (ICIEV), 2014 International Conference on.
Sadiku, M. N. (2014). *Elements of electromagnetics* (1 ed.): Oxford university press.
Samukic, A. (1998). *UMTS universal mobile telecommunications system: development of standards for the third generation.* Paper presented at the Global Telecommunications Conference, 1998. GLOBECOM 1998. The Bridge to Global Integration. IEEE.
Saraswati, S., & Agrawal, N. (2016). Improvement of the Performance of Microstrip Patch Antenna. *International Journal of Computer Applications, 148*(10).
Sarma, S. S., & Akhtar, M. J. (2016). *A dual band meandered printed dipole antenna for RF energy harvesting applications.* Paper presented at the Antennas and Propagation (APCAP), 2016 IEEE 5th Asia-Pacific Conference on.
Shahzad, K. (2013). *Scheduling in energy harvesting systems with hybrid energy storage.* University of Maryland, College Park.
Song, N. S., Chin, K. L., Liang, D. B. B., & Anyi, M. (2006). *Design of broadband dual-frequency microstrip patch antenna with modified sierpinski fractal geometry.* Paper presented at the Communication systems, 2006. ICCS 2006. 10th IEEE Singapore International Conference on.
Stiles, J. (2010). Tapered Lines. from http://www.ittc.ku.edu/~jstiles/723/handouts/section_5_8_Tapered_Lines_package.pdf
Sun, H., Guo, Y.-x., He, M., & Zhong, Z. (2013). A dual-band rectenna using broadband yagi antenna array for ambient RF power harvesting. *IEEE Antennas and Wireless Propagation Letters, 12*(1), 918-921.
Tawk, Y., Ayoub, F., Christodoulou, C., & Costantine, J. (2015). *An array of inverted-F antennas for RF energy harvesting.* Paper presented at the Antennas and Propagation & USNC/URSI National Radio Science Meeting, 2015 IEEE International Symposium on.
Technologies, A. (1999). HSMS-2850 Series "Surface Mount Zero Bias Schottky Detector Diodes". (1).
Thidé, B. (2004). *Electromagnetic field theory* (1 ed.): Upsilon Books Uppsala.
Varma, V. K. (2012). Wireless Fidelity—WiF. from https://www.ieee.org/about/technologies/emerging/wifi.pdf
Wang, D., & Negra, R. (2014). *Novel TriBand RF Rectifier Design for Wireless Energy Harvesting.* Paper presented at the Microwave Conference (GeMIC), 2014 German.
Wang, J., Gao, Q., Yu, Y., Wang, H., & Jin, M. (2012). Radio-triggered power management in wireless sensor networks *Wireless Sensor Networks-Technology and Applications* (1 ed.): InTech.

Wang, X., Zhao, Z., Chen, G., & He, F. (2014). *RF energy harvesting with broadband antenna.* Paper presented at the Transportation Electrification Asia-Pacific (ITEC Asia-Pacific), 2014 IEEE Conference and Expo.

Wen, J., Xie, D., Liu, X., Guo, H., Liu, C., & Yang, X. (2016). *Wideband collar-shaped antenna for RF energy harvesting.* Paper presented at the Electromagnetic Compatibility (APEMC), 2016 Asia-Pacific International Symposium on.

Zainuddin, N., Zakaria, Z., Husain, M., Derus, B. M., Aziz, M. A., Mutalib, M., & Othman, M. (2013). *Design of wideband antenna for RF energy harvesting system.* Paper presented at the Instrumentation, Communications, Information Technology, and Biomedical Engineering (ICICI-BME), 2013 3rd International Conference on.

Zakaria, Z., Zainuddin, N., Aziz, M. A., Husain, M., & Mutalib, M. (2013). *Dual-band monopole antenna for energy harvesting system.* Paper presented at the Wireless Technology and Applications (ISWTA), 2013 IEEE Symposium on.

Zheng, C., & Li, T. (2011). *Development of an exponential tapered impedance transformer for UHF-PD sensor.* Paper presented at the Electric Power Equipment-Switching Technology (ICEPE-ST), 2011 1st International Conference on.

Zhou, Z., Liao, W., Zhang, Q., Han, F., & Chen, Y. (2016). *A multi-band fractal antenna for RF energy harvesting.* Paper presented at the Antennas and Propagation (APSURSI), 2016 IEEE International Symposium on.

Appendix 1:

Surface Mount Zero Bias Schottky Detector Diodes

HSMS-2850 Series

Agilent Technologies
Innovating the HP Way

Surface Mount Zero Bias Schottky Detector Diodes

Technical Data

HSMS-2850 Series

Features

- Surface Mount SOT-23/ SOT-143 Packages
- Miniature SOT-323 and SOT-363 Packages
- High Detection Sensitivity: up to 50 mV/µW at 915 MHz
- Low Flicker Noise: -162 dBV/Hz at 100 Hz
- Low FIT (Failure in Time) Rate*
- Tape and Reel Options Available
- Matched Diodes for Consistent Performance
- Better Thermal Conductivity for Higher Power Dissipation

* For more information see the Surface Mount Schottky Reliability Data Sheet.

Pin Connections and Package Marking

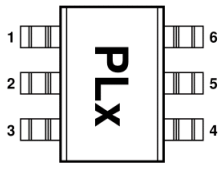

Notes:
1. Package marking provides orientation and identification.
2. See "Electrical Specifications" for appropriate package marking.

SOT-23/SOT-143 Package Lead Code Identification (top view)

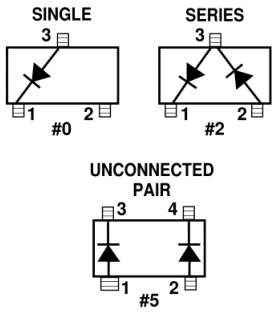

SOT-323 Package Lead Code Identification (top view)

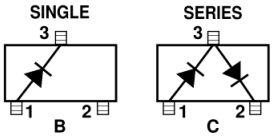

SOT-363 Package Lead Code Identification (top view)

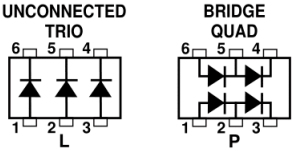

Description

Agilent's HSMS-285x family of zero bias Schottky detector diodes has been designed and optimized for use in small signal (P_{in} <-20 dBm) applications at frequencies below 1.5 GHz. They are ideal for RF/ID and RF Tag applications where primary (DC bias) power is not available.

Important Note: For detector applications with input power levels greater than –20 dBm, use the HSMS-282x series at frequencies below 4.0 GHz, and the HSMS-286x series at frequencies above 4.0 GHz. The HSMS-285x series IS NOT RECOMMENDED for these higher power level applications.

Available in various package configurations, these detector diodes provide low cost solutions to a wide variety of design problems. Agilent's manufacturing techniques assure that when two diodes are mounted into a single package, they are taken from adjacent sites on the wafer, assuring the highest possible degree of match.

SOT-23/SOT-143 DC Electrical Specifications, T_C = +25°C, Single Diode

Part Number HSMS-	Package Marking Code[1]	Lead Code	Configuration	Maximum Forward Voltage V_F (mV)		Typical Capacitance C_T (pF)
2850 2852 2855	P0 P2 P5	0 2 5	Single Series Pair[2,3] Unconnected Pair[2,3]	150	250	0.30
Test Conditions				I_F = 0.1 mA	I_F = 1.0 mA	V_R = –0.5 V to –1.0V f = 1 MHz

Notes:
1. Package marking code is in white.
2. ΔV_F for diodes in pairs is 15.0 mV maximum at 1.0 mA.
3. ΔC_T for diodes in pairs is 0.05 pF maximum at –0.5 V.

SOT-323/SOT-363 DC Electrical Specifications, T_C = +25°C, Single Diode

Part Number HSMS-	Package Marking Code[1]	Lead Code	Configuration	Maximum Forward Voltage V_F (mV)		Typical Capacitance C_T (pF)
285B 285C 285L 285P	P0 P2 PL PP	B C L P	Single[2] Series Pair[2,3] Unconnected Trio Bridge Quad	150	250	0.30
Test Conditions				I_F = 0.1 mA	I_F = 1.0 mA	V_R = 0.5 V to –1.0V f = 1 MHz

Notes:
1. Package marking code is laser marked.
2. ΔV_F for diodes in pairs is 15.0 mV maximum at 1.0 mA.
3. ΔC_T for diodes in pairs is 0.05 pF maximum at –0.5 V.

RF Electrical Specifications, T_C = +25°C, Single Diode

Part Number HSMS-	Typical Tangential Sensitivity TSS (dBm) @ f = 915 MHz	Typical Voltage Sensitivity γ (mV/µW) @ f = 915 MHz	Typical Video Resistance RV (KΩ)
2850 2852 2855 285B 285C 285L 285P	–57	40	8.0
Test Conditions	Video Bandwidth = 2 MHz Zero Bias	Power in = –40 dBm R_L = 100 KΩ, Zero Bias	Zero Bias

Absolute Maximum Ratings, T_C = +25°C, Single Diode

Symbol	Parameter	Unit	Absolute Maximum[1]	
			SOT-23/143	SOT-323/363
P_{IV}	Peak Inverse Voltage	V	2.0	2.0
T_J	Junction Temperature	°C	150	150
T_{STG}	Storage Temperature	°C	-65 to 150	-65 to 150
T_{OP}	Operating Temperature	°C	-65 to 150	-65 to 150
θ_{jc}	Thermal Resistance[2]	°C/W	500	150

ESD WARNING: Handling Precautions Should Be Taken To Avoid Static Discharge.

Notes:
1. Operation in excess of any one of these conditions may result in permanent damage to the device.
2. T_C = +25°C, where T_C is defined to be the temperature at the package pins where contact is made to the circuit board.

Equivalent Linear Circuit Model

HSMS-285x chip

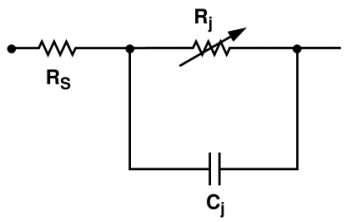

R_S = series resistance (see Table of SPICE parameters)

C_j = junction capacitance (see Table of SPICE parameters)

$$R_j = \frac{8.33 \times 10^{-5}\ nT}{I_b + I_s}$$

where

I_b = externally applied bias current in amps

I_s = saturation current (see table of SPICE parameters)

T = temperature, °K

n = ideality factor (see table of SPICE parameters)

Note:

To effectively model the packaged HSMS-285x product, please refer to Application Note AN1124.

SPICE Parameters

Parameter	Units	HSMS-285x
B_V	V	3.8
C_{J0}	pF	0.18
E_G	eV	0.69
I_{BV}	A	3 E-4
I_S	A	3 E-6
N		1.06
R_S	Ω	25
P_B (V_J)	V	0.35
P_T (XTI)		2
M		0.5

Typical Parameters, Single Diode

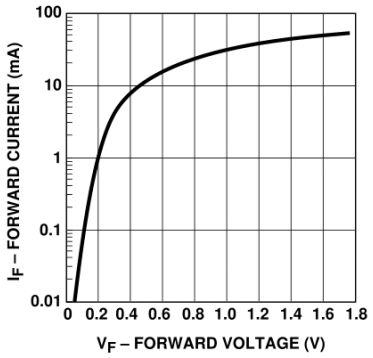

Figure 1. Typical Forward Current vs. Forward Voltage.

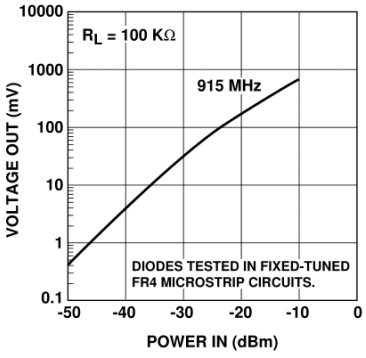

Figure 2. +25°C Output Voltage vs. Input Power at Zero Bias.

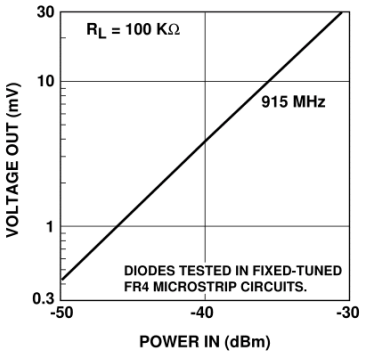

Figure 3. +25°C Expanded Output Voltage vs. Input Power. See Figure 2.

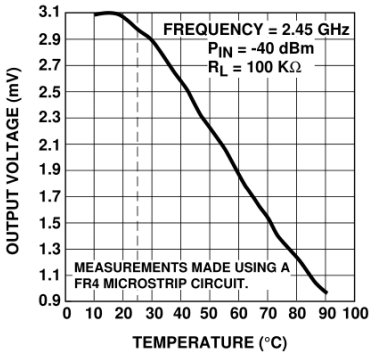

Figure 4. Output Voltage vs. Temperature.

Applications Information

Introduction

Agilent's HSMS-285x family of Schottky detector diodes has been developed specifically for low cost, high volume designs in small signal (P_{in} < -20 dBm) applications at frequencies below 1.5 GHz. At higher frequencies, the DC biased HSMS-286x family should be considered.

In large signal power or gain control applications (P_{in} > -20 dBm), the HSMS-282x and HSMS-286x products should be used. The HSMS-285x zero bias diode is not designed for large signal designs.

Schottky Barrier Diode Characteristics

Stripped of its package, a Schottky barrier diode chip consists of a metal-semiconductor barrier formed by deposition of a metal layer on a semiconductor. The most common of several different types, the passivated diode, is shown in Figure 5, along with its equivalent circuit.

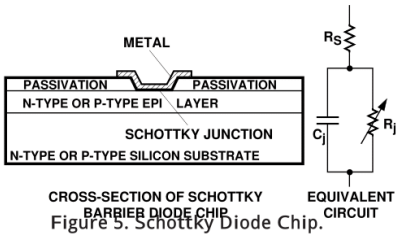

Figure 5. Schottky Diode Chip.

R_S is the parasitic series resistance of the diode, the sum of the bondwire and leadframe resistance, the resistance of the bulk layer of silicon, etc. RF energy coupled into R_S is lost as heat—it does not contribute to the rectified output of the diode. C_J is parasitic junction capacitance of the diode, controlled by the thickness of the epitaxial layer and the diameter of the Schottky contact. R_j is the junction resistance of the diode, a function of the total current flowing through it.

$$R_j = \frac{8.33 \times 10^{-5}\, n\, T}{I_S + I_b} = R_V - R_s$$

$$= \frac{0.026}{I_S + I_b} \text{ at } 25°C$$

where

n = ideality factor (see table of SPICE parameters)
T = temperature in °K
I_S = saturation current (see table of SPICE parameters)
I_b = externally applied bias current in amps

I_S is a function of diode barrier height, and can range from picoamps for high barrier diodes to as much as 5 µA for very low barrier diodes.

The Height of the Schottky Barrier

The current-voltage characteristic of a Schottky barrier diode at room temperature is described by the following equation:

$$I = I_S \left(\exp\left(\frac{V - IR_S}{0.026}\right) - 1\right)$$

On a semi-log plot (as shown in the Agilent catalog) the current graph will be a straight line with inverse slope 2.3 X 0.026 = 0.060 volts per cycle (until the effect of R_S is seen in a curve that droops at high current). All Schottky diode curves have the same slope, but not necessarily the same value of current for a given voltage. This is determined by the saturation current, I_S, and is related to the barrier height of the diode.

Through the choice of p-type or n-type silicon, and the selection of metal, one can tailor the characteristics of a Schottky diode. Barrier height will be altered, and at the same time C_J and R_S will be changed. In general, very low barrier height diodes (with high values of I_S, suitable for zero bias applications) are realized on p-type silicon. Such diodes suffer from higher values of R_S than do the n-type. Thus, p-type diodes are generally reserved for small signal detector applications (where very high values of R_V swamp out high R_S) and n-type diodes are used for mixer applications (where high L.O. drive levels keep R_V low).

Measuring Diode Parameters

The measurement of the five elements which make up the low frequency equivalent circuit for a packaged Schottky diode (see Figure 6) is a complex task. Various techniques are used for each element. The task begins with the elements of the diode chip itself.

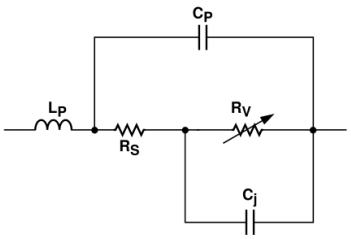

FOR THE HSMS-285x SERIES
C_P = 0.08 pF
L_P = 2 nH
C_j = 0.18 pF
R_S = 25 Ω
R_V = 9 KΩ

Figure 6. Equivalent Circuit of a Schottky Diode.

R_S is perhaps the easiest to measure accurately. The V-I curve is measured for the diode under forward bias, and the slope of the curve is taken at some relatively high value of current (such as 5 mA). This slope is converted into a resistance R_d.

$$R_S = R_d - \frac{0.026}{I_f}$$

R_V and C_J are very difficult to measure. Consider the impedance of C_J = 0.16 pF when measured at 1 MHz — it is approximately 1 MΩ. For a well designed zero bias Schottky, R_V is in the range of 5 to 25 KΩ, and it shorts out the junction capacitance. Moving up to a higher frequency enables the measurement of the capacitance, but it then shorts out the video resistance. The best measurement technique is to mount the diode in series in a 50 Ω microstrip test circuit and measure its insertion loss at low power levels (around -20 dBm) using an HP8753C network analyzer. The resulting display will appear as shown in Figure 7.

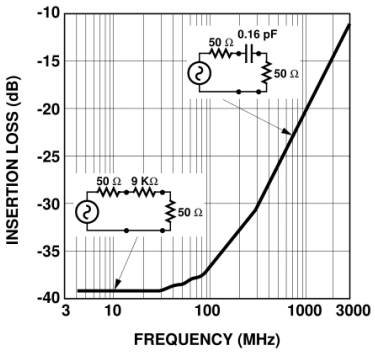

Figure 7. Measuring C_J and R_V.

At frequencies below 10 MHz, the video resistance dominates the loss and can easily be calculated from it. At frequencies above 300 MHz, the junction capacitance sets the loss, which plots out as a straight line when frequency is plotted on a log scale. Again, calculation is straightforward.

L_P and C_P are best measured on the HP8753C, with the diode terminating a 50 Ω line on the input port. The resulting tabulation of S_{11} can be put into a microwave linear analysis program having the five element equivalent circuit with R_V, C_J and R_S fixed. The optimizer can then adjust the values of L_P and C_P until the calculated S_{11} matches the measured values. Note that extreme care must be taken to de-embed the parasitics of the 50 Ω test fixture.

Detector Circuits

When DC bias is available, Schottky diode detector circuits can be used to create low cost RF and microwave receivers with a sensitivity of -55 dBm to -57 dBm.[1] These circuits can take a variety of forms, but in the most simple case they appear as shown in Figure 8. This is the basic detector circuit used with the HSMS-285x family of diodes.

In the design of such detector circuits, the starting point is the equivalent circuit of the diode, as shown in Figure 6.

Of interest in the design of the video portion of the circuit is the diode's video impedance — the other four elements of the equivalent circuit disappear at all reasonable video frequencies. In general, the lower the diode's video impedance, the better the design.

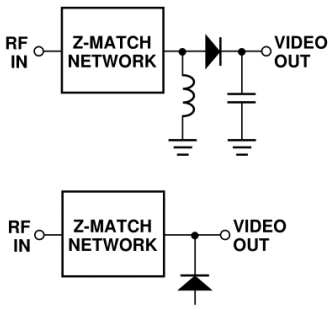

Figure 8. Basic Detector Circuits.

The situation is somewhat more complicated in the design of the RF impedance matching network, which includes the package inductance and capacitance (which can be tuned out), the series resistance, the junction capacitance and the video resistance. Of these five elements of the diode's equivalent circuit, the four parasitics are constants and the video resistance is a function of the current flowing through the diode.

$$R_V \approx \frac{26{,}000}{I_S + I_b}$$

where

I_S = diode saturation current in μA

I_b = bias current in μA

Saturation current is a function of the diode's design,[2] and it is a constant at a given temperature. For the HSMS-285x series, it is typically 3 to 5 μA at 25°C.

Saturation current sets the detection sensitivity, video resistance and input RF impedance of the zero bias Schottky detector diode.

[1] Agilent Application Note 923, *Schottky Barrier Diode Video Detectors.*

[2] Agilent Application Note 969, *An Optimum Zero Bias Schottky Detector Diode.*

Since no external bias is used with the HSMS-285x series, a single transfer curve at any given frequency is obtained, as shown in Figure 2.

The most difficult part of the design of a detector circuit is the input impedance matching network. For very broadband detectors, a shunt 60 Ω resistor will give good input match, but at the expense of detection sensitivity.

When maximum sensitivity is required over a narrow band of frequencies, a reactive matching network is optimum. Such networks can be realized in either lumped or distributed elements, depending upon frequency, size constraints and cost limitations, but certain general design principals exist for all types.[3] Design work begins with the RF impedance of the HSMS-285x series, which is given in Figure 9.

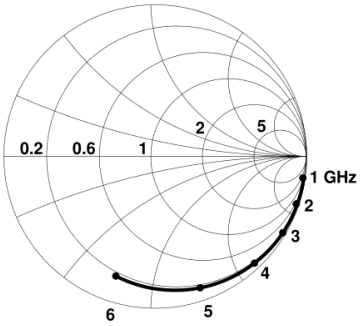

Figure 9. RF Impedance of the HSMS-285x Series at -40 dBm.

915 MHz Detector Circuit

Figure 10 illustrates a simple impedance matching network for a 915 MHz detector.

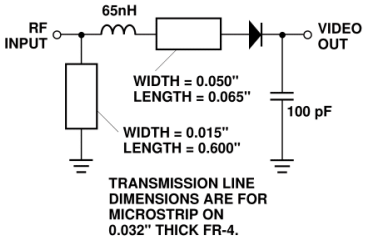

Figure 10. 915 MHz Matching Network for the HSMS-285x Series at Zero Bias.

A 65 nH inductor rotates the impedance of the diode to a point on the Smith Chart where a shunt inductor can pull it up to the center. The short length of 0.065" wide microstrip line is used to mount the lead of the diode's SOT-323 package. A shorted shunt stub of length <λ/4 provides the necessary shunt inductance and simultaneously provides the return circuit for the current generated in the diode. The impedance of this circuit is given in Figure 11.

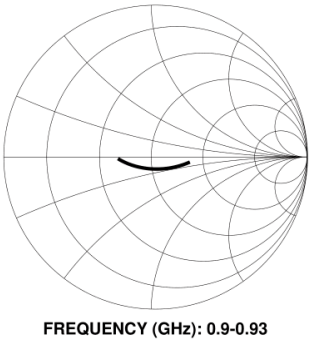

Figure 11. Input Impedance.

The input match, expressed in terms of return loss, is given in Figure 12.

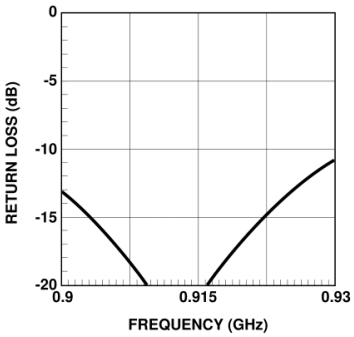

Figure 12. Input Return Loss.

As can be seen, the band over which a good match is achieved is more than adequate for 915 MHz RFID applications.

Voltage Doublers

To this point, we have restricted our discussion to single diode detectors. A glance at Figure 8, however, will lead to the suggestion that the two types of single diode detectors be combined into a two diode voltage doubler[4] (known also as a full wave rectifier). Such a detector is shown in Figure 13.

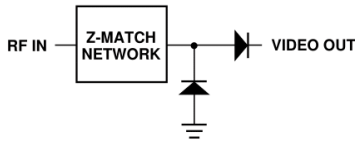

Figure 13. Voltage Doubler Circuit.

Such a circuit offers several advantages. First the voltage outputs of two diodes are added in series, increasing the overall value of voltage sensitivity for the network (compared to a single diode detector). Second, the RF impedances of the two diodes are added in parallel, making the job of reactive matching a bit easier.

[3] Agilent Application Note 963, *Impedance Matching Techniques for Mixers and Detectors.*
[4] Agilent Application Note 956-4, *Schottky Diode Voltage Doubler.*
[5] Agilent Application Note 965-3, *Flicker Noise in Schottky Diodes.*

Such a circuit can easily be realized using the two series diodes in the HSMS-285C.

Flicker Noise

Reference to Figure 5 will show that there is a junction of metal, silicon, and passivation around the rim of the Schottky contact. It is in this three-way junction that flicker noise[5] is generated. This noise can severely reduce the sensitivity of a crystal video receiver utilizing a Schottky detector circuit if the video frequency is below the noise corner. Flicker noise can be substantially reduced by the elimination of passivation, but such diodes cannot be mounted in non-hermetic packages. p-type silicon Schottky diodes have the least flicker noise at a given value of external bias (compared to n-type silicon or GaAs). At zero bias, such diodes can have extremely low values of flicker noise. For the HSMS-285x series, the noise temperature ratio is given in Figure 14.

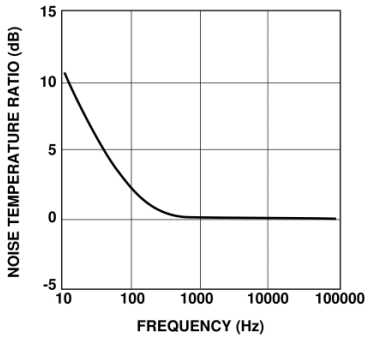

Figure 14. Typical Noise Temperature Ratio.

Noise temperature ratio is the quotient of the diode's noise power (expressed in dBV/Hz) divided by the noise power of an ideal resistor of resistance R = R_V.

For an ideal resistor R, at 300°K, the noise voltage can be computed from

$$v = 1.287 \times 10^{-10} \sqrt{R} \text{ volts/Hz}$$

which can be expressed as

$$20 \log_{10} v \quad \text{dBV/Hz}$$

Thus, for a diode with R_V = 9 KΩ, the noise voltage is 12.2 nV/Hz or -158 dBV/Hz. On the graph of Figure 14, -158 dBV/Hz would replace the zero on the vertical scale to convert the chart to one of absolute noise voltage vs. frequency.

Diode Burnout

Any Schottky junction, be it an RF diode or the gate of a MESFET, is relatively delicate and can be burned out with excessive RF power. Many crystal video receivers used in RFID (tag) applications find themselves in poorly controlled environments where high power sources may be present. Examples are the areas around airport and FAA radars, nearby ham radio operators, the vicinity of a broadcast band transmitter, etc. In such environments, the Schottky diodes of the receiver can be protected by a device known as a limiter diode.[6] Formerly available only in radar warning receivers and other high cost electronic warfare applications, these diodes have been adapted to commercial and consumer circuits.

Agilent offers a complete line of surface mountable PIN limiter diodes. Most notably, our HSMP-4820 (SOT-23) can act as a very fast (nanosecond) power-sensitive switch when placed between the antenna and the Schottky diode, shorting out the RF circuit temporarily and reflecting the excessive RF energy back out the antenna.

Assembly Instructions

SOT-323 PCB Footprint

A recommended PCB pad layout for the miniature SOT-323 (SC-70) package is shown in Figure 15 (dimensions are in inches). This layout provides ample allowance for package placement by automated assembly equipment without adding parasitics that could impair the performance. Figure 16 shows the pad layout for the six-lead SOT-363.

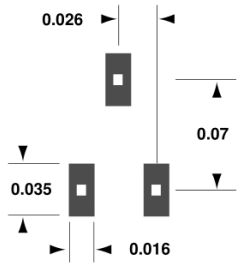

Figure 15. PCB Pad Layout (dimensions in inches).

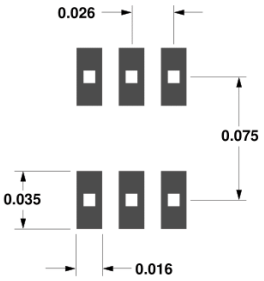

Figure 16. PCB Pad Layout (dimensions in inches).

[6] Agilent Application Note 1050, *Low Cost, Surface Mount Power Limiters.*

SMT Assembly

Reliable assembly of surface mount components is a complex process that involves many material, process, and equipment factors, including: method of heating (e.g., IR or vapor phase reflow, wave soldering, etc.) circuit board material, conductor thickness and pattern, type of solder alloy, and the thermal conductivity and thermal mass of components. Components with a low mass, such as the SOT packages, will reach solder reflow temperatures faster than those with a greater mass.

Agilent's diodes have been qualified to the time-temperature profile shown in Figure 17. This profile is representative of an IR reflow type of surface mount assembly process.

After ramping up from room temperature, the circuit board with components attached to it (held in place with solder paste) passes through one or more preheat zones. The preheat zones increase the temperature of the board and components to prevent thermal shock and begin evaporating solvents from the solder paste. The reflow zone briefly elevates the temperature sufficiently to produce a reflow of the solder.

The rates of change of temperature for the ramp-up and cool-down zones are chosen to be low enough to not cause deformation of the board or damage to components due to thermal shock. The maximum temperature in the reflow zone (T_{MAX}) should not exceed 235°C.

These parameters are typical for a surface mount assembly process for Agilent diodes. As a general guideline, the circuit board and components should be exposed only to the minimum temperatures and times necessary to achieve a uniform reflow of solder.

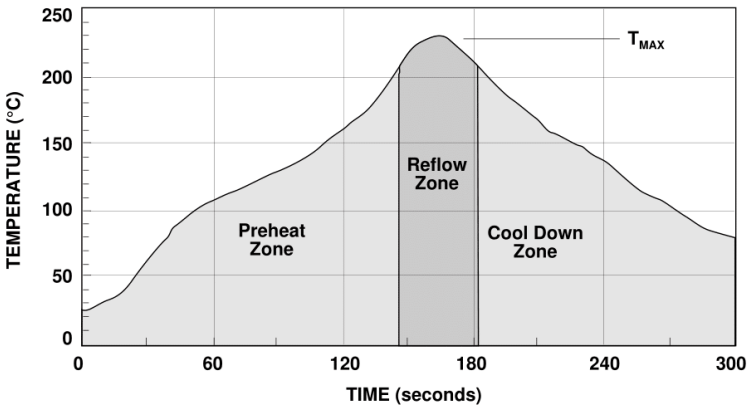

Figure 17. Surface Mount Assembly Profile.

Package Dimensions

Outline 23 (SOT-23)

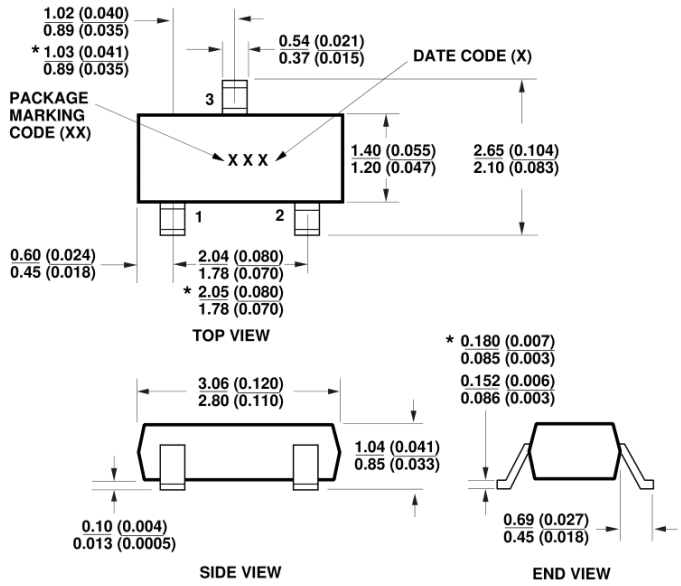

* THESE DIMENSIONS FOR HSMS-280X AND -281X FAMILIES ONLY.

DIMENSIONS ARE IN MILLIMETERS (INCHES)

Outline 143 (SOT-143)

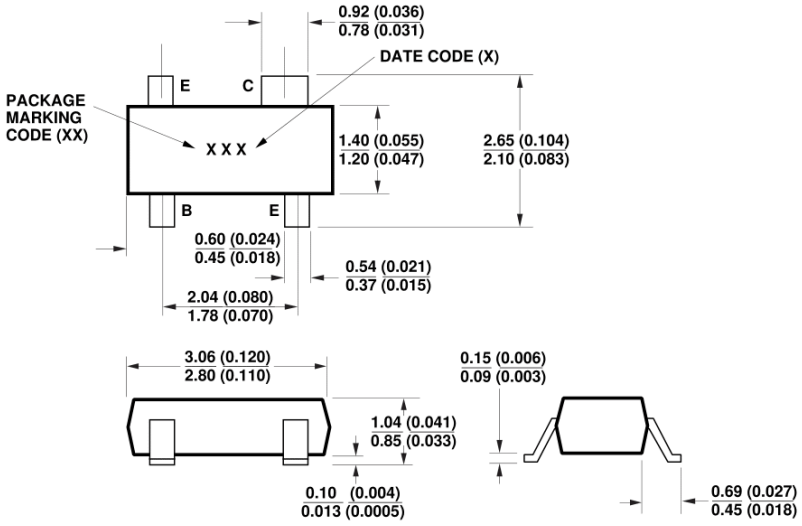

DIMENSIONS ARE IN MILLIMETERS (INCHES)

Outline SOT-323
(SC-70, 3 Lead)

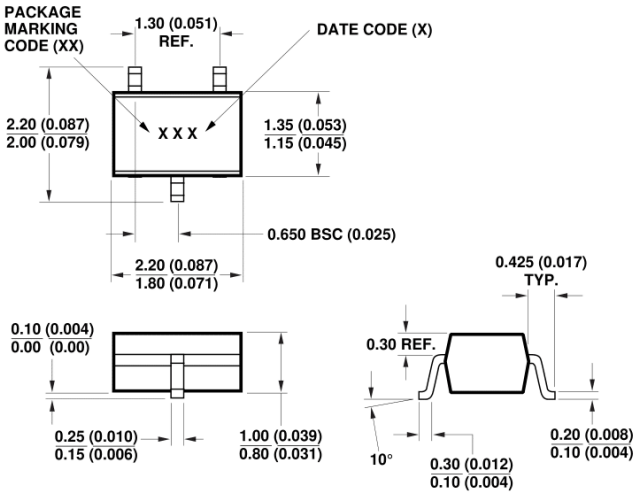

DIMENSIONS ARE IN MILLIMETERS (INCHES)

Outline SOT-363
(SC-70, 6 Lead)

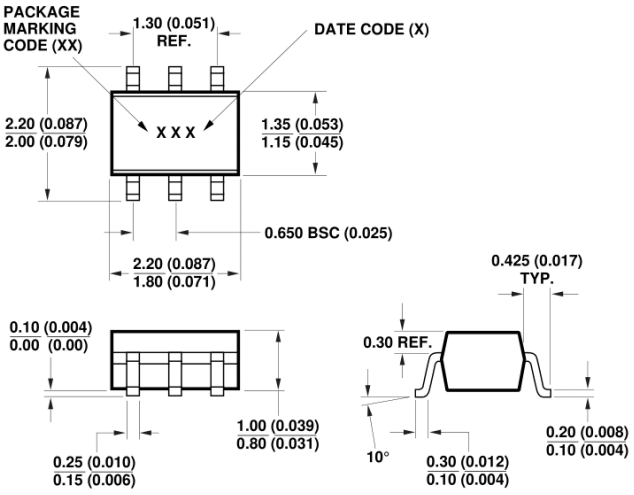

DIMENSIONS ARE IN MILLIMETERS (INCHES)

Part Number Ordering Information

Part Number	No. of Devices	Container
HSMS-285x-TR2*	10000	13" Reel
HSMS-285x-TR1*	3000	7" Reel
HSMS-285x-BLK*	100	antistatic bag

where x = 0, 2, 5, B, C, L and P for HSMS-285x.

Device Orientation

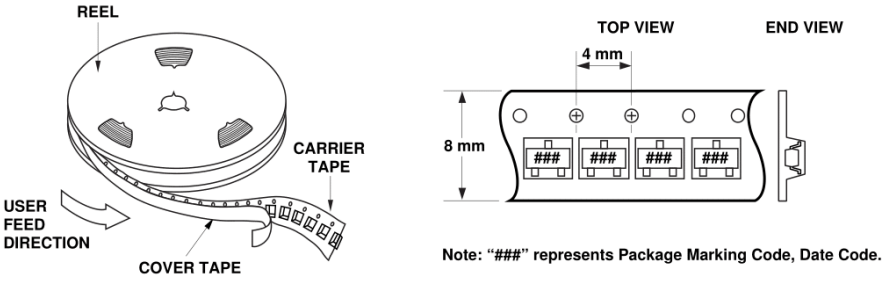

Tape Dimensions and Product Orientation
For Outline SOT-323 (SC-70 3 Lead)

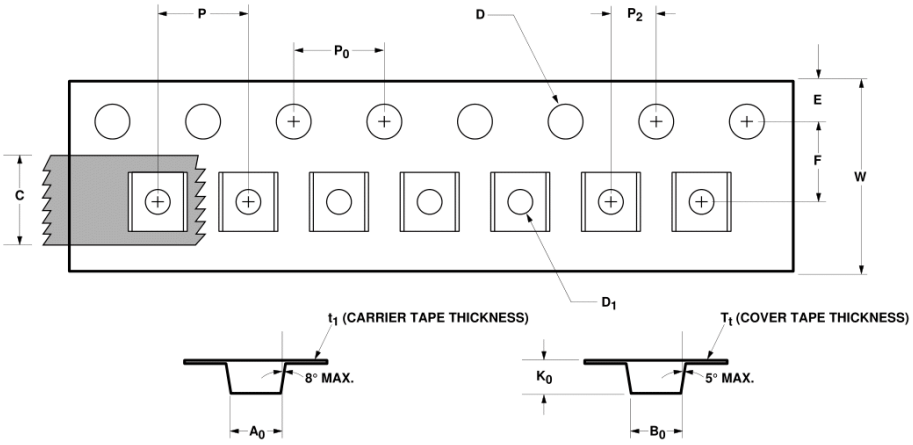

DESCRIPTION		SYMBOL	SIZE (mm)	SIZE (INCHES)
CAVITY	LENGTH	A_0	2.24 ± 0.10	0.088 ± 0.004
	WIDTH	B_0	2.34 ± 0.10	0.092 ± 0.004
	DEPTH	K_0	1.22 ± 0.10	0.048 ± 0.004
	PITCH	P	4.00 ± 0.10	0.157 ± 0.004
	BOTTOM HOLE DIAMETER	D_1	1.00 + 0.25	0.039 + 0.010
PERFORATION	DIAMETER	D	1.55 ± 0.05	0.061 ± 0.002
	PITCH	P_0	4.00 ± 0.10	0.157 ± 0.004
	POSITION	E	1.75 ± 0.10	0.069 ± 0.004
CARRIER TAPE	WIDTH	W	8.00 ± 0.30	0.315 ± 0.012
	THICKNESS	t_1	0.255 ± 0.013	0.010 ± 0.0005
COVER TAPE	WIDTH	C	5.4 ± 0.10	0.205 ± 0.004
	TAPE THICKNESS	T_1	0.062 ± 0.001	0.0025 ± 0.00004
DISTANCE	CAVITY TO PERFORATION (WIDTH DIRECTION)	F	3.50 ± 0.05	0.138 ± 0.002
	CAVITY TO PERFORATION (LENGTH DIRECTION)	P_2	2.00 ± 0.05	0.079 ± 0.002

www.semiconductor.agilent.com
Data subject to change.

Obsoletes 5968-5437E, 5968-5908E,
5968-2355E
5968-7457E (11/99)